

AD-A100 371

NAVAL RESEARCH LAB WASHINGTON DC
POLARIMETRY STUDIES OF IONOSPHERIC MODIFICATION BY ROCKET BOOST--ETC(U)
MAY 81 M H REILLY, L O HARNISH, J M GOODMAN
NRI-MR-4517

F/G 4/1

NL

UNCLASIFIED

1 of 1

AD
A100371

END
DATE
FILMED
7-81
DTIC

LEVEL II

BS

12

NRL Memorandum Report 4517

AD A100371

Polarimetry Studies of Ionospheric Modification by Rocket Boosters

M. H. REILLY, L. O. HARMISH, AND J. M. GOODMAN

Space Science Division

DTIC
ELECTE
JUN 18 1981
S D E

May 27, 1981



NAVAL RESEARCH LABORATORY
Washington, D.C.

Approved for public release; distribution unlimited.

81 6 18 118

FILE COPY

SECURITY CLASSIFICATION OF THIS PAGE (When Data Entered)

REPORT DOCUMENTATION PAGE		READ INSTRUCTIONS BEFORE COMPLETING FORM
1. REPORT NUMBER NRL Memorandum Report 4517	2. GOVT ACCESSION NO. AD-A100 371	3. RECIPIENT'S CATALOG NUMBER
4. TITLE (and Subtitle) POLARIMETRY STUDIES OF IONOSPHERIC MODIFICATION BY ROCKET BOOSTERS .	5. TYPE OF REPORT & PERIOD COVERED Memorandum report - final	
	6. PERFORMING ORG. REPORT NUMBER 251950	
7. AUTHOR(s) M. H. Reilly, L. O. Harnish, and J. M. Goodman	8. CONTRACT OR GRANT NUMBER(s)	
9. PERFORMING ORGANIZATION NAME AND ADDRESS Naval Research Laboratory Washington, D.C. 20375	10. PROGRAM ELEMENT, PROJECT, TASK AREA & WORK UNIT NUMBERS 61153N RR0330244 0149-0-1	
11. CONTROLLING OFFICE NAME AND ADDRESS	12. REPORT DATE May 27, 1981	
	13. NUMBER OF PAGES 89	
14. MONITORING AGENCY NAME & ADDRESS (if different from Controlling Office)	15. SECURITY CLASS. (of this report) UNCLASSIFIED	
	15a. DECLASSIFICATION/DOWNGRADING SCHEDULE	
16. DISTRIBUTION STATEMENT (of this Report) Approved for public release; distribution unlimited.		
17. DISTRIBUTION STATEMENT (of the abstract entered in Block 20, if different from Report)		
18. SUPPLEMENTARY NOTES		
19. KEY WORDS (Continue on reverse side if necessary and identify by block number) Ionosphere Modification Chemical Releases Polarimetry Studies Rocket Booster Effects Faraday Rotation		
20. ABSTRACT (Continue on reverse side if necessary and identify by block number) High altitude releases of certain molecules in booster rocket exhausts are known to deplete electron concentration in the ionosphere dramatically. These effects are exhibited in recent Faraday rotation measurements for the HEAO-C launch from Cape Kennedy on September 20, 1979 and the NOAA-B launch from Vandenberg on May 29, 1980, in which total electron content drop responses to the booster rockets are evident. The polarimetry experiments and data for these nocturnal launches are presented, discussed, and analyzed to obtain time profiles of total electron content (TEC) associated with three different satellite-to-receiver raypaths. Calculations of the (Continued)		

DD FORM 1 JAN 73 1473

EDITION OF 1 NOV 65 IS OBSOLETE
S/N 0102-014-6601

SECURITY CLASSIFICATION OF THIS PAGE (When Data Entered)

20. ABSTRACT (Continued)

booster rocket effect are carried out in detail for the HEAO-C case in an attempt to theoretically simulate the experimental results for the early-time TEC depletion effect from the booster rocket. The calculational model includes a full, three-dimensional integration of the rocket exhaust effect, in which rocket exhaust expansion is treated as thermalized, mutual diffusion in the non-uniform ambient background atmosphere. Results are discussed, and future directions are indicated.

CONTENTS

1.0 INTRODUCTION	1
2.0 THEORY AND COMPUTATIONAL CONSIDERATIONS	3
3.0 THE HEAO-C HOLE STUDY	6
3.1 Experimental Considerations	6
3.2 Data Presentation-The Control Period	9
3.3 The Conversion to TEC	13
3.4 The HEAO-C Booster Perturbation	18
3.5 Theoretical Considerations	20
4.0 THE NOAA-B HOLE STUDY	31
4.1 Experimental Considerations	31
4.2 Data Processing and Presentation	33
4.3 The NOAA-B Booster Perturbation	38
5.0 DISCUSSION AND CONCLUSIONS	38
6.0 ACKNOWLEDGMENTS	41
7.0 REFERENCES	41
APPENDIX A	45
APPENDIX B	65
APPENDIX C	70

Accession For	
NTIS GRA&I	<input checked="" type="checkbox"/>
DTIC TAB	<input type="checkbox"/>
Unannounced	<input type="checkbox"/>
Justification	
By	
Distribution/	
Availability Codes	
Dist	Avail and/or Special
A	

POLARIMETRY STUDIES OF IONOSPHERIC MODIFICATION BY ROCKET BOOSTERS

1.0 INTRODUCTION

The ionic content of the atmosphere has a significant effect on radiowave propagation, particularly at UHF and below. The mechanisms for introducing changes in the ionic content are of interest from a scientific point of view and for its potential in exploitation scenarios, such as in alleviating deleterious effects on radiowave propagation. Induced modification can take the form of producing, removing, or (less likely) moving free electrons in the ionospheric layers that extend roughly between altitudes of 60 and 1200 km.

The natural ionic constitution of the earth's upper atmosphere is largely due to the solar flux in the extreme ultraviolet band (XUV). As a result, electron concentrations are less at night than during the day, but the ionosphere nevertheless persists because of the sluggishness of electronic loss processes, especially at great heights where the atmosphere is extremely sparse. Attempts to produce excess ionization by non-nuclear means have been successful, but the effects have generally been short-lived and limited in geographical extent and altitude. Ion cloud experiments are typically designed to illuminate the benign properties of the medium and thus to effect only minor perturbations in the total system. Ion clouds have been used to investigate upper atmospheric and ionospheric characteristics, and have been especially important in the identification of field aligned phenomena and situation development.

The most extraordinary changes in the constitution of the upper atmosphere by non-nuclear means has been achieved by the removal of ions through the introduction of copious quantities of chemical reagents, such as water (H_2O) and hydrogen gas (H_2) during rocket launches [Mendillo et al., 1975]. Introduction of such molecules into the upper atmosphere, say above 250 km, where atomic

species are dominant, produces an enormous change in the chemistry that governs electron concentration. At these altitudes, electrons are present principally by virtue of vertical diffusion, having been born via the photo-ionization processes that occur primarily at much lower altitudes. Electronic losses near the maximum of the F2 layer and above are extremely small, because three-body processes are rare, and the two-body loss processes are radiative, with a resulting low cross section. This situation is drastically altered by the introduction of reagents, such as H_2O and H_2 , which increase the probability of electron loss by orders of magnitude. Furthermore, chemical reagent releases that occur at night are even more effective, since they do not have to contend with the vertical diffusion of electrons from the lower ionospheric daytime source. Examination of large and geographically extensive reductions in the concentration of electrons in the ionosphere can provide considerable information about the reconstitution of the electronic and ionic distributions in the upper atmosphere, and about sources and sinks.

Mendillo, Baumgardner, and Klobuchar [1979] suggested that the launch of the HEAO-C from Cape Kennedy on 20 Sept. 1979 would provide an excellent opportunity to observe an electron content "hole" in the ionosphere. Furthermore, the event was to be nocturnal rather than daytime as in the well-known SKYLAB case [Mendillo et al., 1975]. The launch occurred at 0128 LUT (Bermuda) and burned within the F-region at approximately 0130 LUT. NRL utilized two Faraday rotation polarimeters, both situated in Bermuda, to conduct its study of the HEAO-C effect. One polarimeter was directed toward ATS-3, while the other was directed toward ATS-5. In addition to these TEC measurements NRL also conducted HF communication and HF OTH radar studies of the event. Preliminary papers which outline NRL's involvement have been presented at a "HEAO-HOLE" workshop/symposium [Proceedings, 1980 a,b] in November, 1979, and the TEC effects were presented at COSPAR [Goodman, 1980]. The overall status of the HEAO-HOLE program has been reviewed by Mendillo, Rote, and Bernhardt [1980]. Reilly [1980] has described theoretical calculations which represent a portion of the experimental data adequately. The theoretical model development is continuing.

Recently it was suggested that an Atlas F launch of a NOAA satellite from Vandenberg during the month of May 1980 would provide another opportunity for studies of rocket-induced TEC diminution [Baumgardner, 1980]. NRL located a polarimeter at a site by the Salton Sea in California with the antenna boresighted to ATS-1 to observe possible effects. The Atlas F launch occurred at approximately 0400 PST on May 29, 1980 and useful data was obtained.

It is the purpose of this report to describe the Bermuda and Salton Sea polarimetry experiments and results, and to indicate how the data are being used to interpret the ionospheric response to booster rocket perturbations. In the next section (Sec. 2) a brief account of background theory for the polarimetry experiment is given. In Sec. 3 the Bermuda polarimetry experiment for the HEAO-C is discussed and analyzed. The Salton Sea experiment for the NOAA-B experiment is similarly treated in Sec. 4. Sec. 5 gives discussion and conclusions based on the results, and indicates future directions.

2.0 THEORY AND COMPUTATIONAL CONSIDERATIONS

The polarimetry experiment is based on the Faraday effect for a magnetoionic medium. In this case the polarization vector of a linearly polarized radiowave is observed to rotate during its passage through the ionosphere from a satellite source to a receiver on the ground. The radiowave frequency (e.g., ~137 MHz) is typically much greater than any electron plasma frequency along the raypath. In this frequency regime the index of refraction is close to unity, raypaths are nearly straight, radiowave polarization is essentially transverse, and characteristic wave polarizations are very nearly left- and right-circular. Explicitly, the Appleton-Hartree refractive index and polarization reduce to [e.g., Budden, 1966]

$$n_k \approx \left[1 - \frac{X}{1 \pm Y_l} \right]^{1/2} \approx 1 - \frac{1}{2} X (1 \mp Y_l)$$

$$X \equiv \omega_p^2(z)/\omega^2 \quad Y_l \equiv e \mathbf{B}(z)/m\omega \cdot \hat{z} \quad (1)$$

$$E_{\omega x} / E_{\omega y} \approx \mp j$$

for the radiowave whose electric field is given by

$$\mathbf{E} = \mathbf{E}_\omega(z) \exp(j\omega t) + c.c. = E_x \hat{x} + E_y \hat{y} \quad (2)$$

along the raypath, which is assumed to be in the \hat{z} direction at a point z along it (i.e., z is considered to be a raypath coordinate). Upper and lower signs in Eq. (1) refer to left- and right- circular polarizations, as denoted by the subscripts L and R , respectively. The expressions in Eq. (1) break down when \mathbf{B} and \hat{z} become very nearly perpendicular, but this is assumed not to happen here. The complex conjugate of the first term on the right in Eq. (2) is denoted by c.c. For the purpose of visualizing the polarization rotation, we note that the two-dimensional vector in Eq. (2) has a simple phasor representation through the definition

$$F = E_x + j E_y. \quad (3)$$

The linearly polarized radiowave is represented in terms of the characteristic circularly polarized waves as

$$\begin{aligned} F(z,t) &= F_L(z,t) + F_R(z,t), \text{ where} \\ F_L(z,t) &= F_\omega(z) \exp -j\omega \left[t - \frac{1}{c} \int_0^z n_L(s,\omega) ds \right] \equiv F_\omega \exp(jA) \\ F_R(z,t) &= F_\omega(t) \exp j\omega \left[t - \frac{1}{c} \int_0^z n_R(s,\omega) ds \right] \equiv F_\omega \exp(jB) \end{aligned} \quad (4)$$

The point z specifies distance along the raypath, and the phasor rotation of F_L or F_R is according to the left-hand or right-hand rule, respectively, where the thumb of the hand is in the direction of propagation, and the fingers curl in the direction of polarization (i.e., phasor) rotation with time at a given point. By combining the exponential terms the field can be written as

$$F(z,t) = 2 F_\omega \cos \left(\frac{A-B}{2} \right) \exp j \left(\frac{A+B}{2} \right) \quad (5)$$

which clearly shows the Faraday rotation of the polarization vector to be

$$\phi = \frac{A+B}{2} = \frac{\omega}{2c} \int_0^{z_r} [n_L - n_R] ds = \frac{\omega}{2c} \int_0^{z_r} XY_1 ds, \quad (6)$$

where z_r is the distance along the raypath to the receiver. In terms of the altitude variable h , $ds = -dh \sec \chi$, where χ is the raypath zenith angle, and the amount of Faraday rotation in radians is evaluated for MKS units as

$$\begin{aligned} \phi &= 2.9714 \times 10^{-2} f^2 I \\ \text{where } I &= \int_0^{h_1} H \cos \theta \sec \chi N dh = \int_0^{h_1} MN dh \\ &\equiv \bar{M} \int_0^{h_1} N dh \equiv \bar{M} T. \end{aligned} \quad (7)$$

Here, h_s is the height of the satellite, f is the radio frequency (Hz), H is the magnetic field strength (amp. turns/m.), and N is the electron density (m^{-3}). In the last line a mean value of M is extracted, i.e., \bar{M} , thus isolating the factor T , which is of physical interest. It is total vertical electron content (TEC - in el/m^2) up to the height h_f . It has been shown [Titheridge, 1972] that if \bar{M} is evaluated as the value of M at a height of 420 km along the raypath, with $h_f = 2000$ km., then the last line of Eq. (7) is accurate within 5% under most conditions. This is the procedure adopted in subsequent calculations. The "mean ionospheric point" or "ionospheric pierce point" at 420 km altitude will later be referred to as the IPP. Changes in T , i.e. ΔT , due to ionospheric variations will thus be inferred from measured changes in ϕ according to Eq. (7):

$$\Delta T = (33.654 f^2 / \bar{M}) \Delta \phi \quad (MKS). \quad (8)$$

It is, however, often convenient to express T in units of $10^{16} el/m^2$ (i.e., "TEC units"), f in MHz ($= 10^6$ Hz), ϕ in degrees ($^\circ$), and \bar{M} in oersteds, where $H = 1$ oersted is equivalent to a magnetic field $B = 1$ gauss $= 10^5$ gamma in a nonmagnetic medium. In these units the preceding expression becomes

$$\Delta T (10^{16} el/m^2) = 7.3811 \times 10^{-7} \frac{f (MHz)^2}{\bar{M} (oersted)} \Delta \phi (^\circ), \quad (9)$$

and this is the one we find most useful. The incorporation of second order effects (e.g., as an extension of Eq. (1)) would not significantly enhance the accuracy of Eq. (9) for the high radiowave frequencies of interest here [Ross, 1965].

From knowledge of satellite position, which is not strictly geostationary, and receiver location the value of \bar{M} in Eq. (9) is calculated for the times appropriate to the polarimetry experiment according to a standard magnetic field model [Cain and Sweeney, 1970]. This enables TEC variations to be inferred from measured polarization rotation changes according to Eq. (9). To fix the absolute value of TEC, the "baseline ambiguity" must be removed, and this is done by comparison of the data with calibrated TEC values routinely published by AFGL for nearby stations. This procedure will be specified below.

3.0 THE HEAO-C HOLE STUDY

3.1 Experimental Considerations

As seen in Fig. 1, Bermuda was in a unique position to observe TEC effects at aspects approximately perpendicular to the HEAO-C booster rocket track. Other polarimeter receivers were located along the Florida coast to view rocket booster perturbations to the ionosphere at aspects approximately parallel to the rocket track. The latter results are contained in recent HEAO-C Workshop Proceedings reports [Proceedings, 1980 a,b]. Observation of the HEAO-C launch in the NRL experiment was made from the NASA STDN Facility on the eastern end of Bermuda. Two separate polarimeter systems were used. One system used a NASA crossed-yagi antenna on the roof which was pointed at ATS-5. A similar crossed-yagi antenna was mounted on the roof and pointed at ATS-3. Both ATS-3 and ATS-5 are nominally geosynchronous satellites which have linearly polarized VHF downlinks.

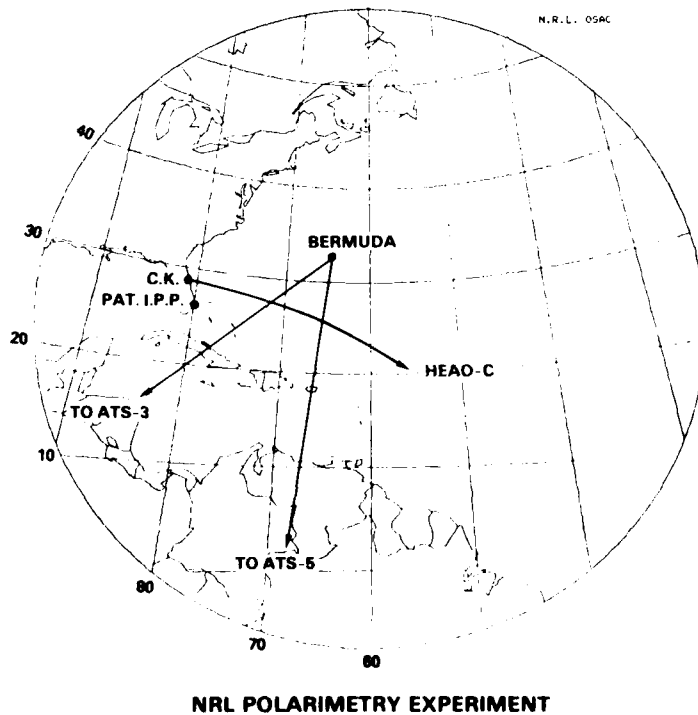


Fig. 1 — Perspective of the NRL Bermuda polarimetry experiment in a gnomonic projection

The satellite signals were processed as shown in Fig. 2. The received signals were fed to quadrature hybrids through coaxial cables phase-matched to within $\pm 1^\circ$. The hybrids' right- and left- hand circular outputs were fed into Teledyne Micronetics Faraday Polarization Tracking Systems, Model 6501 B. These polarimeters electronically simulate antenna rotation at a rate of 18Hz by phase-shifting one of the inputs with respect to the other. The signals are then combined in a 90° hybrid. After amplification and filtering, the signal is phase-compared to a reference signal, and is then applied to a dual phase meter with ϕ and $\phi + 180^\circ$ outputs, where ϕ is the signal phase angle. These outputs, along with an AGC output and a NASA 36 time code were then recorded on an 8-channel chart recorder. Filter networks directly in front of the AGC outputs were modified to correct an impedance mismatch with the chart recorder.

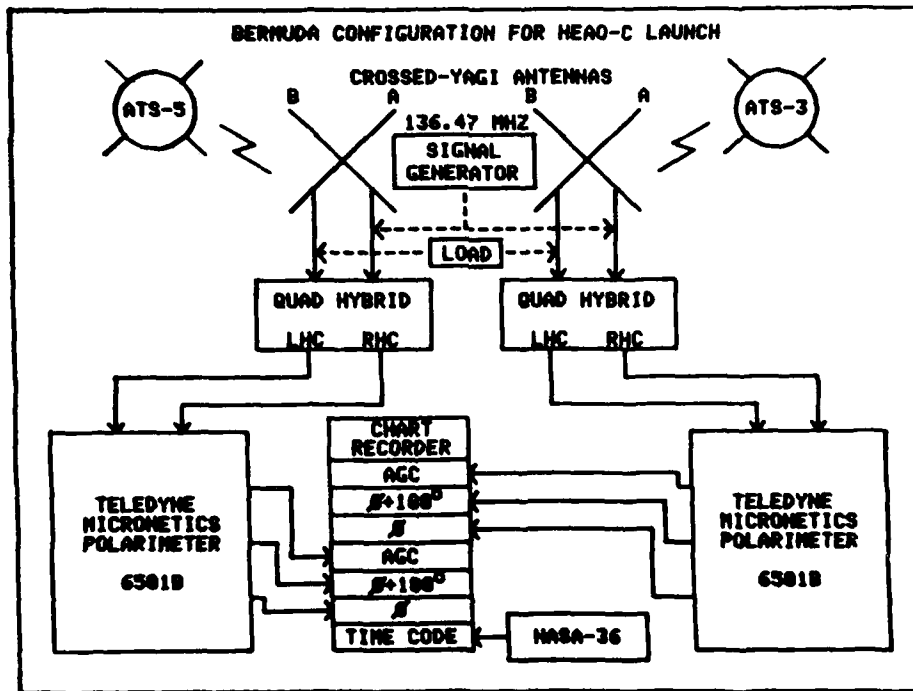


Fig. 2 — Block diagram of the apparatus for the Bermuda polarimetry experiments

Because of the fact that the satellites are not strictly geostationary, the diurnal patterns of their earth projections are figure-eights having latitudinal extents defined by the orbit inclinations. The ray-path IPP projection on the earth's surface will also vary for each satellite. These effects are displayed on a rectangular lat.-lon. grid in Fig. 3 for the day of the launch of HEAO-C, i.e., Sept. 20, 1979. The figure-eights of the satellite and associated IPP earth projections are shown for the 24 hour period. Also shown are the satellite-to-receiver raypaths at the times of closest approach of the rocket to the raypaths. The times are given as GMT values, four hours later than local time. The booster rocket trajectory is shown in Fig. 3 up to the point of burnout (the tip of the arrow).

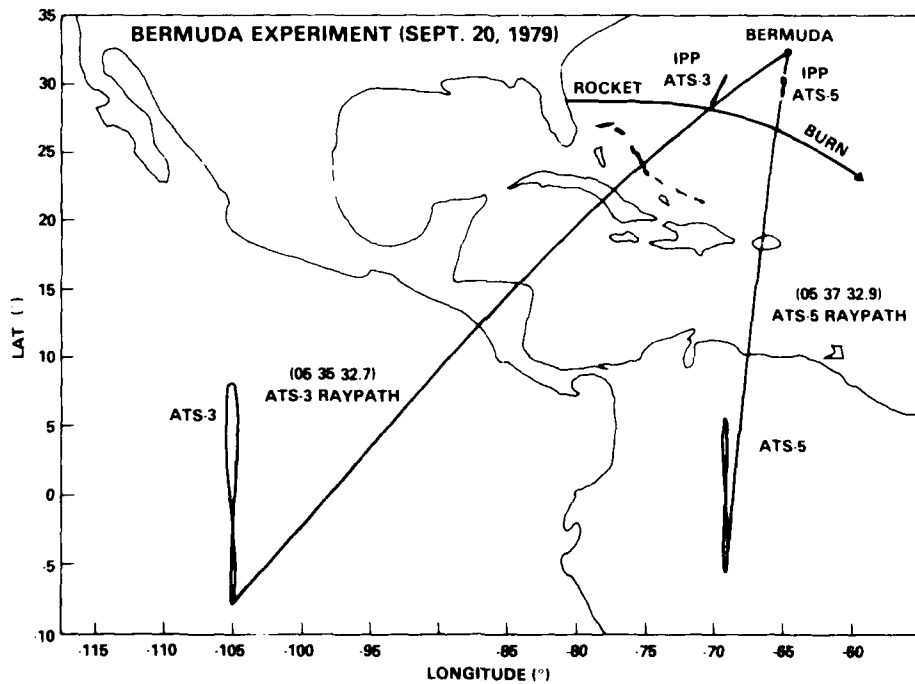


Fig. 3 — Rectangular lat.-lon. grid projection of the Bermuda polarimetry experiment. Features shown are the diurnal patterns of the satellites and associated IPP points on the raypaths to Bermuda for Sept. 20, the rocket trajectory during its burn, and the raypaths at the times of closest approach of the rocket

Over a month's worth of data was obtained from the ATS-5 source. This was used as a control. During the experimental period the satellite position varied, not only because of the aforementioned figure-eight diurnal behavior, but also because of a slow drift of the figure-eight pattern itself over a

longer period of time. It was, however, sufficient, to keep the antenna boresight directions for the satellites fixed. Some parameters of the NRL radio beacon experiments are given in Table 1.

Table 1 — NRL Radio Beacon Experiments
Station Location: Bermuda 32.35°N, 64.66°W
antenna beamwidths 30° nominal

Satellite source	ATS-3	ATS-5
Location	100°W (nominal)	69°W (nominal)
Frequency (MHz)	136.47	136.47
Azimuth (deg)	239 (average)	191 (average)
Elevation (deg)	31 (average)	53 (average)
Sub-ionospheric point @ 420 km	29 °N (nominal) 70°W (nominal)	30 °N (nominal) 65°W (nominal)
Time Coverage	Sept. 17 - Sept. 23	Aug. 15 - Sept. 23

A sample of the strip chart data is shown during the period of the launch in Fig. 4. Time was recorded in code at the bottom of the chart, and the other channels, starting at the top, were ATS-3 AGC, ATS-3 " $\phi + 180^\circ$ ", ATS-3 " ϕ ", ATS-5 AGC, ATS-5 " $\phi + 180^\circ$ ", and ATS-5 " ϕ ". The ATS-3 AGC channel did not perform properly and was ultimately ignored. The ATS-5 AGC dynamic range was approximately 23 dB. The series of "downward" ramps following the launch time are indicative of a rapid reduction in TEC.

3.2 Data Presentation-The Control Period

The polarization angles were scaled at ten-minute intervals during the time coverage of the experiment (cf. Table 1), except during the HEAO-C launch period when the data was scaled at one-minute intervals. The scaling accuracy is estimated as ± 1 mm on the chart paper or $\pm 4^\circ$ for the Faraday rotation angle in this case. From an evaluation of Eq. (9), this translates to a TEC uncertainty of about $\pm 0.1 \times 10^{16}$ el/m². This should be viewed as a random reading error.

The scaled data were put on punched cards, and plots of the rotation angle were generated. As an intermediate step, minimum values of ϕ , which occurred a short time after the HEAO-C launch, were set at 55.5° for ATS-3 and 130° for ATS-5. This amounted to a removal of the baseline ambiguity in Eq. (9), so that the relation between T and ϕ is approximately given by Eq. (9) with the " Δ " symbols removed. Details of the baseline ambiguity removal will be given shortly. The Faraday rotation angle

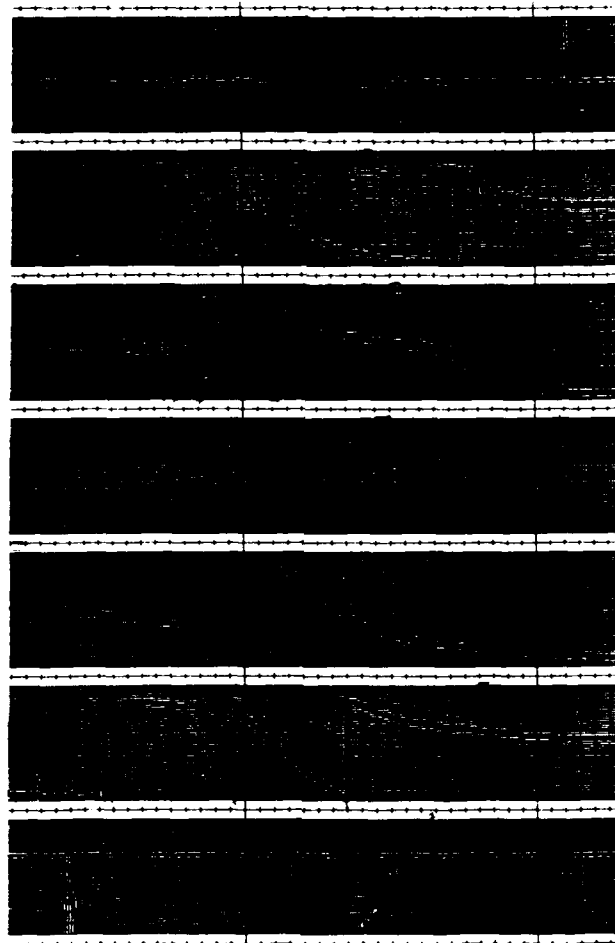


Fig 4 — Strip chart data for the period of the launch of HEAO-C

data plots are given in Appendix A for ATS-5 and in Appendix B for ATS-3. The TEC values can be calculated from these angles ϕ from the relation

$$T (10^{16} \text{el}/\text{m}^2) \approx 1.3747 \times 10^{-2} \phi (^\circ) / \bar{M} (\text{oersted}) \quad (10)$$

The ATS-5 compilation is much larger; it was deemed sufficient to extend the control period for only one of the Bermuda polarimeters.

A compilation of polarization and related geophysical data is given for ATS-5 in Tables 2 and 3 and for ATS-3 in Table 4. Maximum and minimum values of ϕ for each day are given along with their times of occurrence. Also indicated are the Fredericksburg A-indices, which measure daily magnetic

Table 2 — ATS-5 Polarization Data and Related Geophysical Data (August)

DATA	A_{fr}	SSN	MAXIMUM		MINIMUM	
			ϕ deg	TIME (Loc.)	ϕ deg	TIME (Loc.)
8/17/79	7	138	1742	1830	1070	2200
8/18/79	8	138	1966	2049	622	0530
8/19/79	40	310	1790	0000	874	2330
8/20/79	29	259	1754	1730	470	0509
8/21/79	28	335	1350	1839	562	0500
8/22/79	15	262	1622	1839	706	0339
8/23/79	7	261	1794	1330	730	0519
8/24/79	9	315	2094	1419	558	0509
8/25/79	16	256	2030	1149	730	0509
8/26/79	16	236	1298	1309	822	0509
8/27/79	13	277	1798	1130	690	0509
8/28/79	13	221	1982	1249	654	0500
8/29/79	44	169	1754	1730	674	0530
8/30/79	13	169	1302	1039	630	0539
8/31/79	13	214	1678	1339	630	0519

Table 3 — ATS-5 Polarization Data and Related Geophysical Data (September)

DATA	A_{fr}	SSN	MAXIMUM		MINIMUM	
			ϕ deg	TIME (Loc.)	ϕ deg	TIME (Loc.)
9/1/79	7	216	1878	1319	626	0519
9/2/79	6	169	1614	1419	654	0509
9/3/79	7		1978	1239	590	0500
9/4/79	11	201	1934	1439	702	0519
9/5/79	14	208	1718	1109	574	0519
9/6/79	14	223	1634	1130	710	0539
9/7/79	4	231	1770	1519	530	0509
9/8/79	6	181	1830	1349	530	0519
9/9/79	3	150	1962	1309	550	0530
9/10/79	8	253	2046	1519	490	0500
9/11/79	14	190	1586	1330	646	0449
9/12/79	5	223	2006	1600	542	0519
9/13/79	6	247	2134	1500	554	0519
9/14/79	6	240	1746	1549	554	2349
9/15/79	7	243	1658	1300	386	0500
9/16/79	8	233	1610	1519	270	0509
9/17/79	10	202	1678	1419	362	0519
9/18/79	45	278	1254	0009	258	0609
9/19/79	7	282	1778	1330	166	0530
9/20/79	18	207	2146	1400	130	0530
9/21/79	16	194	1962	1100	534	0539
9/22/79	5	291	1790	1409	354	0509
9/23/79	5	395	1074	0749	530	0530

Table 4 — ATS-3 Polarization Data and Related Geophysical Data (September)

DATE	A_{fr}	SSN	MAXIMUM		MINIMUM	
			ϕ deg	TIME (Loc.)	ϕ deg	TIME (Loc.)
9/17/79	10	202	1675	1400	935	0819
9/18/79	45	278	1421	0000	345	0500
9/19/79	7	282	1575	1300	203	0539
9/20/79	18	207	1911	1239	35	0230
9/21/79	16	194	1835	1109	583	0549
9/22/79	5	291	1761	1730	473	0530
9/23/79	5	395	1359	0749	831	0049

activity, and Boulder sunspot numbers (SSN). Note that times of occurrence are local times, four hours earlier than GMT.

Inspection of the data in Appendix A for ATS-5 reveals daytime variations in TEC somewhat larger in August than for September. On the other hand, the variation of minimum TEC (just prior to sunrise) is smaller in August than for September. In the data for Sept. 18, 1979, the values of TEC are substantially reduced. This is a well-known result of high magnetic storm activity and related heating of the thermosphere, which were prevalent conditions on Sept. 18. Many of the large scale features of the ATS-5 data are in common with ATS-3 data in Appendix B.

Figure 5 is a plot of the average ATS-5 ϕ for the "quiet" portions of the time period between 17 August and 23 September. Periods of TEC depression on Sept. 18 and 19, which resulted from magnetic storms, and on Sept. 20, which resulted from the HEAO-C launch, were excluded from this average. The extrema in the figure are smeared somewhat because of their time variation in the daily plots of Appendix A. Of note is the enhancement in TEC which occurs at approximately 0500 GMT, roughly five hours before the pre-sunrise minimum. This is apparently a regular feature of the midlatitude ionosphere. Kersley et al. [1980] have previously observed a post-sunset maximum in TEC for data obtained in Caribbean zone.

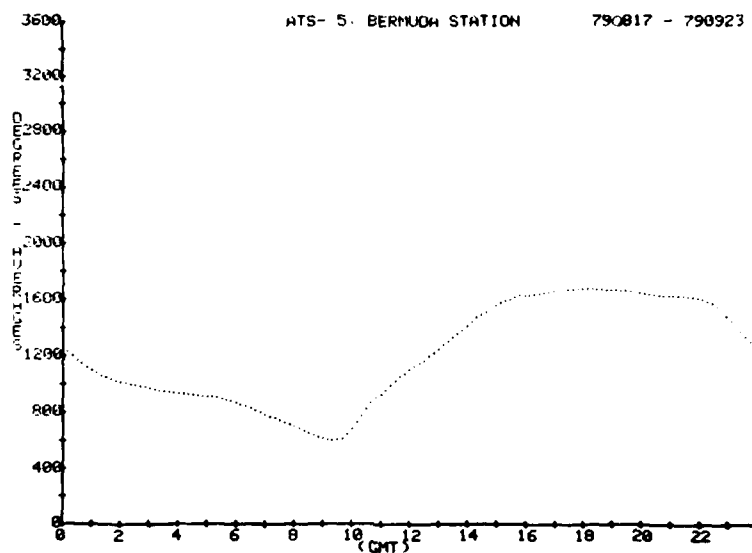


Fig. 5 — Average diurnal behavior of the ATS-5 Faraday rotation angle for the "un-perturbed" ionosphere. Time period for the average was 8/17-9/23, 1979, excluding the magnetic storm data in 9/18/0040Z-9/19/1050Z and the HEAO-C depression of TEC in 9/20/0540Z-9/20/1100Z.

3.3 The Conversion to TEC

Faraday rotation angle data are converted to TEC values through Eq. (9), which for this case becomes

$$T = C + 1.3747 \times 10^{-2} \phi \text{ (}^\circ\text{)} / \bar{M} \text{ (oersted)}, \quad (11)$$

where T and C are in TEC units. The determination of the constant C amounts to the removal of the baseline ambiguity previously mentioned. If the value of ϕ at a particular time t_0 is given as ϕ_0 in the data, which has been essentially arbitrarily scaled during the recording period, and the TEC is known from other information, the value of C (or an equivalent correction to ϕ) can be determined from Eq. (11). First, a set of \bar{M} -values are needed, and the calculation of these proceeds as indicated in Sec. 2.0. The results are included in Fig. 6 for ATS-5 and in Fig. 7 for ATS-3. In each of these figures there are three curves. The one defined by x-marks was provided to us by J. Klobuchar of AFGL before the HEAO-C launch, and is appropriate to Sept. 5, 1979. The other curves were computed by us recently from satellite one-line orbit elements for the satellites as inferred by J. Eisele at NRL from NAVSPASUR five-line orbit elements. The one-line elements were appropriate to Sept. 20, 1979, the

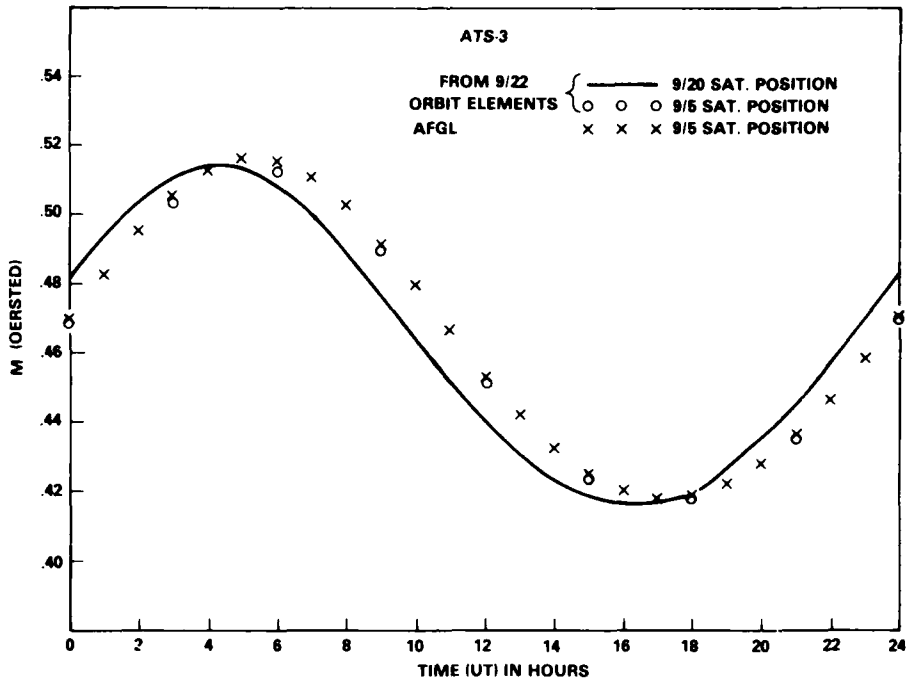


Fig. 6 - Calculated \bar{M} factors for ATS-5

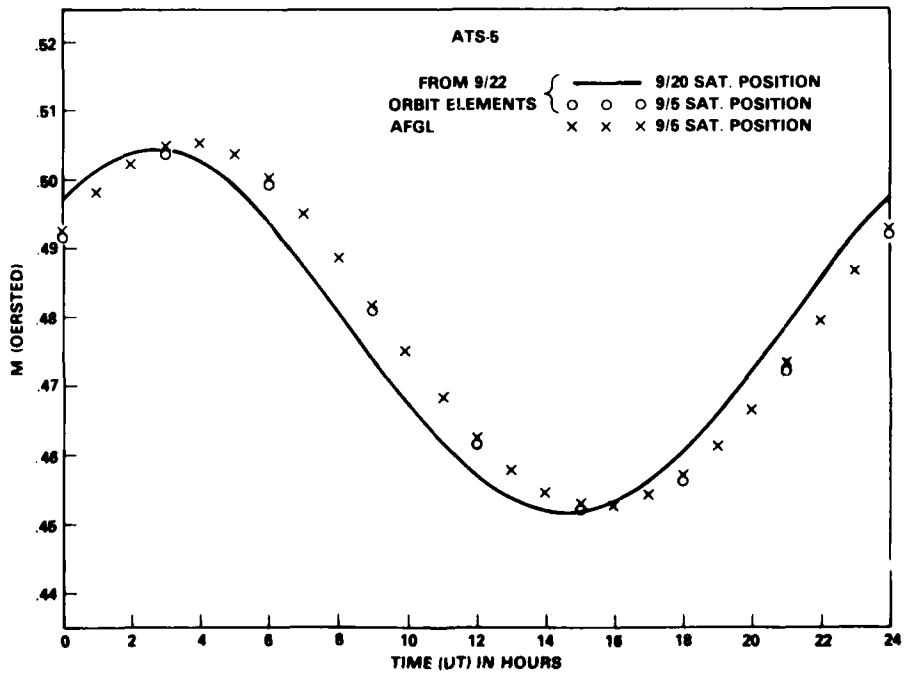


Fig. 7 - Calculated \bar{M} factors for ATS-3

day of the HEAO-C launch, and the solid line \bar{M} -factor curves in Figs. 6 and 7 are applicable for this date. As a check on the calculations, the one-line elements were used to determine a curve for Sept. 5, as identified by 0-marks in Figs. 6 and 7. This agrees quite closely with the AFGL curve, as hoped, and the difference between the Sept. 5 and Sept. 20 curves is a result of slowly varying changes in the satellite positions. These differences are small, however, compared to the diurnal variations exhibited. Incidentally, the one-line orbit elements were previously used in the calculations of Fig. 3.

The constant C in Eq. (11) has been determined by trying to fit TEC values routinely tabulated by AFGL for Patrick AFB near Cape Kennedy. The IPP earth projection for Patrick is shown in Fig. 1. The Patrick AFB TEC values are shown as the solid curve in Fig. 8 for several days surrounding the HEAO-C launch. The constant C was initially chosen to obtain an estimated best fit of Patrick TEC maxima for Sept. 14-17. The resultant ATS-5 TEC values, which were calculated from the Bermuda data in conjunction with the AFGL \bar{M} -factor values in Fig. 6, are shown as x-marks in Fig. 8. The agreement with Patrick AFB values is good enough to allow some confidence in this procedure. The notable exception, of course, is the TEC dropout evident in the Bermuda data near the pre-sunrise minimum on Sept. 20. This is an effect of the HEAO-C launch, which is not seen in the Patrick TEC values. Inspection of raypath geometries in Fig. 1 makes this plausible. Strong TEC depression on Sept. 18 results from magnetic storm conditions, and there is some question of the validity of the Patrick TEC values for a 24 hour period on either side of the HEAO-C launch [Klobuchar, 1979], but these considerations do not seem to affect the validity of our procedure for removing the baseline ambiguity. While C , as initially determined, does a good job on the fit of TEC maxima during magnetically quiet days preceding the launch, the minima values are not similarly well fit. Accordingly, a correction of -2 TEC units was added to obtain a final C value with an estimated uncertainty of ± 2 TEC units. The final value of C adopted thus requires a shift of all the x-mark values in Fig. 8 by two TEC units downward.

The calculated TEC values for the ATS-5 raypath on the morning of Sept. 20, the day of the HEAO-C launch, are shown in Fig. 9. Also shown are the unperturbed Patrick TEC values with straight

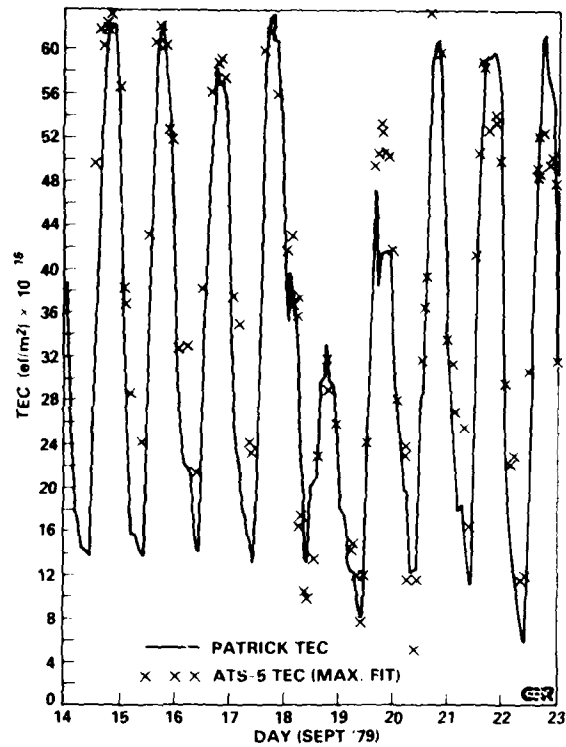


Fig. 8 — Comparison of Patrick TEC with Bermuda TEC, as calculated from the polarimetry data to obtain the best fit of Patrick TEC maxima for Sept. 14-17

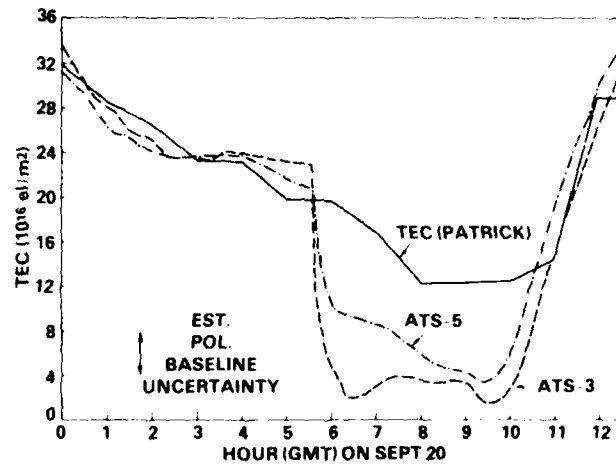
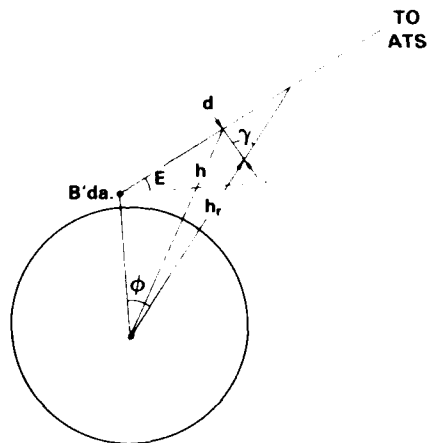


Fig. 9 — Final TEC determination from Bermuda polarimetry data for Sept. 20. Hourly Patrick TEC values are connected by straight lines (see text).

lines drawn between values of the hourly tabulation. These unperturbed values are questionable in view of the above remarks. The ATS-3 TEC values were similarly computed from the AFGL \bar{M} -values in Fig. 7. The constant C for this case was chosen to obtain agreement with the ATS-5 TEC value at 2.9 hours (GMT) on Sept. 20. The result of this is the ATS-3 curve in Fig. 10. While somewhat arbitrary, the above procedure is still estimated to give results within the estimated uncertainty of ± 2 TEC units for the baseline ambiguity removal, which is shown by the double-arrowed line in Fig. 9. The original polarization angle data was corrected by the C values determined, and it is this corrected data which appears in Appendix A and Appendix B. Hence, $C \approx 0$ in Eq. (11) for these data.



<u>SAT.</u>	<u>$\phi(^{\circ})$</u>	<u>$h_r(\text{km})$</u>	<u>$h(\text{km})$</u>	<u>$d(\text{km})$</u>	<u>$\gamma(^{\circ})$</u>
ATS-3	6.6	389.549	429.089	47.391	33.565
ATS-5	5.8	464.464	597.86	219.948	53.395

CR

Fig. 10 — Determination of the orientation of the raypaths with respect to the rocket at closest approach

Although the TEC curves for ATS-3 and ATS-5 were calculated from AFGL \bar{M} -values for Sept. 5 in Figs. 6 and 7, instead of the slightly more accurate Sept. 20 \bar{M} values in these figures, the corrections are deemed to be insignificant. A systematic 2% error in \bar{M} values is not significant in a theory which makes a possible 5% error in extracting an effective average \bar{M} values at a raypath altitude of 420 km.

3.4 The HEAO-C Booster Perturbation

On September 20, 1979 NASA's third High-Energy Astrophysical Observatory (HEAO-C) was launched from Cape Kennedy at 0528 (GMT) (lift-off time) by an Atlas-Centaur booster rocket system. The second-stage Centaur rocket was ignited at an altitude of 211 km and burned up to an altitude of about 501 km along the trajectory shown in Fig. 3, which was supplied to us after the launch by NASA, Goddard [Ketterer, 1979]. Along its trek through the ionosphere, rocket exhaust molecules were injected at the rate of about $5.9 \times 10^{26} \text{ s}^{-1}$ for H_2 and $9.8 \times 10^{26} \text{ s}^{-1}$ for H_2O [Mendillo, Baumgardner, and Klobuchar, 1979].

Especially at F-region heights in the ionosphere, where the resident species of ions and atoms are predominantly monatomic, these molecules turn out to have a substantial chemical effect [Mendillo, Hawkins, and Klobuchar, 1975]. After charge-exchange collisions of these molecules with O^+ ions, the associated positive molecular ions very efficiently diminish the population of electrons in their vicinity through a molecular dissociative recombination process. As a manifestation of this electron removal, TEC records show a drop-out effect, as seen in Figs. 4 and 9 and in the polarization angle data for Sept. 20 in Appendix A and Appendix B.

The spatial and temporal development of the ionosphere hole may be partially understood from the experimental data and from calculation of the relative geometry of the booster rocket trajectory with respect to the satellite-to-receiver raypaths (cf. Fig. 3). The intersection of the rocket trajectory and raypath projections on the earth occur at the times indicated in Fig. 3. The latitudes and longitudes of the intersection points, as well as the associated azimuthal and elevation angles of the raypaths from Bermuda, are given in Table 5. These values were used to calculate parameters of physical interest for the orientation of the rocket with respect to the raypaths at the distances of closest approach, as given by Fig. 10. The parameters are: the angular displacement ϕ from Bermuda to the rocket, the altitude h_r of the rocket, the altitude h of the raypath point and its distance from the rocket d , and the angle away from zenith γ of the line connecting the rocket to the closest approach point on the raypath. The TEC

Table 5 — Raypath Parameters for Intersection with the Rocket Trajectory

	Intersection Pts.		Raypath Look Angles	
			from Bermuda	
	Lat. (°N)	Lon (°W)	Az (°)	El. (°)
<i>Sat.</i>				
ATS-3	28.038	70.512	231.19	26.921
ATS-5	26.583	65.493	187.43	47.574

diminution effect is expected to be relatively large for ATS-3, since the rocket came within 48 km of the ATS-3 raypath, and this is observed to be the case in Fig. 9. The ATS-5 effect is surprisingly large, however, considering that the rocket distance of closest approach to the raypath is 220 km. The preceding computations were carried out for a standard ellipsoidal earth model [Bate, Mueller, and White, 1971], but the results were found not to be significantly different for a spherical earth approximation.

It is noted with some interest that the TEC in Fig. 9, as observed along the Bermuda to ATS-5 path, continues to slowly decrease following the abrupt drop near the time of the HEAO-C launch. The TEC corresponding to ATS-3 drops more precipitously, as would be expected, but thereafter does not continue a monotonic decline. This indicates that the TEC along the ATS-3 path is virtually exhausted ($\leq 2 \times 10^{16}/\text{m}^2$) following the event, whereas the ATS-5 value ($\sim 10^{17}$ electrons/ m^2) is still subject to normal diurnal "influences." Note in fact that the TEC for the ATS-3 path begins to increase by 0230 local time (i.e., 0630 GMT) and continues this pattern until approximately 0530 where it reveals a slight pre-sunrise depression. Close inspection of both curves reveals an oscillation in the TEC with maxima near 0320 and 0500. There is no reason to associate this oscillation with the modification event. Since the oscillation is roughly in phase for both paths, then it is possibly the manifestation of a Travelling Ionospheric Disturbance (TID) propagating in the North-South plane. Indeed, Kersley et al. [1980] have observed TEC oscillating prior to sunrise to be a regular feature of the Caribbean zone.

A second peculiarity of the HEAO-HOLE event is the fact that the usual sunrise enhancement in TEC occurred somewhat earlier on the day of the event than on other control days. This peculiarity will be discussed later. Note also that the AGC trace for ATS-5 in Fig. 4 exhibits an increase in the "scintillation" amplitude following the event. (Recall that the ATS-3 record was inoperable.)

3.5 Theoretical Considerations

The sharp TEC reduction edges in Fig. 9 near 0536 are correlated with the passage of the rocket beneath the raypaths. During this time Faraday rotation angles were being measured at one-minute time intervals, and so it is possible to magnify the behavior of these reduction edges. It is thus opportune to test theoretical models for the reactive diffusion flow of rocket exhaust out to the raypaths during the initial hole-formation process. On a longer time scale the hole is coupled to the protonosphere and the rest of its surroundings in a hole-filling or motion process. For now, however, only the hole-formation problem will be addressed.

In Figs. 11 and 12 are TEC reduction edge values for ATS-5 and ATS-3, as inferred from Faraday rotation data measured at one-minute intervals. These values, given by the dots in these figures, are inferred from the Sept. 20 \bar{M} -factors (solid curves in Figs. 6 and 7) and the polarization baseline values already established. The solid-line curves in Figs. 11 and 12 are based on calculations which will be described later. Rocket lift-off (t) and closest approach (c.a.) times are indicated by vertical tick-marks in these figures.

In order to form a theoretical model for the TEC data (given by the dots in Figs. 11 and 12) for the hole-formation, it is necessary to know raypath geometries, the rocket trajectory, and parameters of the rocket exhaust diffusion and electron recombination chemistry. The raypath geometries have already been deduced from the satellite and receiver coordinates. The post-launch rocket trajectory was furnished to us [Ketterer, 1979] as a numerical computer tabulation. This information has been condensed by least-squares fitting of the data for latitude, longitude, and altitude of the rocket vs. time by

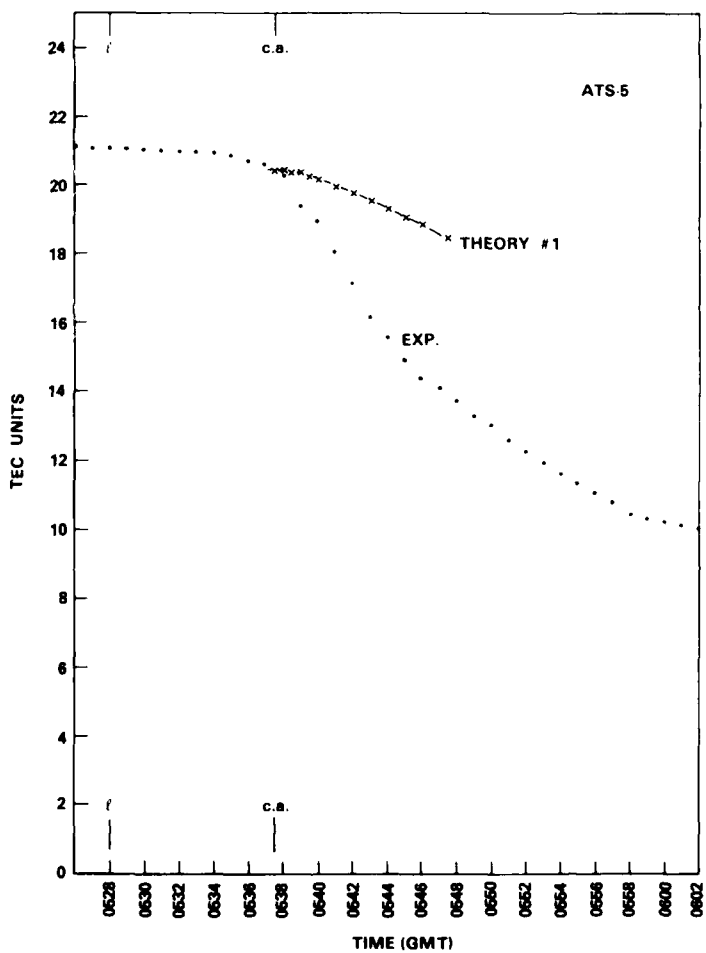


Fig. 11 - ATS-5 raypath TEC reduction edge following the HEAO-C launch. Experimental values are shown by dots, and diffusion theory results by the solid line. Tick marks show liftoff (l) and closest approach (c.a.) times for the booster rocket. See text.

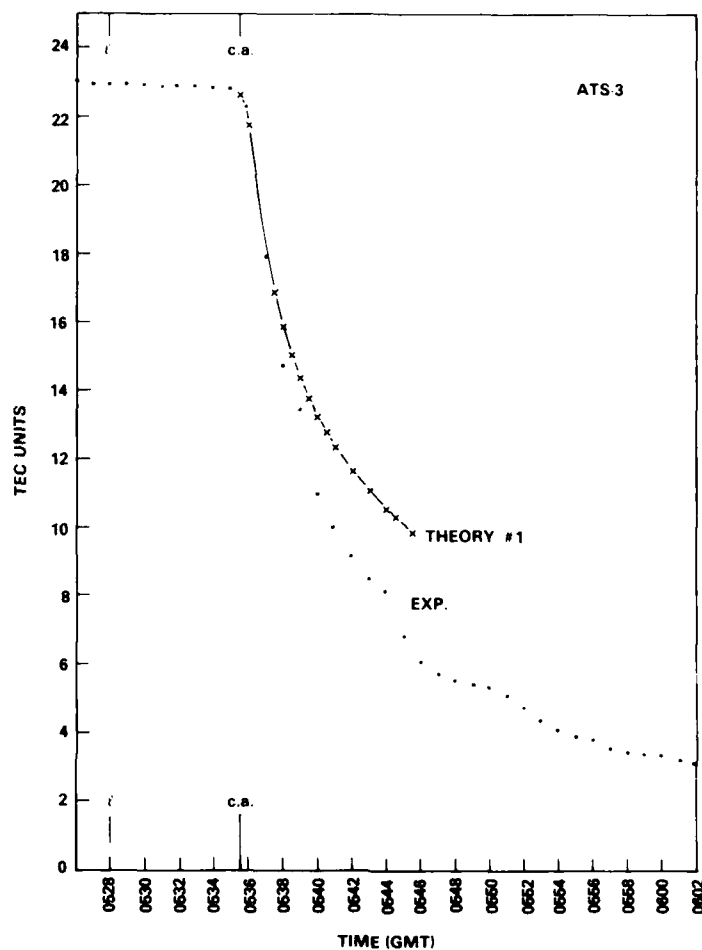


Fig. 12 — ATS-3 raypath TEC reduction edge, similar to Fig. 11

third order polynomials in time intervals which span roughly 100 seconds on either side of the times of closest approach of the rocket to the raypaths. Each function is thus represented as

$$f(t) = A_0 + A_1(t - t_0) + A_2(t - t_0)^2 + A_3(t - t_0)^3$$

$$(t_i \leq t \leq t_f) \quad (12)$$

in a particular time interval, where the expansion coefficients differ from one interval to the next. Each interval spans 40 seconds, and virtually no loss of accuracy is suffered in going from the original numerical tabulation of the rocket trajectory to its representation by Eq. (12). The least-squares coefficients are given in Table 6. This is also a convenient polynomial interpolation for computations. The times in Table 6 are seconds elapsed from rocket ignition, which occurred about 11 seconds prior

Table 6 — HEAO-C Rocket Trajectory

Times(s)	Coeff.	Lat (°N)	Lon (°W)	Alt. (km)
$t_i = 360$	A_0	.2844700+02	.7342239+02	.3235836+03
$t_0 = 380$	A_1	-.3177181-02	-.3402256-01	.9012024+00
$t_f = 400$	A_2	-.1957200-04	-.2565766-04	-.1095331-02
	A_3	-.4808718-07	.4793922-07	.3797260-06
$t_i = 400$	A_0	.2828544+02	.7201993+02	.3579588+03
$t_0 = 420$	A_1	-.5009446-02	-.3620018-01	.8207689+00
$t_f = 440$	A_2	-.2595862-04	-.2547159-04	-.9768056-03
	A_3	.5307621-07	.2283004-06	-.3425513-05
$t_i = 440$	A_0	.2804170+02	.7053048+02	.3891821+03
$t_0 = 460$	A_1	-.7217561-02	-.3834927-01	.7425942+00
$t_f = 480$	A_2	-.3154827-04	-.2894422-04	-.9153887-03
	A_3	-.2548177-06	-.1069609-06	-.1063423-05
$t_i = 480$	A_0	.2769605+02	.6895017+02	.4173544+03
$t_0 = 500$	A_1	-.1006428-01	-.4066669-01	.6653089+00
$t_f = 520$	A_2	-.3877873-04	-.2776726-04	-.9726081-03
	A_3	-.2305383-06	.1620504-06	.2942168-05
$t_i = 520$	A_0	.2722391+02	.6728029+02	.4424225+03
$t_0 = 540$	A_1	-.1360834-01	-.4283429-01	.5857062+00
$t_f = 560$	A_2	-.4833377-04	-.2692919-04	-.1022886-02
	A_3	-.1039103-06	-.7401390-07	-.2355698-05
$t_i = 560$	A_0	.2659643+02	.6552412+02	.4641209+03
$t_0 = 580$	A_1	-.1791637-01	-.4493112-01	.4965629+00
$t_f = 600$	A_2	-.5808527-04	-.2534641-04	-.1234636-02
	A_3	-.7949663-08	-.3452735-07	-.1411592-05
$t_i = 600$	A_0	.2578113+02	.6368800+02	.4818781+03
$t_0 = 620$	A_1	-.2304305-01	-.4685309-01	.3878363+00
$t_f = 640$	A_2	-.7249729-04	-.2335664-04	-.1520375-02
	A_3	-.1543421-06	.1590936-06	-.3994210-05
$t_i = 640$	A_0	.2461925+02	.6158653+02	.4956792+03
$t_0 = 664$	A_1	-.3002765-01	-.4863451-01	.2432487+00
$t_f = 686$	A_2	-.8727188-04	-.1757357-04	-.2076613-02
	A_3	-.4812080-07	.8732465-07	-.2904853-04

to lift-off at 0528 at Cape Kennedy. The closest approach times are at 460.495 sec for the ATS-3 ray-path and 580.692 sec for the ATS-5 raypath. Rocket burnout is about 712 sec after ignition.

For calculation of the TEC dropout effect, it is necessary to specify a transport model by which rocket exhaust molecules ultimately reach the raypath and subsequently remove electrons along it. A

simplified approach is to assume that rocket exhaust molecules are immediately thermalized through collisions with the ambient background gas, and subsequently diffuse out to the raypath. This is in the spirit of earlier calculations ([Mendillo et al., 1975], [Forbes and Mendillo, 1976] and [Mendillo and Forbes, 1978]). An appropriate expression for the gas concentration resulting from a point release is given for times not too large by [Bernhardt, 1979a]

$$\begin{aligned}
 n_i(x,y,z,t) &= \frac{N_0}{(4\pi D_0 t)^{3/2}} \exp \left[-z \left(\frac{3}{4H_a} + \frac{1}{2H_i} \right) - A(z,t) \right]; \\
 A(z,t) &= A_1(z)t + A_2(z)/(4D_0 t); \\
 A_1(z) &= \beta_i + \frac{D_0}{4} \left[\frac{1}{H_a} - \frac{1}{H_i} \right]^2 \exp [z/2H_a] \\
 A_2(z) &= 4H_a^2 (1 - \exp[-z/2H_a])^2 + (x^2 + y^2) \exp [-z/2H_a] \quad (13)
 \end{aligned}$$

Here, N_0 molecules are released at the origin at $t = 0$ in an atmosphere whose density varies exponentially in the z direction as $\exp [-z/H_a]$. The parameters D_0 and H_a are the diffusion coefficient and scale height, respectively, of the atmosphere at the point of release, and $H_i = kT/m_i g$ is the scale height of the injected gas. The parameter β_i is associated with chemical loss of the injected species through collisions with ambient molecules.

Equation (13) is applied to find the rocket exhaust concentrations at points along the raypath for times up to ten minutes past the time of closest approach of the rocket. This is done at each point along the raypath by replacing N_0 in Eq. (13) by $\dot{N}_0 \delta t$ and integrating along the rocket trajectory given in Table 6, i.e., such $N_0 \delta t$ puffs, where $\delta t = 2$ seconds, are summed along the rocket trajectory by Simpson's Rule. In this way the concentrations of water molecules $n_w(r,t)$ and hydrogen (H_2) molecules $n_H(r,t)$ are found along each of the raypaths for ATS-3 and ATS-5. The parameters used for \dot{N}_0 were $5.9 \times 10^{26} \text{ s}^{-1}$ for H_2 and $9.8 \times 10^{26} \text{ s}^{-1}$ for H_2O [Mendillo, Baumgardner, and Klobuchar, 1979]. The diffusion coefficients D_0 are inversely proportional to the neutral ambient background density $n_a(\mathbf{x})$, which consists principally of oxygen atoms, and thus depend on the altitude of release. They also depend on background thermospheric temperature. For this calculation the values $n_a D_0 = 1.43 \times 10^{20} \text{ cm}^{-1} \text{ s}^{-1}$ for H_2 and $2.32 \times 10^{19} \text{ cm}^{-1} \text{ s}^{-1}$ for H_2O , which are appropriate for an exospheric temperature $T_\infty = 1500 \text{ K}$, have been taken from Schunk [1978]. These values are consistent with

those used by Mendillo and co-workers. The model atmosphere used to evaluate D_0 , H_a , and H_i along the rocket trajectory was taken from Banks and Kockarts [1973] for $T_\infty = 1500^\circ\text{K}$. The values for β_i in Eq. (13) were computed at the raypath, as discussed below.

It remains now to specify the recombination chemistry. Hydrogen and water molecules at the ray-path remove electrons in basically a two-step chemical process. First, molecular ions are formed through charge exchange collisions with O^+ ions:



This is followed rapidly by dissociative electron recombination with these molecular ions:



Electron recombination with atomic ions is a much less efficient electron removal process. Loss of H_2 occurs through the reaction



with no comparably significant loss process for H_2O [Mendillo and Forbes, 1978]. The recombination chemistry is further discussed by Zinn, Sutherland, and co-workers [1980 a,b], from whom the rate constants in Eqs. (14) and (15) were obtained. They point out that the products of recombination with H_2O^+ in Eq. (15) can result in the removal of another electron, but this does not appear to be important in the present case. For one thing, the reaction channel which results in the H_2 product is only about 15% efficient. Furthermore, the other reaction channel which results in the formation of OH , as also in the decay process of Eq. (16), frequently leads to the formation of O_2 by reaction with O , and O_2 is relatively slow to transfer an electron to O^+ to form O_2^+ . Hence, on the time scale of interest here (~ 10 min), this process is unimportant. It appears, therefore, that the simplification of Eqs. (15) and (16) for the recombination chemistry will not result in any serious error.

The loss process of Eq. (16) is related to the loss parameter β_{H_2} in Eq. (13). The relation is

$$\beta_{H_2} = \gamma \bar{n}_o,$$

where \bar{n}_o is some average background oxygen atom concentration; β_i is treated as a constant in the derivation of Eq. (13). Actually, the oxygen concentration varies in the altitude interval between points on the rocket trajectory and raypath, but in the calculation of β_i , the oxygen concentration at the raypath point has been used. Regardless, this loss effect turns out to be unimportant in the calculation of TEC reduction for the raypaths considered here and for the time interval considered. This is consistent with the findings of Forbes and Medillo [FM 1976, MF 1978].

The calculation of TEC reduction proceeds, as mentioned above, by first using Eq. (13) to determine the space-time dependence of H_2 and H_2O concentrations along a raypath. This information is fed into the rate equations associated with Eqs. (14) and (15):

$$\begin{aligned} \frac{\partial [O^+]}{\partial t} &= - \left\{ k_H [H_2] + k_w [H_2O] \right\} [O^+] \\ \frac{\partial [e^-]}{\partial t} &= - \left\{ \alpha_H [OH^+] + \alpha_w [H_2O^+] \right\} [e^-] \\ \frac{\partial [OH^+]}{\partial t} &= k_H [H_2] [O^+] - \alpha_H [e^-] [OH^+] \\ \frac{\partial [H_2O^+]}{\partial t} &= k_w [H_2O] [O^+] - \alpha_w [e^-] [H_2O^+], \end{aligned} \quad (17)$$

where square brackets refer to the concentration of the molecule represented by the enclosed symbol. These coupled first-order differential equations are numerically integrated by the Runge-Kutta method to yield the concentration of O^+ , e^- , OH^+ , and H_2O^+ as a function of time at each of several points along the raypath. The procedure thus far invokes a decoupling of the diffusion and recombination chemistry effects which has been previously justified in a separate investigation (not related to HEAO-C) by Forbes and Mendillo [1976] for the sort of time period of interest here (up to ten minutes past the closet approach times). The calculation of TEC at any time then involves only an integration of electron concentration in the altitude coordinate along the raypath.

Another necessary ingredient of the calculation, beginning with the solution of the rate equations, is a model ionosphere which specifies the initial (and equal) O^+ and e^- concentrations along the raypath. Unfortunately, not much is known about the unperturbed ionosphere along the HEAO-C booster rocket trajectory, other than its TEC. Calculations were ultimately performed for different ionospheric models and rate constant values. The results for a specific set of parameters are shown as the solid-line curves in Figs. 11 and 12. The diffusion parameters values for these curves were mentioned above. The rate constants of Eqs. (14)-(16) have the values in Table 7, and the model ionosphere for these curves is taken to be a Chapman distribution which integrates to 22 TEC units. Hence, the electron concentration n_e is a function of altitude h according to

$$n_e(h) = N_m \exp \left\{ (1/2) [1 - y - \exp(-y)] \right\} \\ y \equiv (h - h_m) / H, \quad (18)$$

where the parameters for the scale height H and maximum concentration N_m at the altitude h_m are given the values

$$N_m = 8.873 \times 10^5 \text{ cm}^{-3}, \quad h_m = 370 \text{ km}, \quad \text{and} \quad H = 60 \text{ km}.$$

in the calculations for the solid curves in Figs. 11 and 12. It is seen that the calculations essentially agree with experiment for ATS-3, but disagree with experiment for ATS-5.

Table 7 — Rate Constants for the Recombination Chemistry

Constant*	Units	Value†
k_H	$10^{-9} \text{ cm}^3 \text{ s}^{-1}$	2.0
k_w		2.4
α_H	$10^{-7} \text{ cm}^3 \text{ s}^{-1}$	2.0
α_w		3.0
γ_H	$10^{-12} \text{ cm}^3 \text{ s}^{-1}$	2.0

*Nomenclature given by Eqs. (14) and (15) in text

†All from [Zinn and Sutherland, 1980], except γ_H taken from [Mendillo and Forbes, 1978]

Some progress in understanding the preceding discrepancy between calculations and experiment for ATS-5 can be made by varying parameters of the calculation to see what happens. This is done in Table 8, where the first column labels the parameters x , the second column gives the units of x , the

Table 8 — TEC Response to Parameter Changes

x Parameter	x Units	x_0 Unperturbed	Δx	Sat ATS-	Δ TEC (10)
$n_a D_H$	$10^{19} \text{cm}^{-1} \text{s}^{-1}$	14.3	-3.3	3	-.069
				5	-.039
$n_a D_w$	$10^{19} \text{cm}^{-1} \text{s}^{-1}$	2.32	-.52	3	.486
				5	.279
k_H	$10^{-9} \text{cm}^3 \text{s}^{-1}$	2.0	.4	3	-.184
				5	-.163
k_w	$10^{-9} \text{cm}^3 \text{s}^{-1}$	2.4	-.4	3	.309
				5	.168
α_H	$10^{-7} \text{cm}^3 \text{s}^{-1}$	2.0	.5	3	.054
				5	.003
α_w	$10^{-7} \text{cm}^3 \text{s}^{-1}$	3.0	-.5	3	.003
				5	.009
γ_H	$10^{-12} \text{cm}^3 \text{s}^{-1}$	2.0	-2.0	3	-.466
				5	-.192
W_N	km s^{-1}	0.	.1	3	-.900
				5	-.987
W_E	km s^{-1}	0.	.1	3	-.250
				5	-.401

third column gives the unperturbed value of x in these units, the fourth column gives the change Δx in these units, the fifth column labels the satellite for which the calculation was performed, and the sixth column gives the change in TEC after 10 minutes, i.e., Δ TEC (10) in TEC units due to the change Δx . Calculations were performed for the model ionosphere specified by Eq. (18) and the parameters cited there. Two new winds parameters W_N and W_E appear in Table 8. These are northerly and easterly neutral wind speeds at the rocket altitude. The wind calculations assumed that the diffusion patterns were carried at the wind speed. Evidently, a north ionospheric wind could enhance the TEC reduction rate by blowing the rocket exhaust molecules toward the raypaths, which pass over the rocket trajectory.

Some parameter changes have larger effects than others in Table 8, but these sorts of parameter changes, whose magnitudes correspond roughly to plausible uncertainties, do not seem capable of bringing the calculations into agreement with experiment for ATS-5. It is seen from Fig. 11 that a change $\Delta \text{TEC}(10) \approx -4.6$ units is needed for this purpose. In order to assess the effect of changing

the ionospheric model, calculations were repeated for three other ionospheres, all of the form of Eq. (18), but with different parameters. They are all chosen, however, to integrate to 22 TEC units. The results are given in Table 9 for the various model ionospheres in Fig. 13. The other parameters in the calculation were given the unperturbed values in Table 8. The values of Table 8 and Figs. 11 and 12 were calculated for the model #1 ionosphere in Table 9, which is shown as the solid curve in Fig. 13.

Table 9 — TEC Response to Model Ionosphere Changes

#	N_m (10^5 cm^{-3})	h_m (km)	H (km)	ATS-	22-TEC (10)	
1	8.873	370	60	3	12.74	
				5	2.01	
2	9.330	305	40 ($h < h_m$)	3	10.54	
			65 ($h > h_m$)	5	1.49	
3	9.330	370	40 ($h < h_m$)	3	13.41	
			65 ($h > h_m$)	5	2.29	
4	8.837	409	50 ($h < h_m$)	3	13.11	
			65 ($h > h_m$)	5	2.85	
Experiment:					<u>TEC(0) - TEC(10)</u>	
					3	16.05
					5	6.60

Table 9 indicates a substantial dependence of the ATS-5 results on model ionosphere, but nowhere near the amount required to explain the discrepancy between calculations and experiment for this case.

There have recently been calculations by other authors [Zinn, Sutherland, et al., 1980] which have aimed to simulate the Bermuda HEAO-C polarimetry results of the present report, a preliminary version of which were presented in November, 1979 [Proceedings, 1980 a,b]. Although the computation model used by these authors is apparently two-dimensional, as contrasted to the brute-force three-dimensional calculations discussed above, similar results for the hole-formation phase are obtained. They obtain substantial agreement with the ATS-3 results for the TEC reduction edge, but find it difficult to calculate a reduction edge for ATS-5 which is steep enough. Nevertheless, their simulation of the ATS-5 reduction edge seems to be closer to the experimental results than ours, apparently due in some measure to the replacement of diffusive (thermalized) rocket exhaust expansion by free ballistic

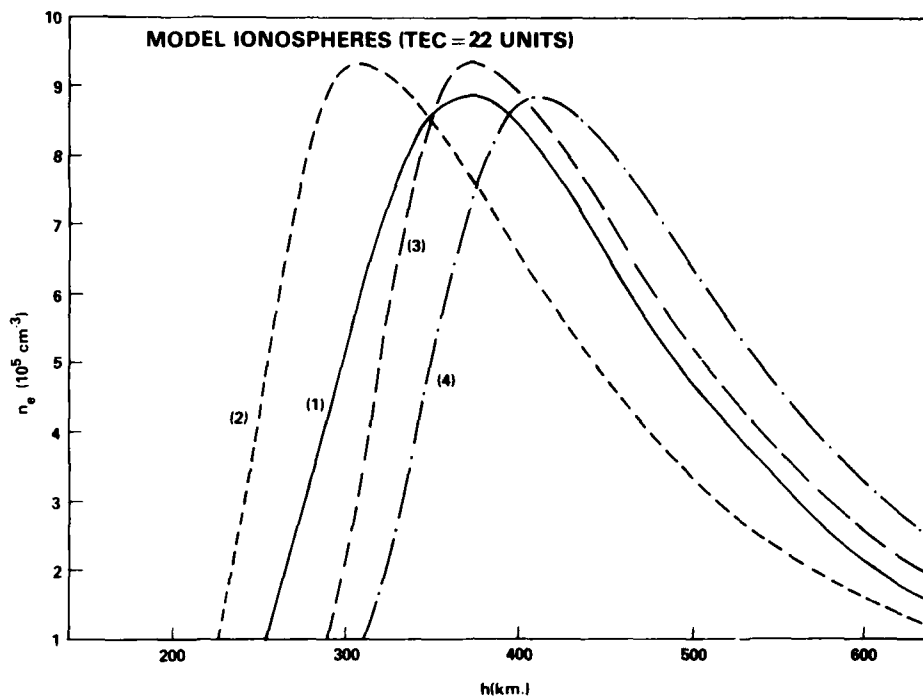


Fig. 13 — Model ionospheres used in diffusion calculations. The solid line curve is used for Fig's. 10 and 11

expansion for early times (relative to the point of release) in their model. Incidentally, their model ionosphere is quite similar to model #4 in Table 9. Indeed, the inclusion of free ballistic expansion at early times is expected to be especially appropriate for high altitude releases, such as that for ATS-5 (cf. Fig. 10). The transition from free rocket exhaust expansion to diffusive expansion has recently been treated theoretically by Bernhardt [1979 b]. It is intended to incorporate these effects into the present calculational model at a future time.

Other effects not considered in the calculations are the variation of results with model atmosphere (e.g., neutral density) changes and rocket trajectory changes. The accuracy of our assumptions about these is *unknown*. Certainly we have used the best information available about the rocket trajectory, and the neutral atmosphere data is apparently not available. Another curious feature in the ATS-5 data (cf. Fig. 11), not encompassed by the calculations, is that a TEC reduction effect starts about 3-4 minutes before the time of closest approach of the rocket to the raypath. The cause of this effect is not

understood, although it is very likely not related to the rocket. It is possible that a significant fraction of the discrepancy between calculations and experiment for ATS-5 is due to effects of this nature.

4.0 THE NOAA-B HOLE STUDY

4.1 Experimental Considerations

Figure 14 shows geometrical aspects of the Salton Sea polarimetry experiment. The receiver was located at the Salton Sea Instrument Laboratory, Salton Sea Naval Test Facility, California, in order to observe Faraday rotation perturbations introduced on the ATS-1 VHF transmission at 137.35 MHz. The diurnal figure-eight pattern of ATS-1 and the corresponding pattern of the ionospheric pierce point (IPP) at 420 km altitude on the raypath between satellite and receiver are also shown in Fig. 14.

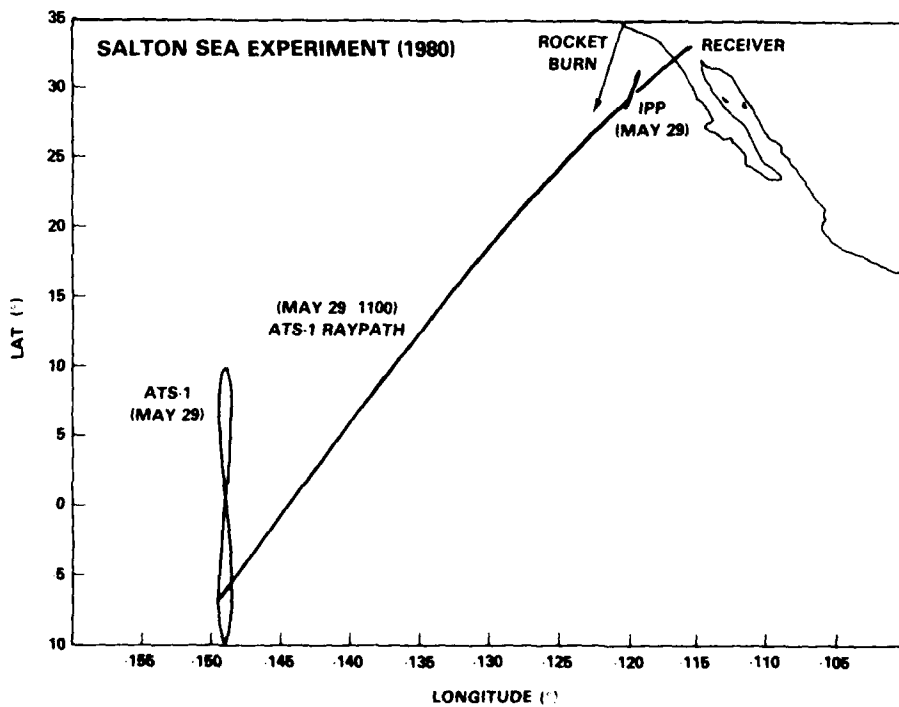


Fig 14 — Rectangular projection of the Salton Sea polarimetry experiment, similar to Fig. 3

The NOAA-B launch occurred at 10:52:59 UT on May 29, 1980 and followed a trajectory indicated in Fig. 14. The ATLAS-F booster rocket shut off its sustainer engine 378 seconds later (10:59:17 UT) at an altitude of 434 km. This burnout point, as indicated by the tip of the arrow in Fig. 14, was the closest approach of the rocket exhaust source to the raypath, which is shown in Fig. 14 for 1100 UT.

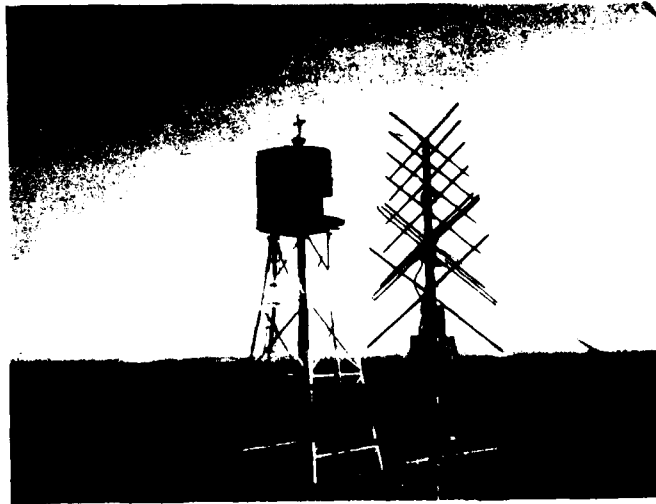


Fig. 15 — Salton Sea receiving antenna. Photo shows the water tower nearby

In the polarimetry experiment a crossed-yagi antenna was mounted on the roof and pointed at ATS-1. The antenna was fixed at an azimuth of 227.23° and an elevation of 38.50° during the course of the experiment. Look angles to the satellite from the receiver are actually computed to vary from 222.1° to 240.2° in azimuth (224.9° at 1100 UT) on May 29 and from 29.1° to 45.6° in elevation (31.6° at 1100 UT). Because of an antenna beamwidth greater than 30° at its 3 db points, however, motion of the satellite position relative to the fixed boresight was an unimportant influence on the data. Although a 40 foot metal water tower was located nearby, it caused no apparent signal distortion. A picture of the antenna and water tower is shown in Fig. 15.

The received signal was fed into a diode switch through cables phase-matched to $\pm 1^\circ$. The switch received its logic from an AFGL Polarimeter Adapter and simulated the antenna rotating at a 27 Hz

rate. The signal was then fed to a Vanguard RF converter and mixed down to 10.7 MHz. Then it was fed to a 10.7 MHz IF filter before being input to an AN/URR 390 HF Receiver, which uses a 1 KHz IF bandwidth. The receiver's detected IF output was fed to the polarimeter adapter's 27 Hz Twin-T filters. The resulting 27 Hz signal was then squared through a Schmidt-Trigger, differentiated, then integrated with the 0° and 180° 27 Hz references, and fed into the output amplifiers. The resulting 0° ϕ and 180° ϕ outputs were recorded on analog tape and strip chart recorders. The R390 AGC output was fed to the polarimeter adapter where it was amplified and offset, and then recorded on analog tape and strip chart recorders. A picture of the polarimetry equipment is shown in Fig. 16, and a block diagram of the system is shown in Fig. 17.

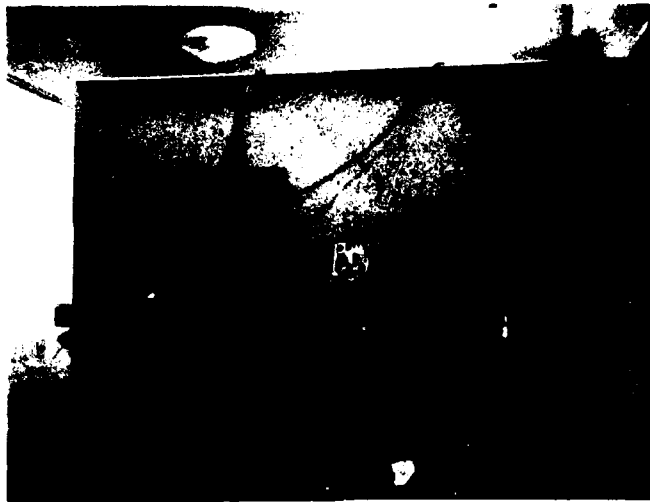


Fig. 16. Salton Sea polarimetry equipment.

4.2 Data Processing and Presentation

The Faraday rotation angle variations of the AIS-1 satellite beacon were measured for May 26-29. The results of these measurements are shown in App. C. No attempt has been made to remove the baseline ambiguity, i.e., only polarization angle changes are significant in the data of App. C. The last figure in App. C is a composite of the rotation angle data, which clearly shows the unusual, abrupt 110° reduction edge associated with the launch of NOAA-B.

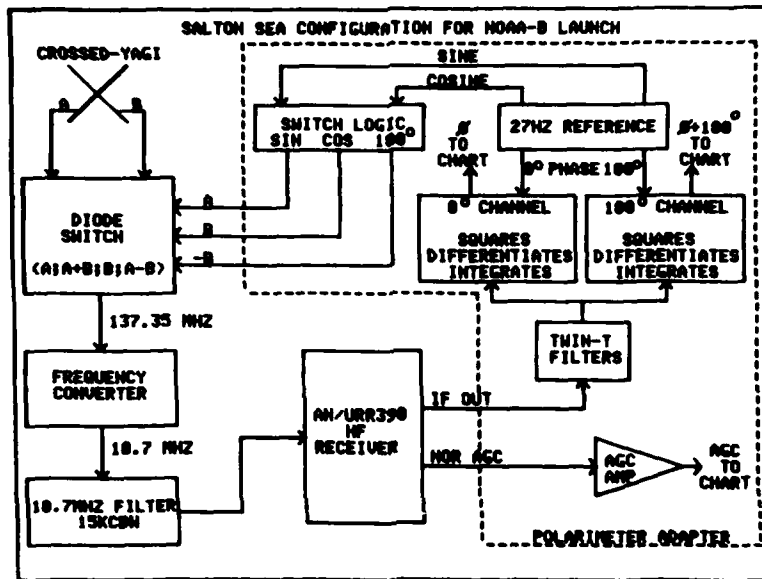


Fig. 17 — Block diagram of the apparatus for the Salton Sea polarimetry experiment

The conversion of Faraday rotation angle to TEC occurs by means of Eq. (9), which is for this case

$$\Delta T (10^{16} \text{ el}/m^2) = 1.7924 \times 10^{-2} \Delta \phi (^\circ) / \bar{M} \text{ (oersted)} \quad (19)$$

The \bar{M} -factors for a raypath altitude of 420 km. are calculated, in the manner specified in the HEAO-C discussion, to have the diurnal variation for May 29 shown in Fig. 18. The baseline ambiguity is removed, i.e., the constant C in the equation corresponding to Eq. (11) is determined, by fitting calculated TEC to values for Laposta, Ca. and Boulder, Col routinely published by AFGL. The result is shown in Fig. 19, where it is seen that the corrected Salton Sea TEC calculations fit the minima for both Laposta and Boulder quite well. More significantly, the TEC curves for Boulder and Salton Sea almost coincide. This is surprising in view of the fact that Laposta is significantly closer to the Salton Sea receiver site (cf. Fig. 14) than Boulder. The published lat.-lon. coordinates for the IPP points are (30°N, 116°W) for Laposta and (37°N, 106°W) for Boulder. In any event, the baseline ambiguity has been removed by this procedure to within an estimated uncertainty of ± 1 TEC unit. The resultant TEC curves for the Salton Sea receiver are shown for May 27-29 in Figs. 20-22 and in composite form in Fig. 23. As in App. C, local time values are used (Pacific Standard Time) which are seven hours

05/29/80 SALTON SEA, CALIFORNIA

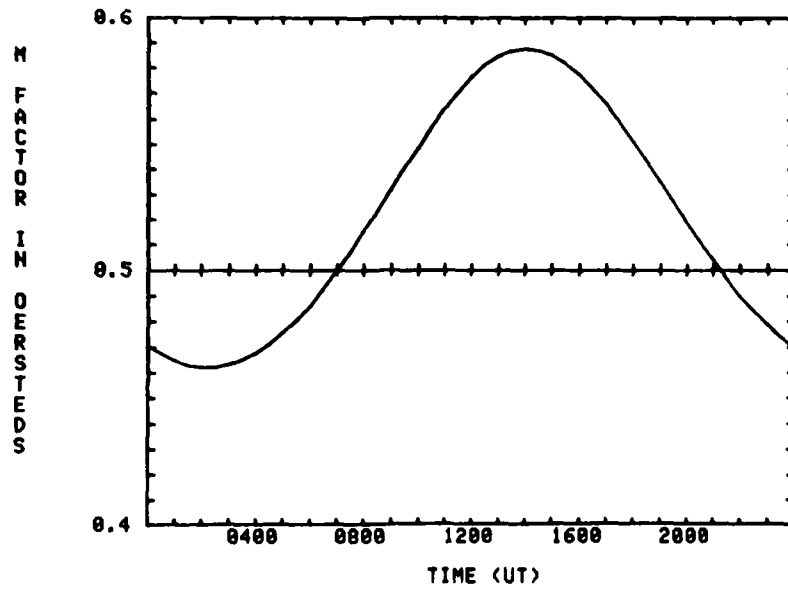


Fig. 18 - Calculated \bar{M} factors for ATS-1

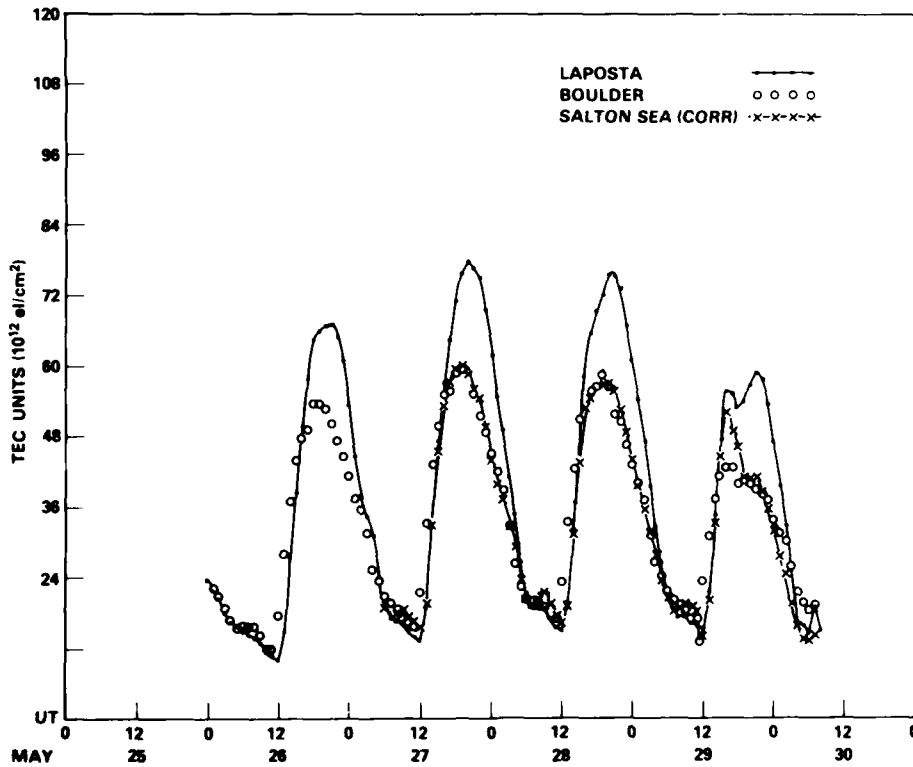


Fig. 19 - Comparison of Laposta and Boulder TEC with Salton Sea TEC, as calculated from the polarimetry data to obtain the best fit of Laposta and Boulder TEC minima. The fit with Boulder TEC is almost exact.

SALTON SEA, CALIFORNIA ATS-1 05/27/80

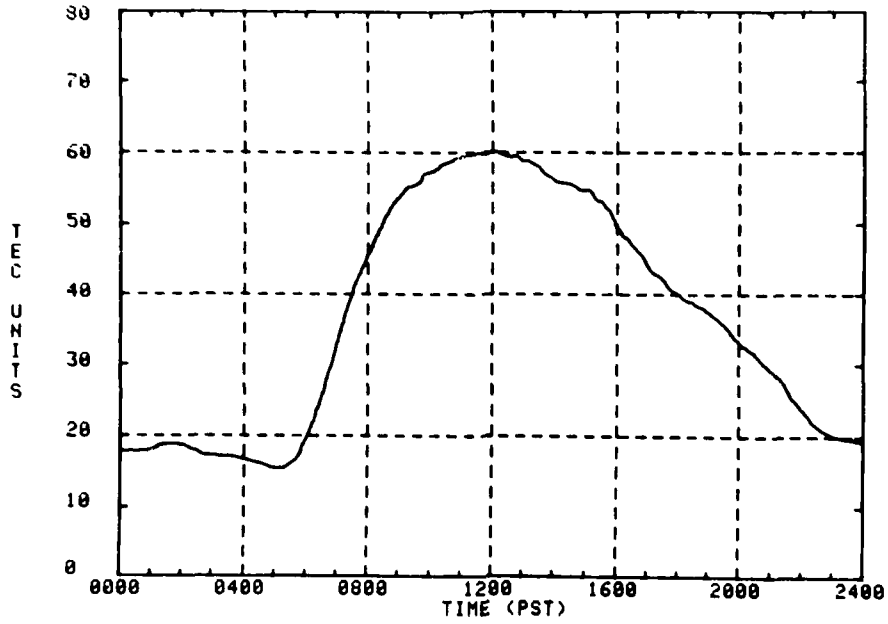


Fig. 20 - TEC determination for May 27

SALTON SEA, CALIFORNIA ATS-1 05/28/80

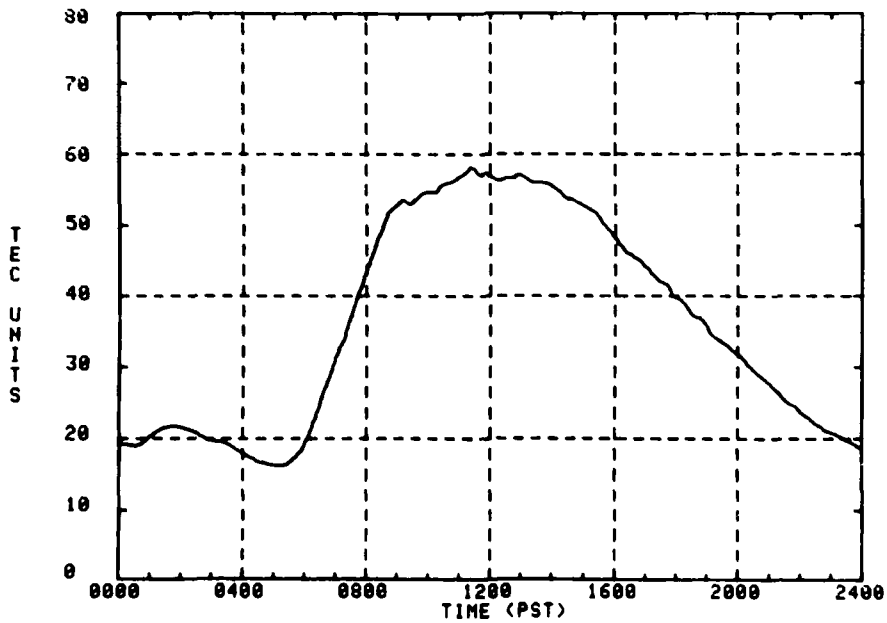


Fig. 21 - TEC determination for May 28

SALTON SEA, CALIFORNIA ATS-1 05-29/80

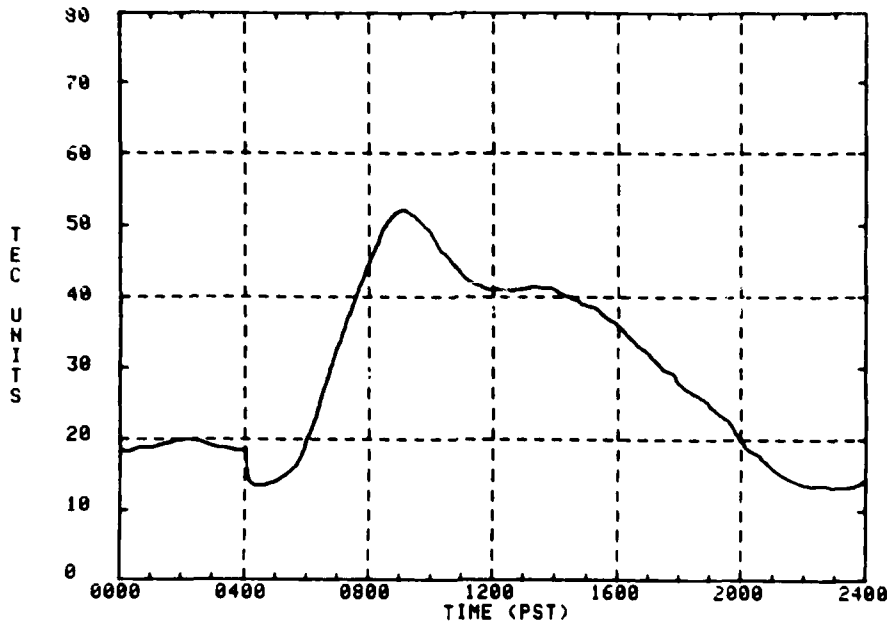


Fig. 22 - TEC determination for May 29

SALTON SEA, CALIFORNIA ATS-1 27,28,29 MAY 80

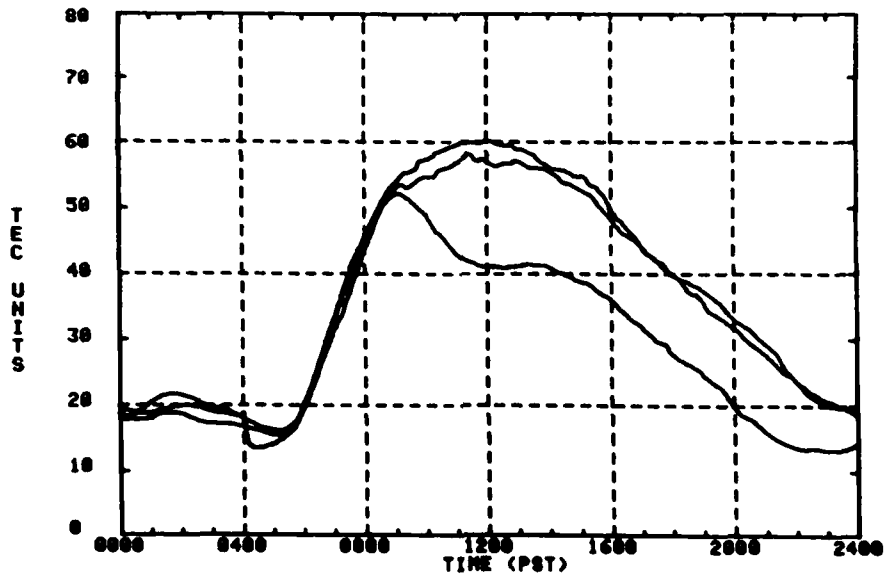


Fig. 23 - Composite TEC behavior for May 27-29

earlier than GMT or UT. The sharp TEC reduction edge near 0400 PST on May 29 characterizes the booster rocket perturbation.

4.3 The NOAA-B Booster Perturbation

With the use of the analog tape recording of the data the TEC reduction edge on May 29 can be further specified, and the time scale can be stretched out. The result is shown in Fig. 24, which also shows tick marks for the time of launch (l) and closest approach (c.a.) of the rocket exhaust source to the raypath. This is indicated by the tip of the arrow in Fig. 14; the booster rocket burned out before it reached a lat.-lon. intersection with the raypath. At the time of burnout, however, the rocket was not too far from the raypath. With respect to parameters defined in connection with Fig. 10, the height of the rocket at burnout was $h_r = 433.7$ km., the height of the closest raypath point was $h = 543.3$ km, the distance of closest approach was $d = 173.0$ km., and the angle away from zenith from the rocket to the closest raypath point was $\gamma = 52.1^\circ$. These numbers are based on the post-launch trajectory obtained from J. Baumgardner and the raypath geometry calculated from the receiver and satellite positions. The raypath geometry at 1100 UT is specified in Table 10.

As seen from Fig. 24, the TEC reduction due to the launch appears to be about 4.5 TEC units in 10 minutes following the closest approach time. We have not attempted to simulate this by calculations yet, but the amount of TEC reduction seems to be roughly consistent with the HEAO-C observations. A noteworthy feature in Fig. 24 is the rather sharp rise in TEC just preceding the TEC reduction edge. This was not observed in the HEAO-C case and is of unknown origin at this time.

5.0 DISCUSSION AND CONCLUSIONS

The polarimetry results, in conjunction with calculations which specify raypath orientations with respect to the booster rocket trajectory, have indicated rapid and dramatic TEC dropout response to chemical modification by rocket exhaust molecules. For releases in the F-region of the ionosphere, significant TEC reduction is seen to develop out to hundreds of kilometers from the rocket centerline

SALTON SEA, CALIFORNIA ATS-1 05/29/80

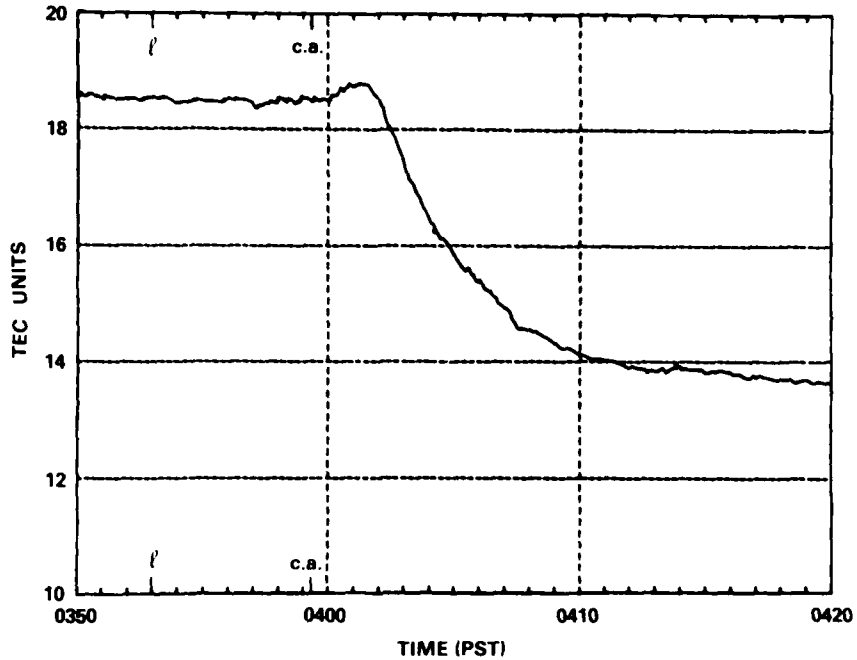


Fig. 24 — ATS-1 raypath TEC reduction edge following the NOAA-B launch, as inferred from the Salton Sea polarimetry data

Table 10 — Salton Sea
to ATS-1 Raypath Parameters
(1100 UT, May 29)

Description	Entity	Value
Receiver Coordinates	Lat.	33.2094°N
	Lon.	115.8707°W
	Alt.	0
Look Angles from Receiver	Az.	224.913°
	El.	31.5746°

on a time scale of ten minutes or so. These findings are consistent with observations by others [Proceedings, 1980 a,b].

The polarimetry experiments and other experiments of opportunity of this type not only are relatively efficient and inexpensive ways to assess the environmental impact of booster rockets, which is of

interest, for example, to the proposed Solar Power Satellite program [Proceedings, 1980 a,b], but also they provide empirical results against which calculational models for ionospheric modification can be tested. This report has tested a particular diffusion model for rocket exhaust expansion which conceivably could explain the polarimetry data on the short time scale (≤ 10 min) associated with the TEC reduction edge. On longer time scales, hole-filling and other modification effects are anticipated. The model tested does not include such effects as ionosphere-protonosphere coupling (taken into account by [Zinn, Sutherland, et al., 1980]). Hence, these longer time scales are outside of the capability of the calculational model tested here, in which rocket exhaust molecules are immediately thermalized by collisions with ambient species and execute motion describable by mutual diffusion theory thereafter. This simplified model is, nevertheless, carried out in a relatively thorough manner; it is a full, numerical, three-dimensional integration of the rocket exhaust effect along the trajectory of the rocket and along the raypaths under consideration. Any defect in the agreement between experiment and calculations therefore tends to be an accurate indicator of the shortcomings of the basic physical assumptions underlying the model. We say "tends to be," because the polarimetry experiments are not as controlled as laboratory experiments; certain parameters of the model are not completely known. Such things as wind speeds, atmospheric densities and temperatures, and rocket trajectory specification errors are not precisely defined. A repeated testing of the model against the empirical results of several experiments should, however, help to remove these uncertainties in the statistical sense. More supporting measurements in future experiments would also help.

The calculational model employed here has been found to be adequate for the ATS-3 raypath through the inner portion of the HEAO-C hole, but it has been found lacking for the ATS-5 raypath, which is further away from the hole axis. By studying the effects of parameter variations within the model, and by comparing with results obtained by Zinn, Sutherland, et al. [1980], we conclude that the ATS-5 results could be indicating deficiencies in the simplified diffusion model for rocket exhaust expansion. It is probably necessary to take account of the transition from free, ballistic expansion to thermalized diffusive expansion for many high altitude releases, as considered theoretically by

Bernhardt [1979b]. This is intended to be the next order of business in calculations for HEAO-C and NOAA-B TEC reduction edges.

There are other effects in the polarimetry results for HEAO-C and NOAA-B which are in need of explanation. We have already alluded to a TEC depletion effect which precedes the rocket passage in the ATS-5 case for the HEAO-C hole and to a TEC enhancement effect which precedes the TEC reduction edge in the case of the NOAA-B hole. Another curious feature of the polarimetry data was noticed for both the HEAO-C (cf. Appendix A and Appendix B) and NOAA-B (cf. Appendix C and Fig. 24) cases. There is a tendency for the TEC recovery from the dropout induced by the booster rocket to begin roughly 1/2 hr before the normal sunrise recovery. This premature sunrise effect may result from the details of the ionosphere-protonosphere coupling, or it may result from hole motion away from the raypath. This is a matter for future investigation.

6.0 ACKNOWLEDGMENTS

The authors would like to thank J. Klobuchar of AFGL for providing polarimetry equipment and some computational support. Helpful exchanges with M. Mendillo and J. Baumgardner are also appreciated. Thanks are due to C. Malik for his instruction on the use of the polarimeters. The authors are also grateful to R. Krausman for the use of his facilities at the Salton Sea site, to S. Stumpf, W. Way, and R. McCoy for their assistance during the HEAO-C experiment at NASA STDN, Bermuda, and to V. B. Richards for his assistance. Data processing and computational support from A. J. Martin, S. Byrd, C. Myers, and J. Eisele of NRL are gratefully acknowledged.

7.0 REFERENCES

1. Banks, P.M. and G. Kockarts, *Aeronomy, Part B*, Academic Press, New York, 1973.
2. Bate, R.R., D.D. Mueller, and J.E. White, *Fundamentals of Astrodynamics*, Dover, New York, 1971.

REILLY, HARNISH, AND GOODMAN

3. Baumgardner, J., Private Communication, Mar. 4, 1980.
4. Bernhardt, P.A., "Three-Dimensional, Time-Dependent Modeling of Neutral Gas Diffusion in a Nonuniform, Chemically Reactive Atmosphere," *J. Geophys. Res.*, 84, p. 793, 1979a.
5. Bernhardt, P.A., "High-Altitude Gas Releases: Transition from Collisionless Flow to Diffusive Flow in a Nonuniform Atmosphere," *J. Geophys. Res.*, 84, p. 4341, 1979b.
6. Budden, K.G., *Radio Waves in the Ionosphere*, Cambridge at the University Press, New York, 1966.
7. Cain, J.C. and R.E. Sweeney, "Magnetic Field Mapping of the Inner Magnetosphere," *J. Geophys. Res.*, 75, p. 4360, 1970.
8. Forbes, J.M. and M. Mendillo, "Diffusion Aspects of Ionospheric Modification by the Release of Highly Reactive Molecules into the F-Region," *J. Atm. and Terr. Physics*, 38, p. 1299, 1976.
9. Goodman, J.M., "The Utilization of Radio Beacons as Diagnostic Tools in the Study of Ionospheric Modification Events," (presented at COSPAR Conference) Warsaw, Poland, May, 1980.
10. Kersley, L., J. Aarons, and J.A. Klobuchar, "Nighttime Enhancements in Total Electron Content Near Arecibo and their association with VHF Scintillations," *J. Geophys. Res.*, 85, p. 4214, 1980.
11. Ketterer, Don, Code 572, NASA, Goddard Space Flight Center, Greenbelt, Md. 20771, 1979.
12. Klobuchar, J., Private Communication, 1979.
13. Mendillo, M., G.S. Hawkins, and J.A. Klobuchar, "A Large Scale Hole in the Ionosphere Caused by the Launch of Skylab," *Science*, 187, p. 343, 1975.
14. Mendillo, M., G.S. Hawkins, and J.A. Klobuchar, "A Sudden Vanishing of the Ionospheric F Region Due to the Launch of Skylab," *J. Geophys. Res.*, 80, p. 2217, 1975.

15. Mendillo, M. and J.M. Forbes, "Artificially Created Holes in the Ionosphere," *J. Geophys. Res.*, 83, p. 151, 1978.
16. Mendillo, M., J. Baumgardner, and J.A. Klobuchar, "Opportunity to Observe a Large Scale Hole in the Ionosphere," *EOS, Trans. Amer. Geophys. Union*, 60, p. 513, July 1979.
17. Mendillo, M., D. Rote, and P.A. Bernhardt, "Preliminary Report on the HEAO Hole in the Ionosphere," *EOS, Trans. Amer. Geophys. Union*, 61, p. 529, July 1980.
18. Proceedings of the Workshop/Symposium on the Preliminary Evaluation of the Ionospheric Disturbances Associated with the HEAO-C Launch, with Applications to the SPS Environmental Assessment, M. Mendillo and B. Baumgardner, Ed's, D.O.E. Report Conf-7911108, 1980a.
19. Proceedings of the Workshop/Symposium. Preliminary Evaluation of the Ionospheric Disturbances Associated with the HEAO-C Launch, with Applications to the SPS Environmental Assessment, M. Mendillo, Ed., Report for D.O.E. contract #31-109-38-5326, 1980b.
20. Reilly, M.H., "Interpretation of Bermuda Polarimetry Data for the HEAO-C Ionospheric Hole." U.R.S.I. North American Radio Science Meeting, Session G.I., Quebec, June 3, 1980.
21. Ross, W.J., "Second-Order Effects in High-Frequency Transionospheric Propagation," *J. Geophys. Res.*, 70, p. 597, 1965.
22. Schunk, R.W., "On the Dispersal of Artificially-Injected Gases in the Night-Time Atmosphere," *Planet. Space Sci.*, 26, p. 605, 1978.
23. Titheridge, J.E., "Determination of Ionospheric Electron Content from the Faraday Rotation of Geostationary Satellite Signals," *Planet. Space Sci.*, 20, p. 353, 1972.
24. Zinn, J. and C.D. Sutherland, "Effects of Rocket Exhaust Products in the Thermosphere and Ionosphere," Los Alamos Scientific Laboratory Report LA-8233-MS, Feb. 1980.

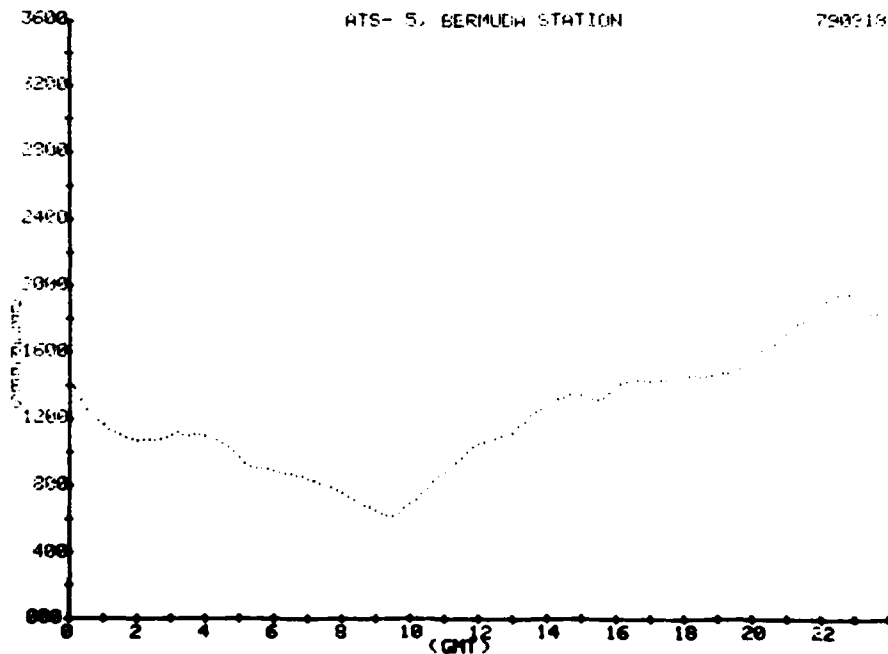
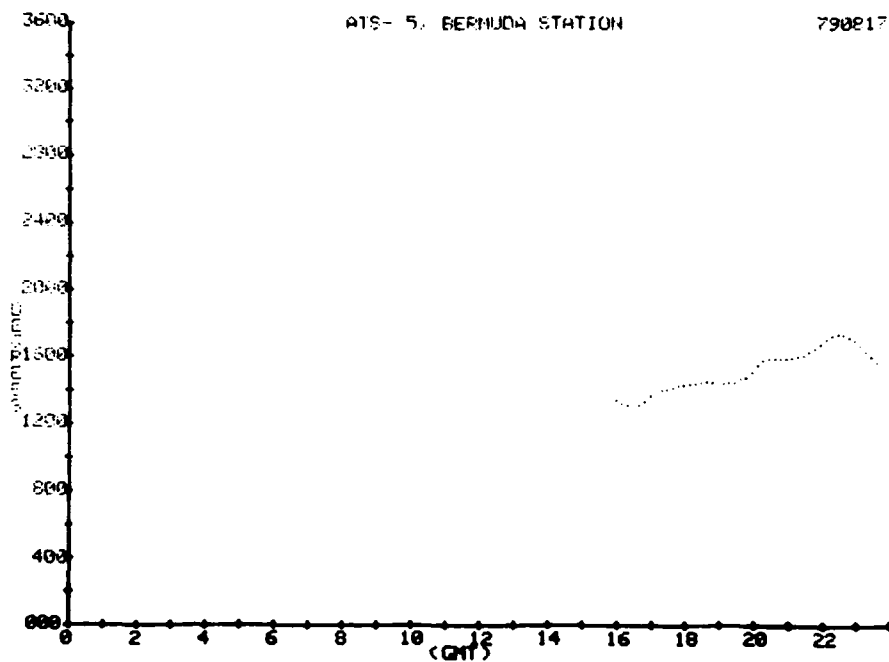
REILLY, HARNISH, AND GOODMAN

25. Zinn, J., C.D. Sutherland, S.N. Stone, L.M. Duncan, and R. Behnke, "Ionospheric Effects of Rocket Exhaust Products—HEAO-C, SKYLAB, and HLLV," Los Alamos Scientific Laboratory Report LA-UR 80-1160-REV, 1980.

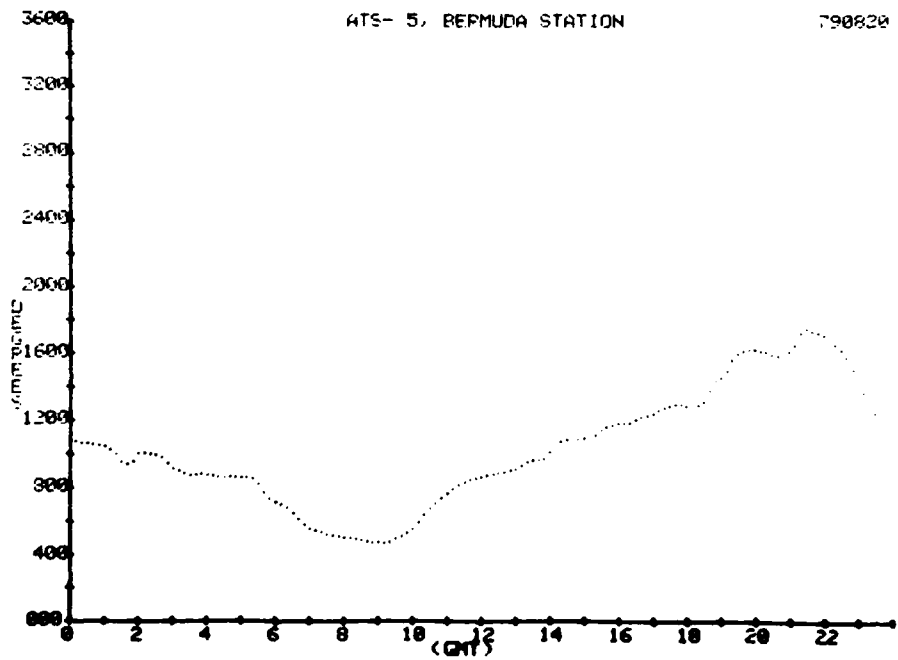
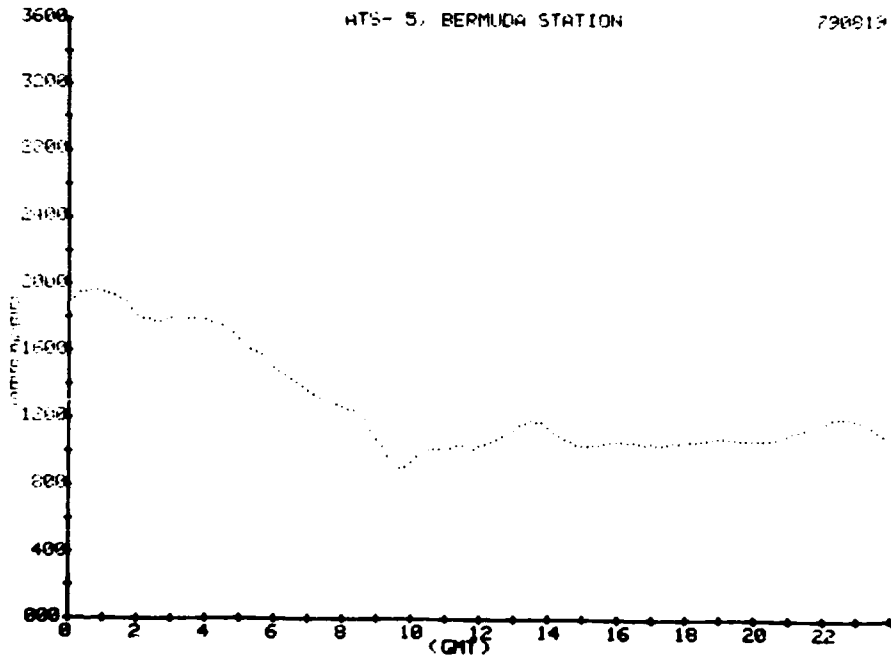
Appendix A

This appendix contains the Faraday rotation data for ATS-5 obtained at Bermuda between Aug. 15 and Sept. 23, 1979. The vertical axis is the Faraday rotation angle ϕ in degrees scaled at ten minute intervals. TEC can be calculated from Eq. (10), but the data given for ϕ must be regarded as uncertain within $\pm 40^\circ$, which uncertainty is inherited from the procedure for removing the baseline ambiguity (cf. Sec. 3.3).

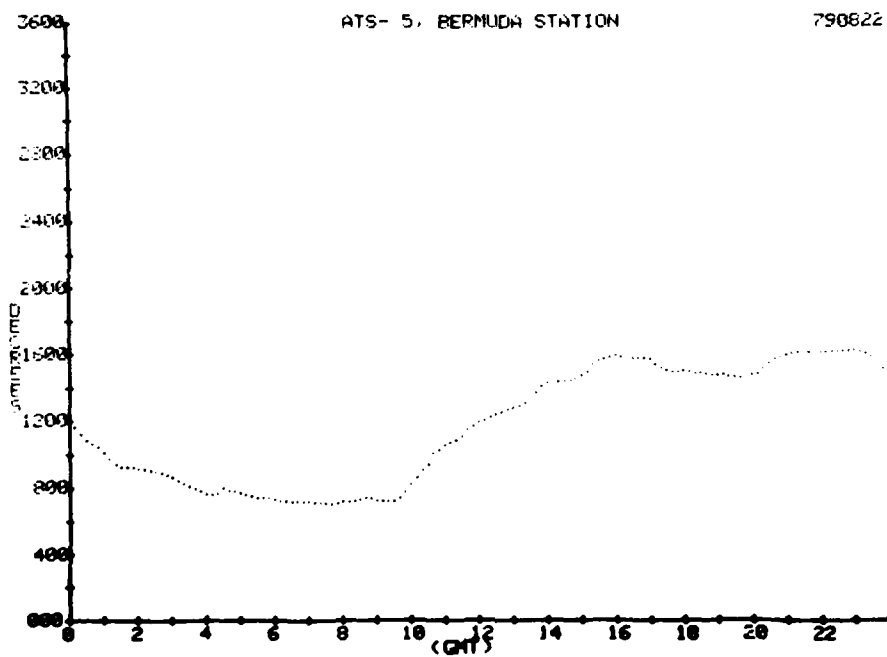
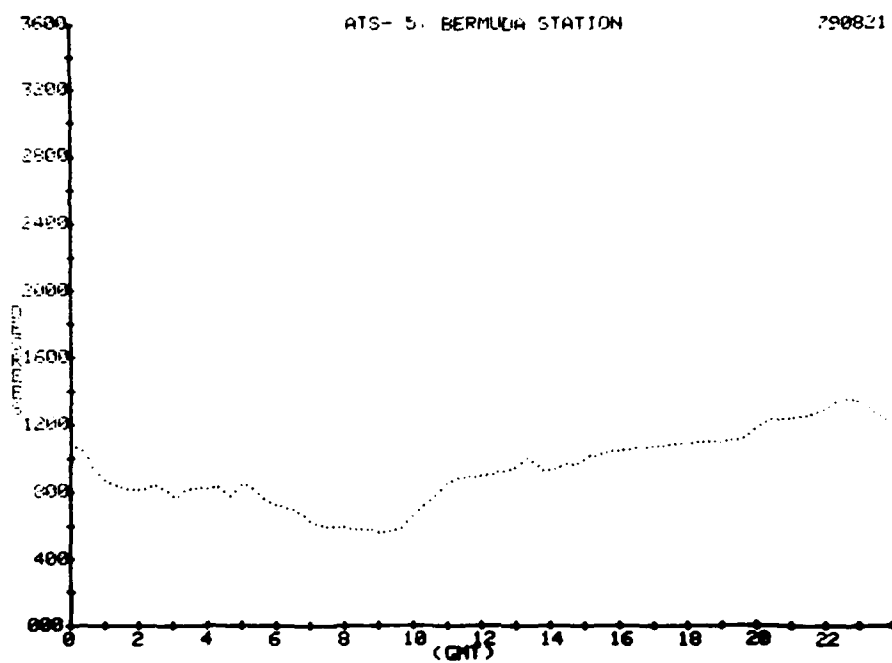
REILLY, HARNISH, AND GOODMAN



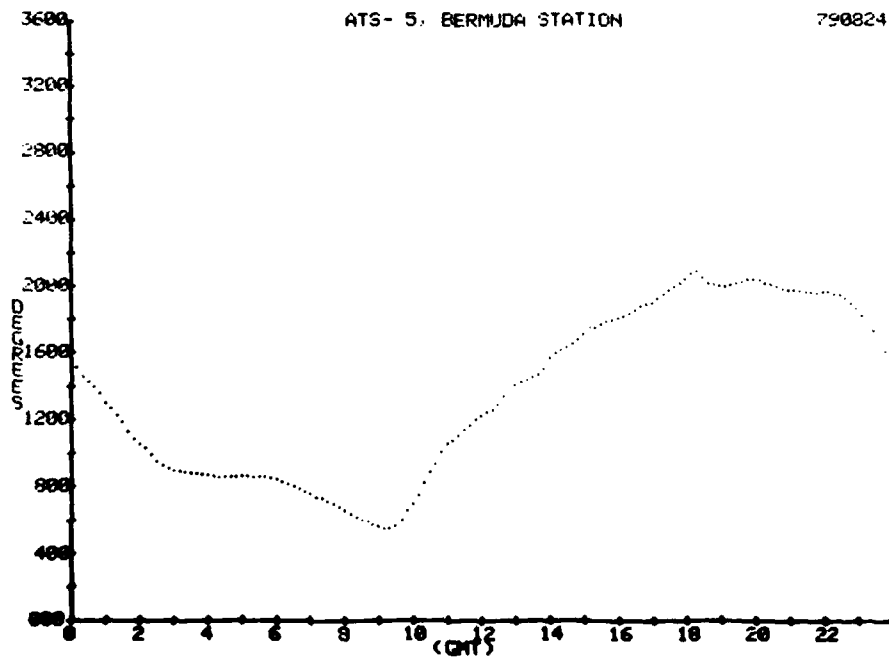
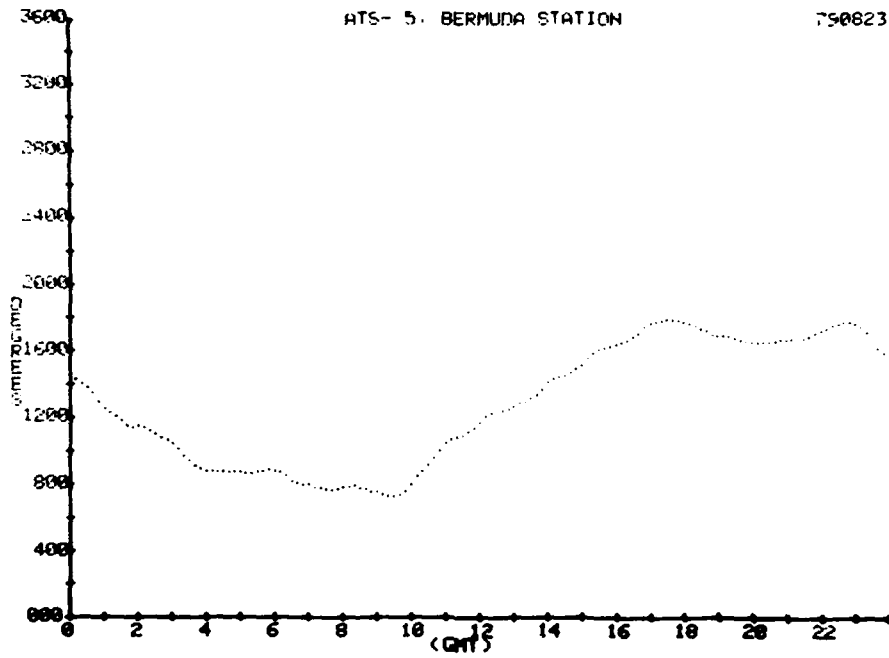
NRL MEMORANDUM REPORT 4517



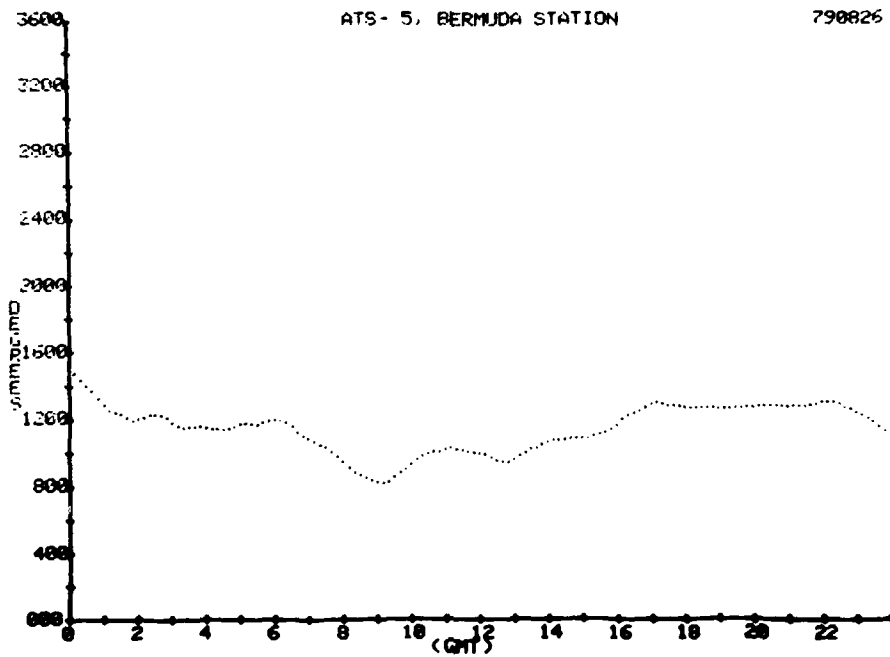
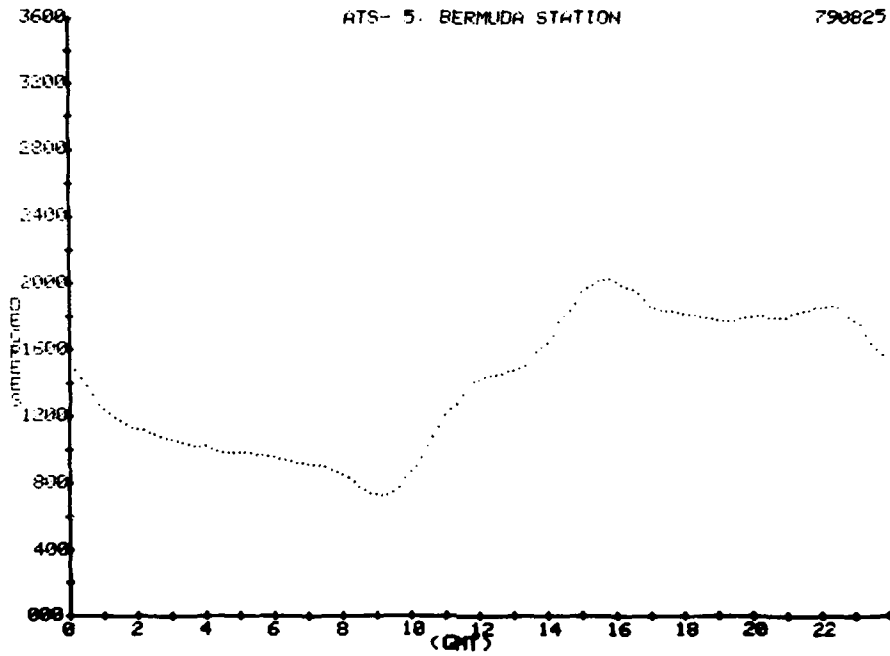
REILLY, HARNISH, AND GOODMAN



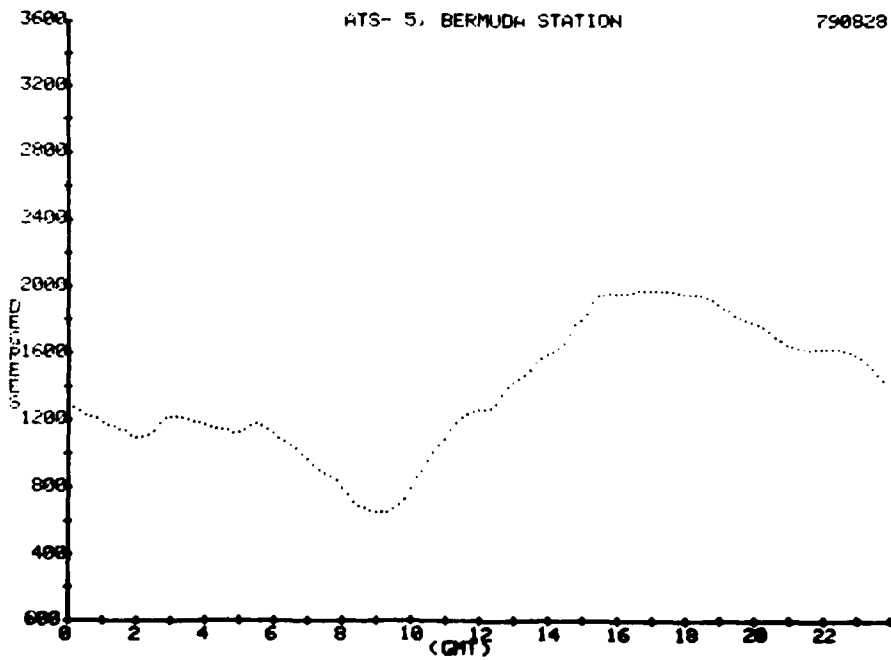
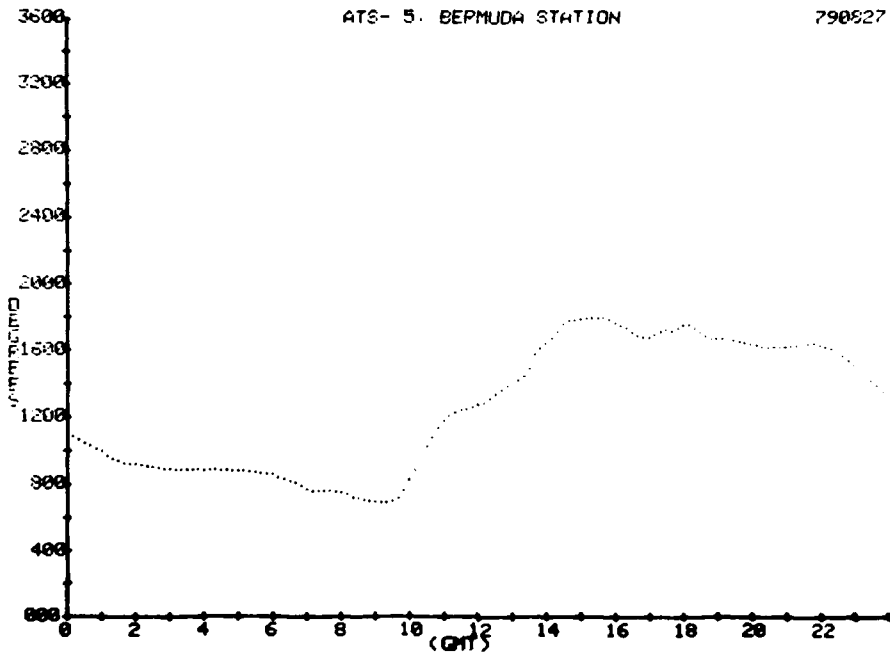
NRL MEMORANDUM REPORT 4517



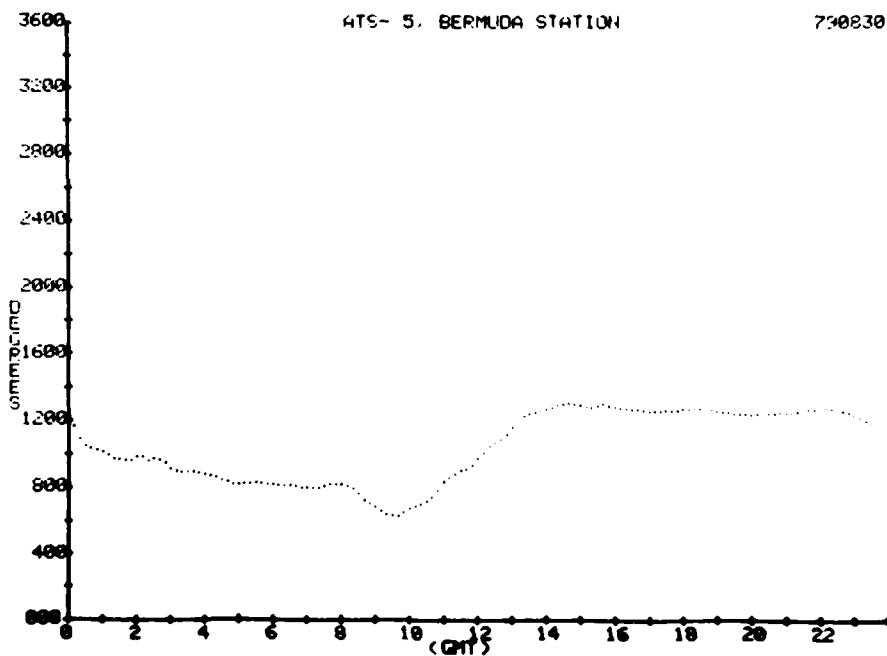
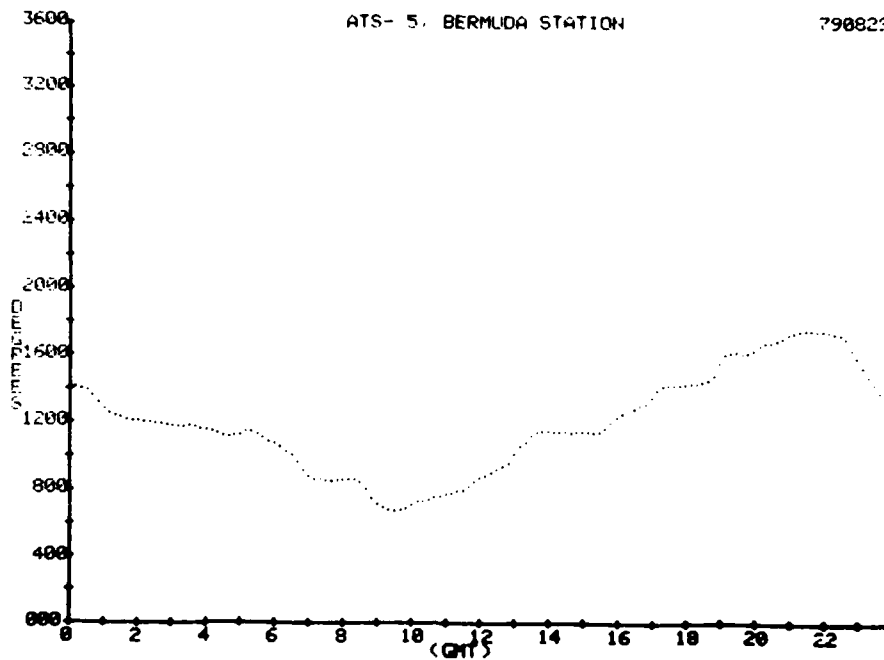
REILLY, HARNISH, AND GOODMAN



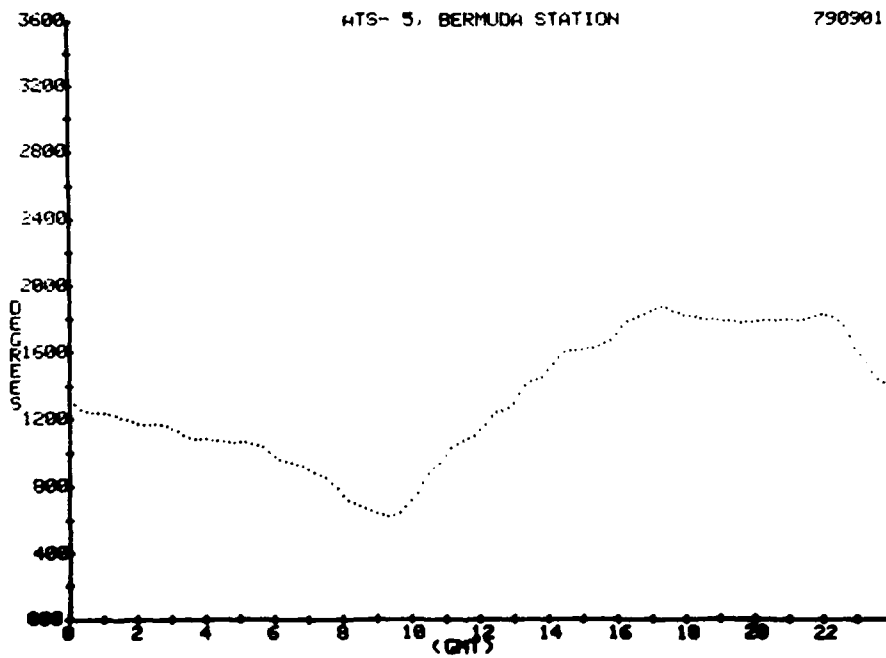
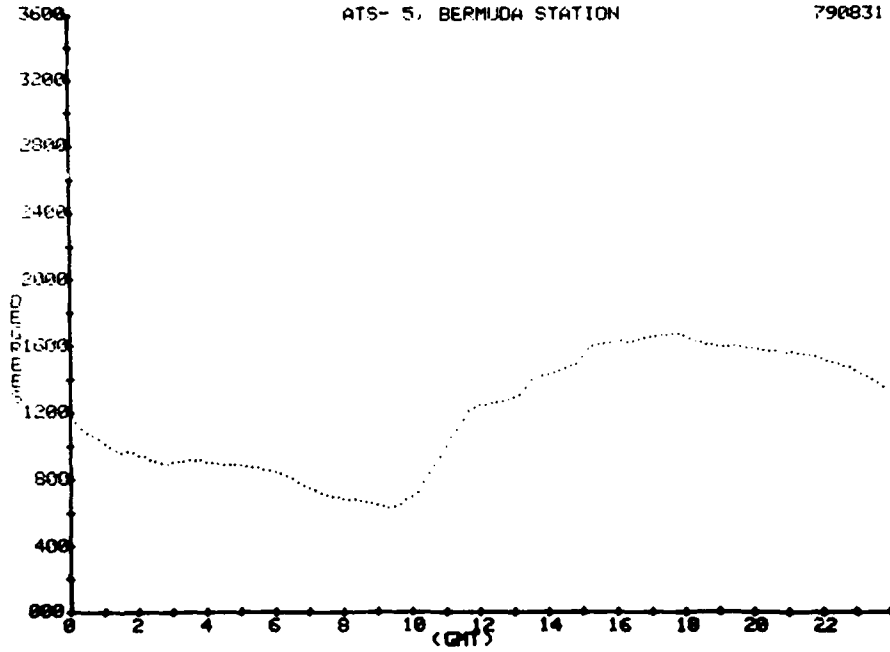
NRL MEMORANDUM REPORT 4517



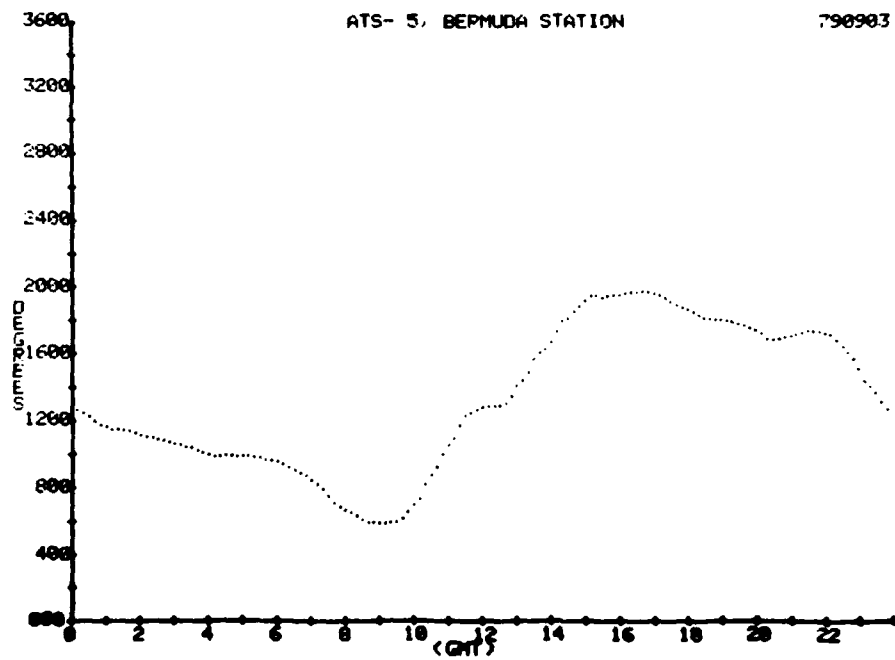
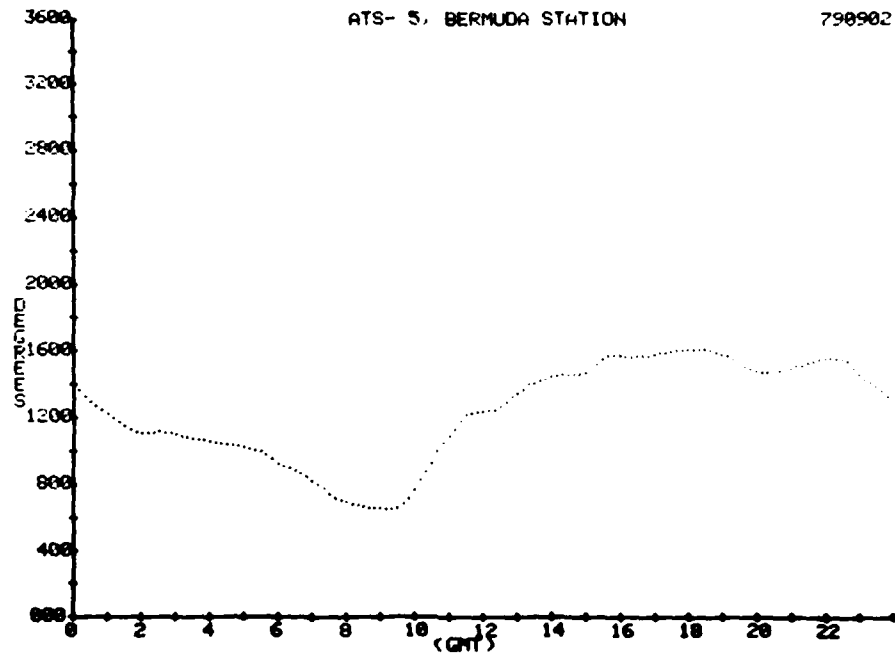
REILLY, HARNISH, AND GOODMAN



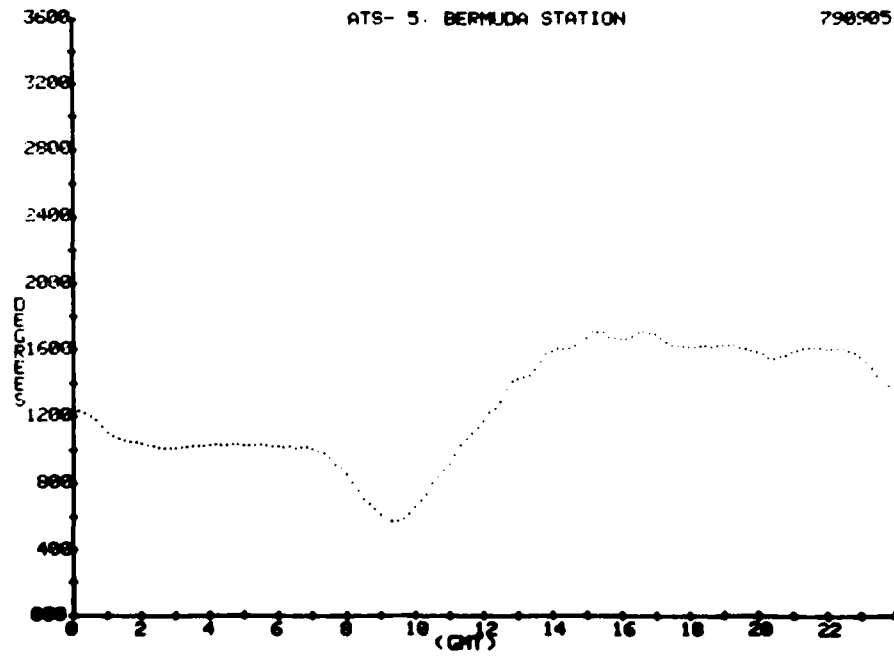
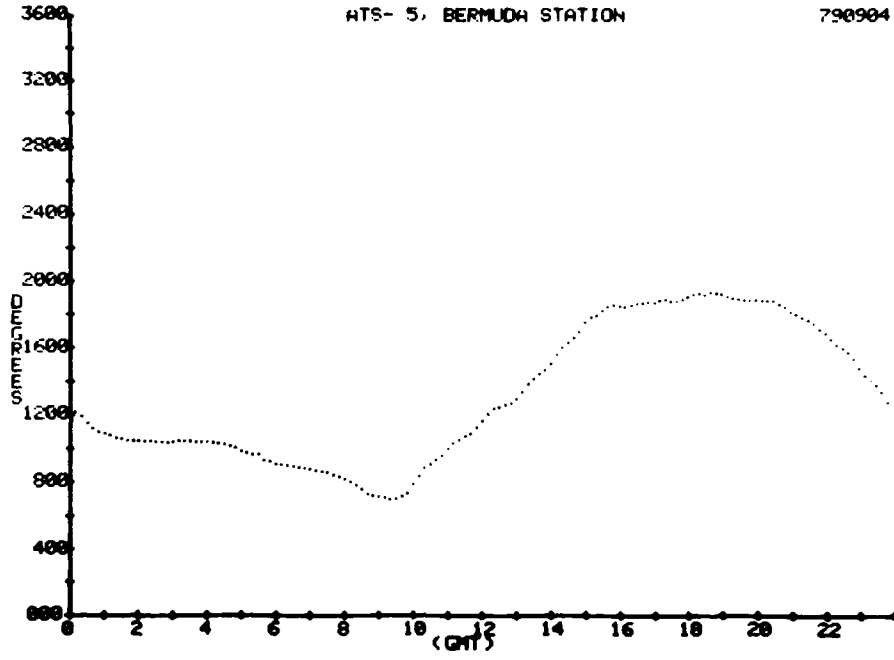
NRL MEMORANDUM REPORT 4517



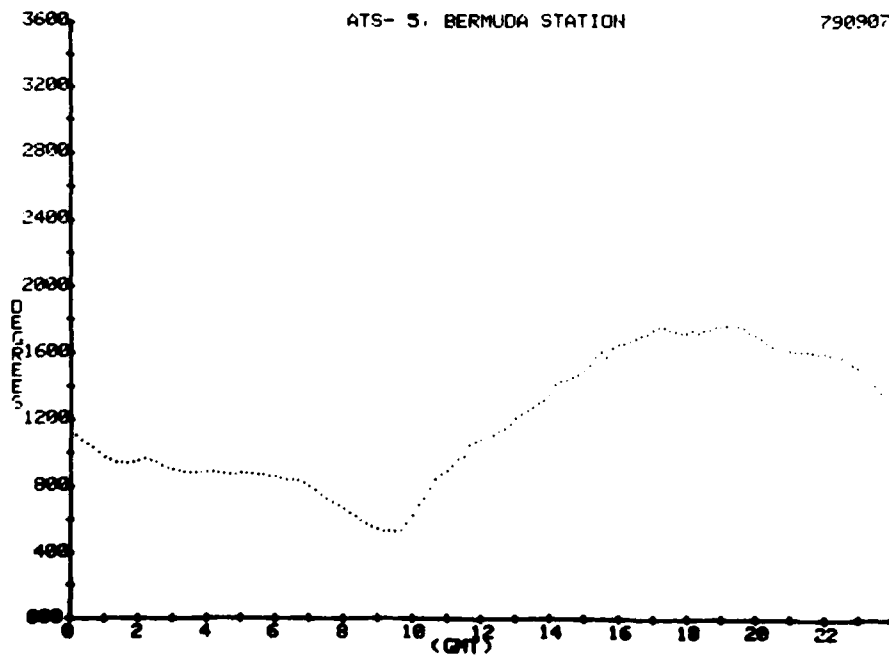
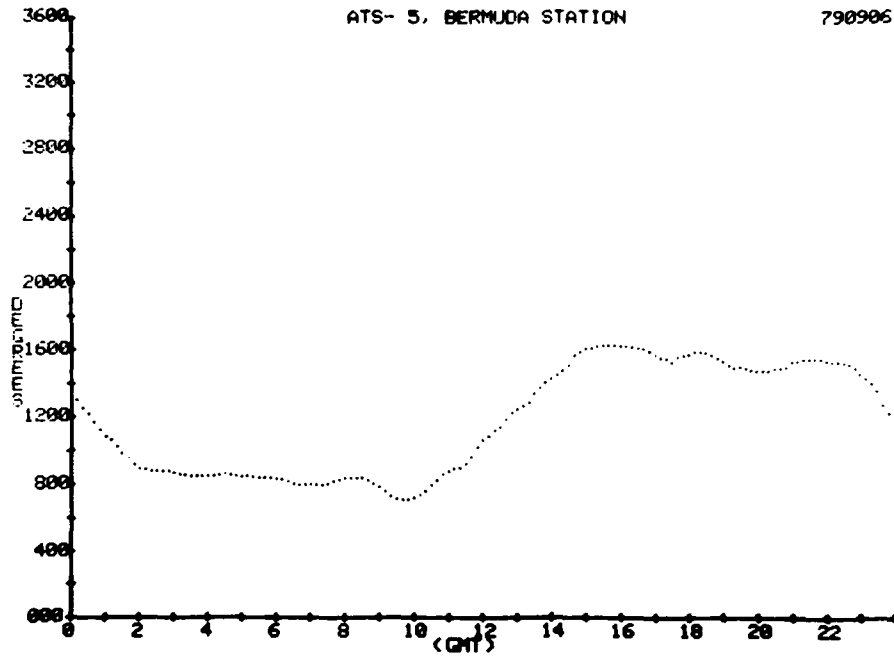
REILLY, HARNISH, AND GOODMAN



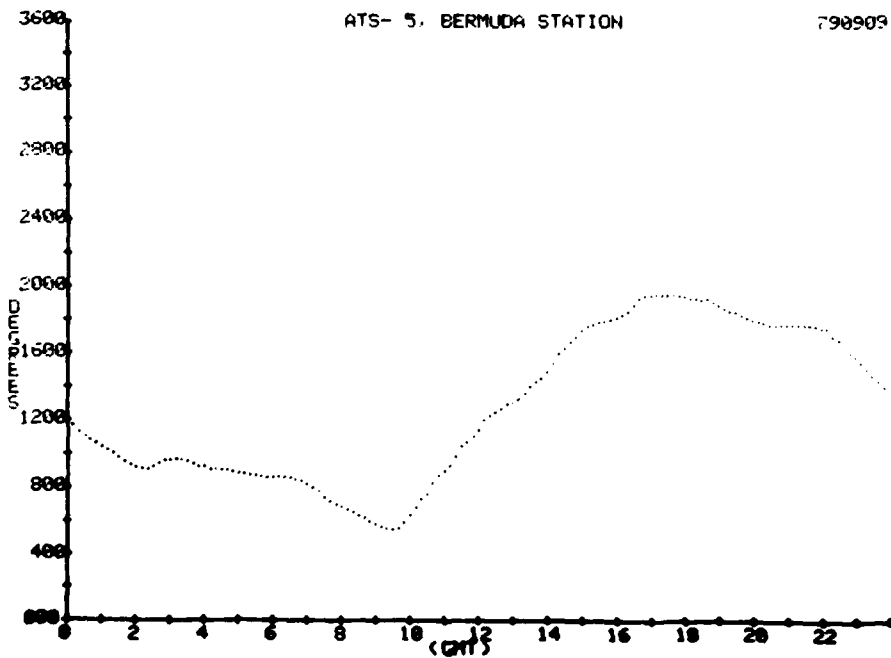
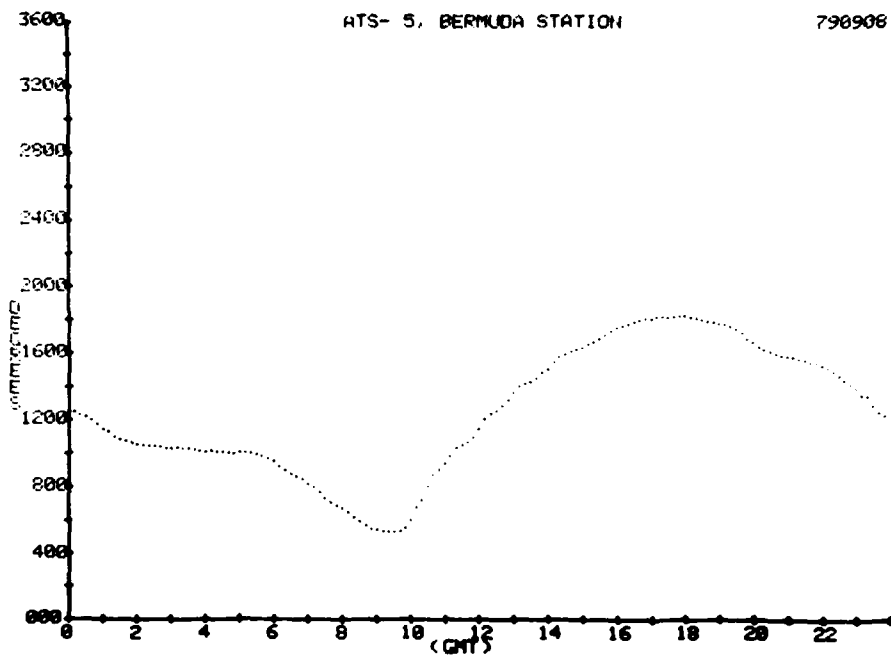
NRL MEMORANDUM REPORT 4517



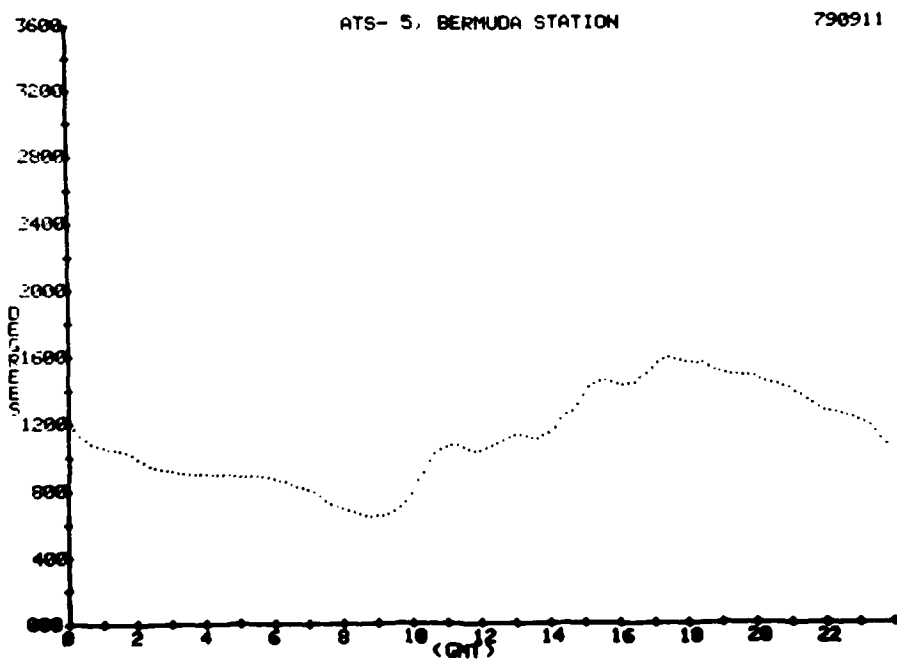
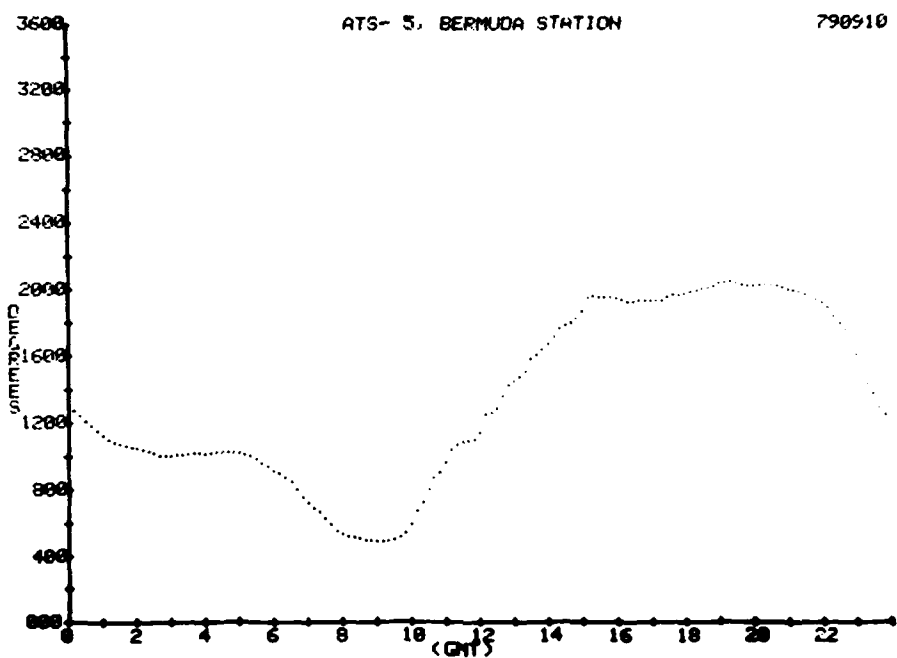
REILLY, HARNISH, AND GOODMAN



NRL MEMORANDUM REPORT 4517



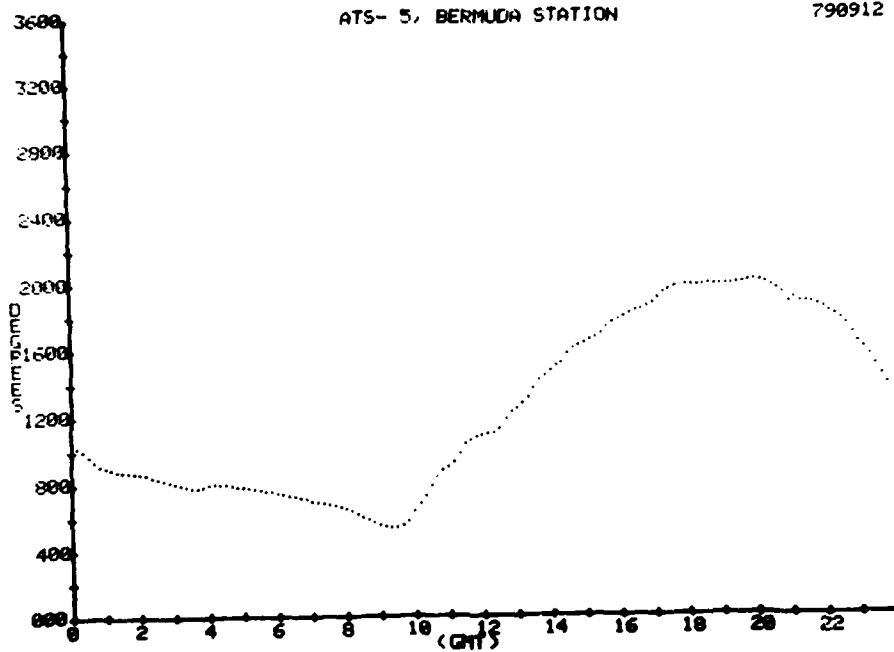
REILLY, HARNISH, AND GOODMAN



NRL MEMORANDUM REPORT 4517

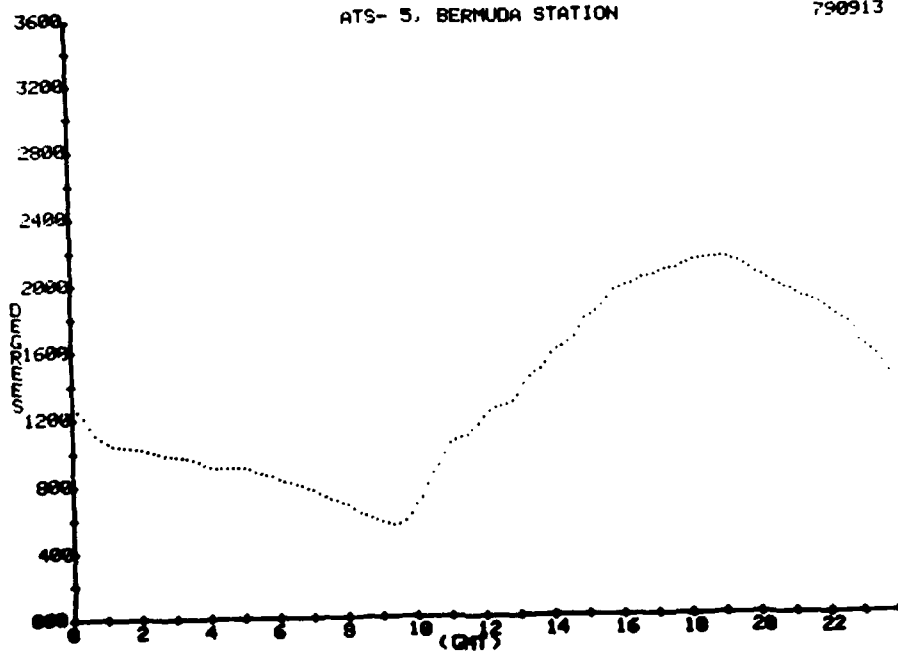
ATS- 5, BERMUDA STATION

790912

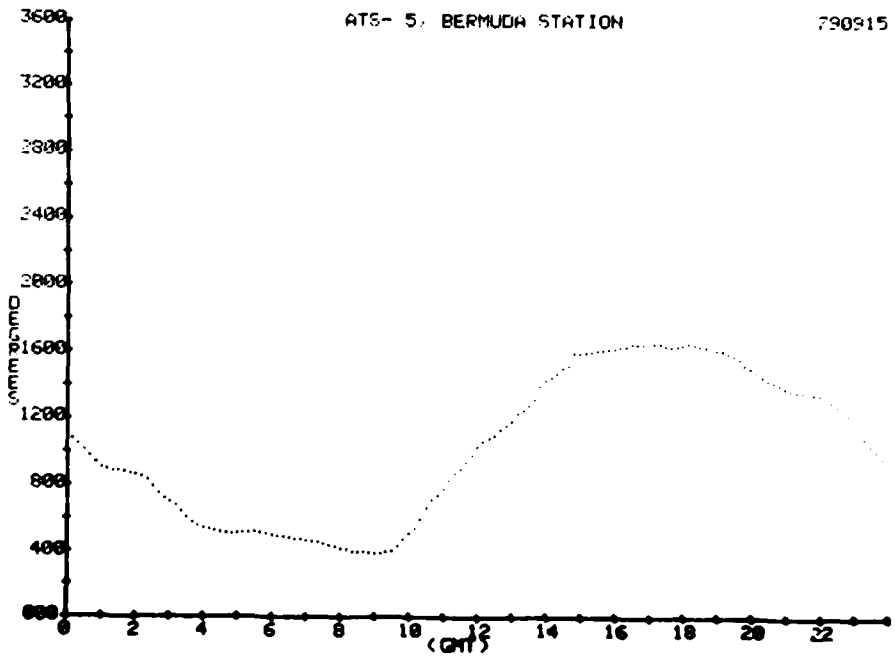
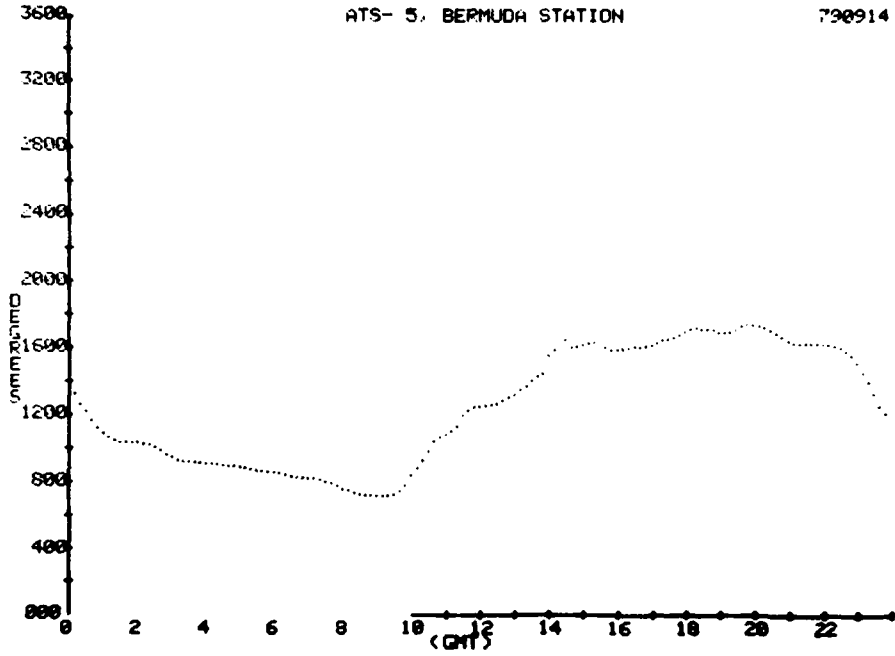


ATS- 5, BERMUDA STATION

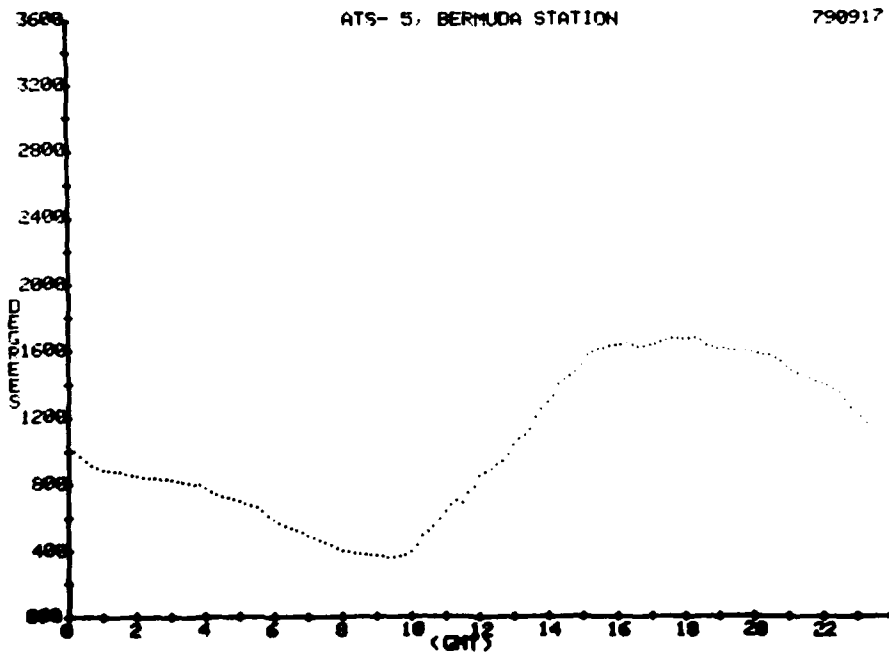
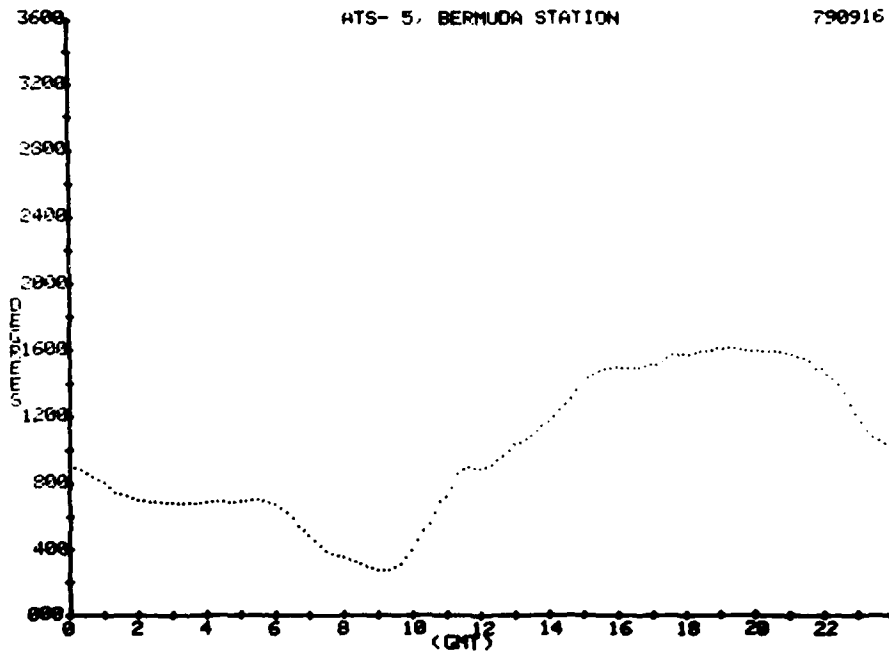
790913



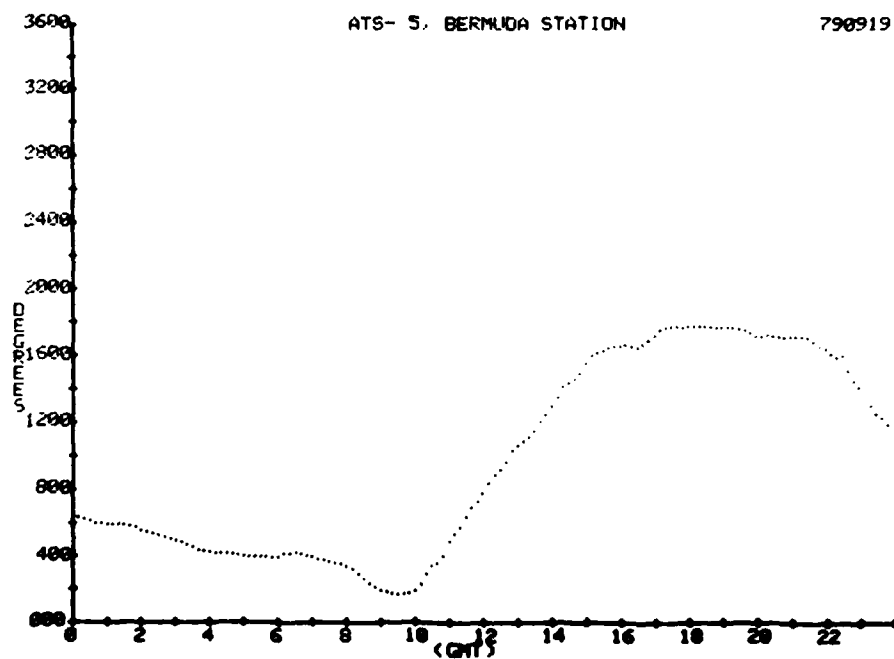
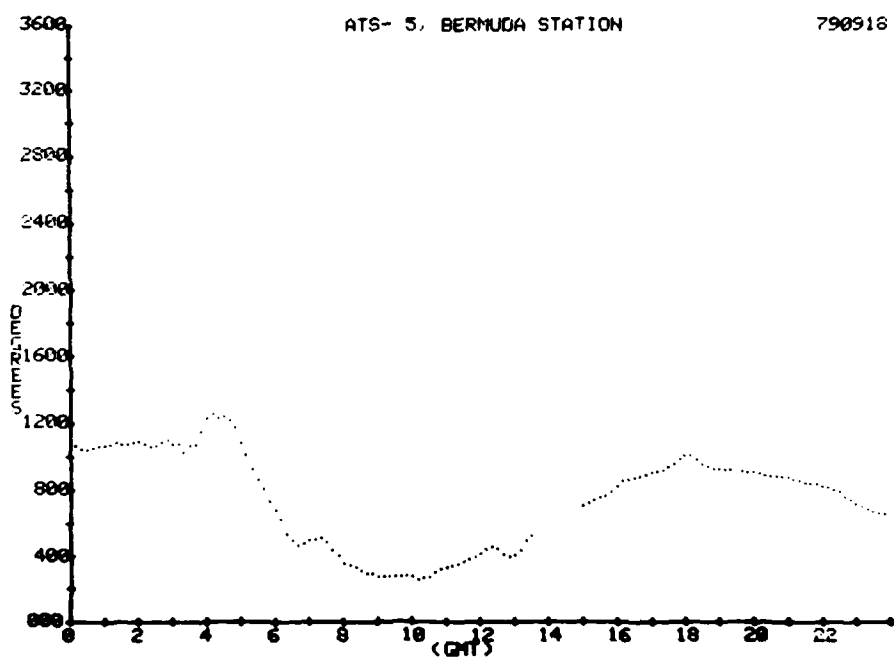
REILLY, HARNISH, AND GOODMAN



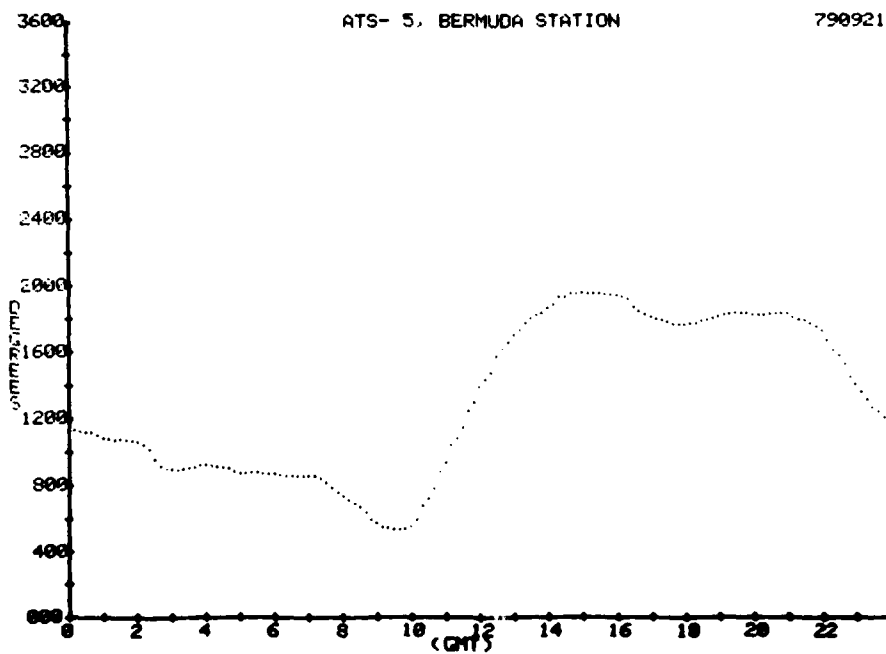
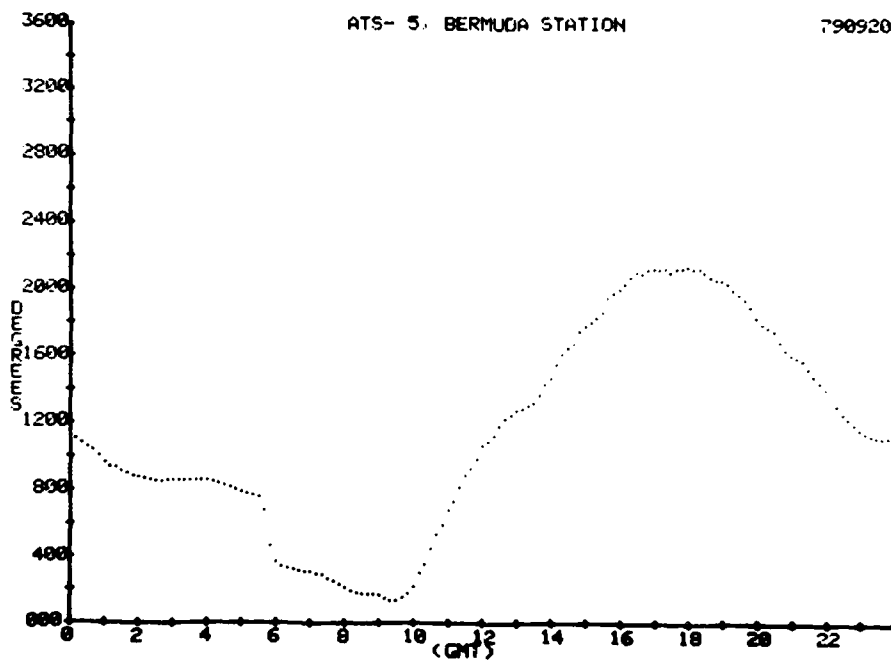
NRL MEMORANDUM REPORT 4517



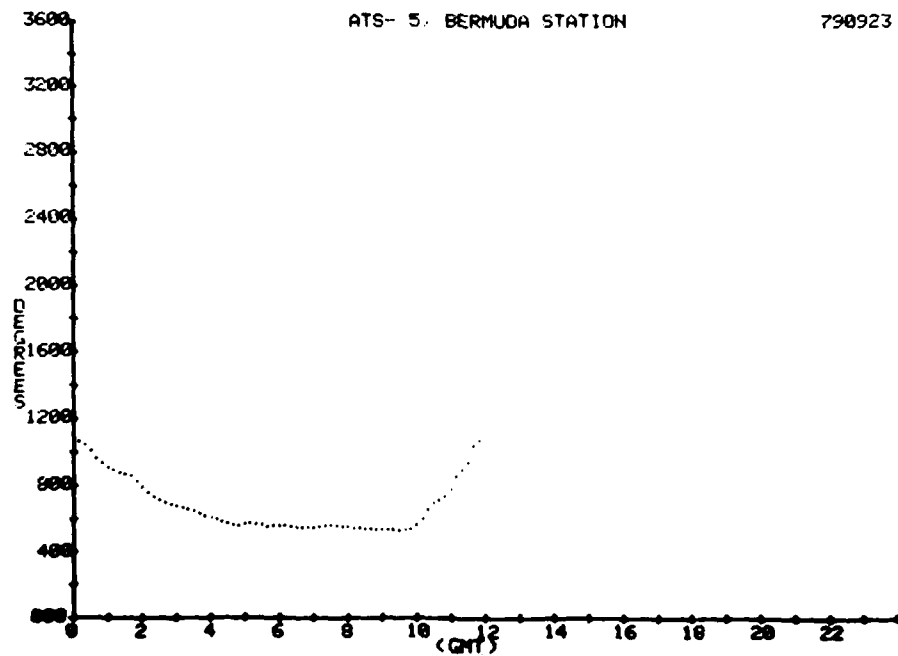
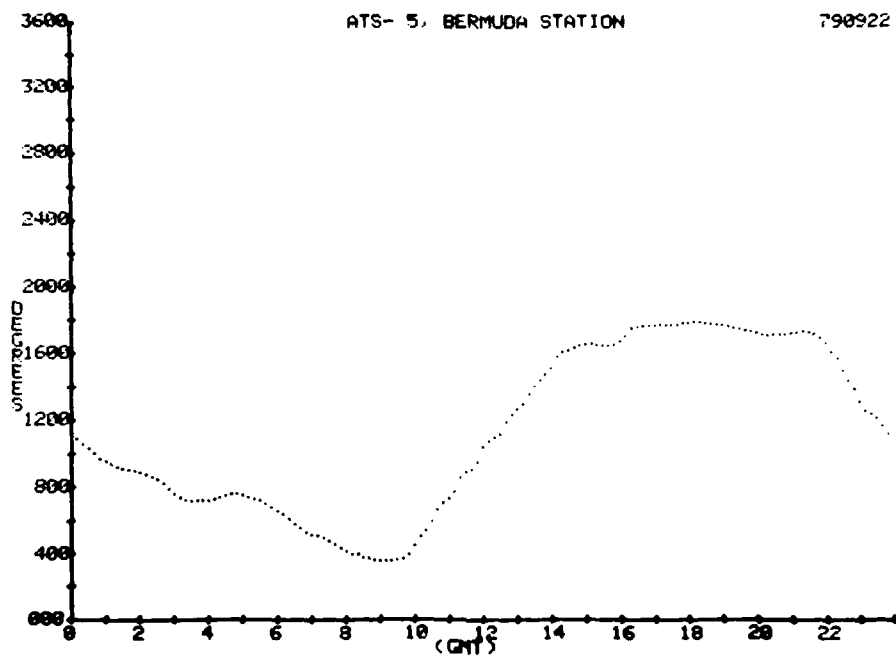
REILLY, HARNISH, AND GOODMAN



NRL MEMORANDUM REPORT 4517



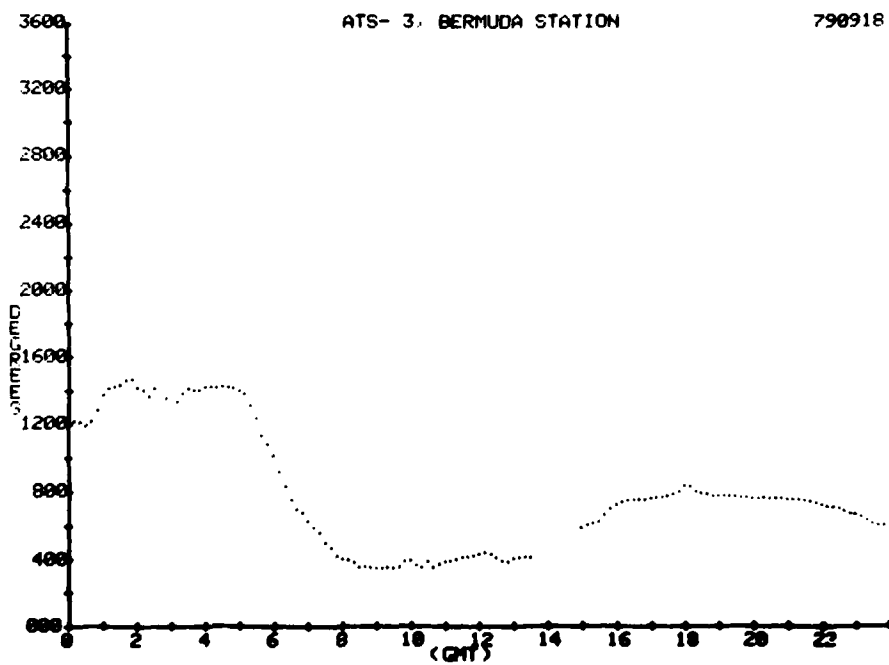
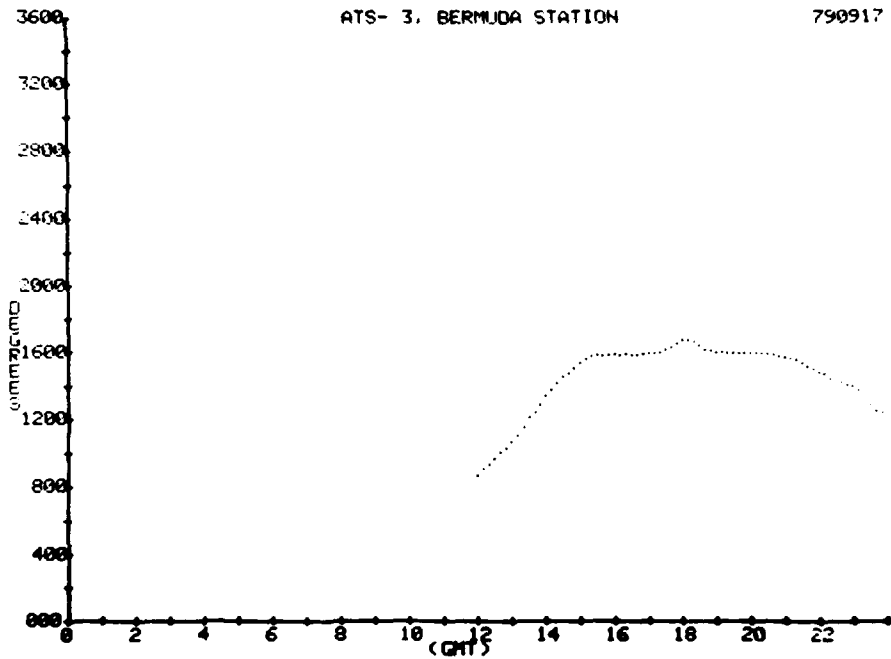
REILLY, HARNISH, AND GOODMAN



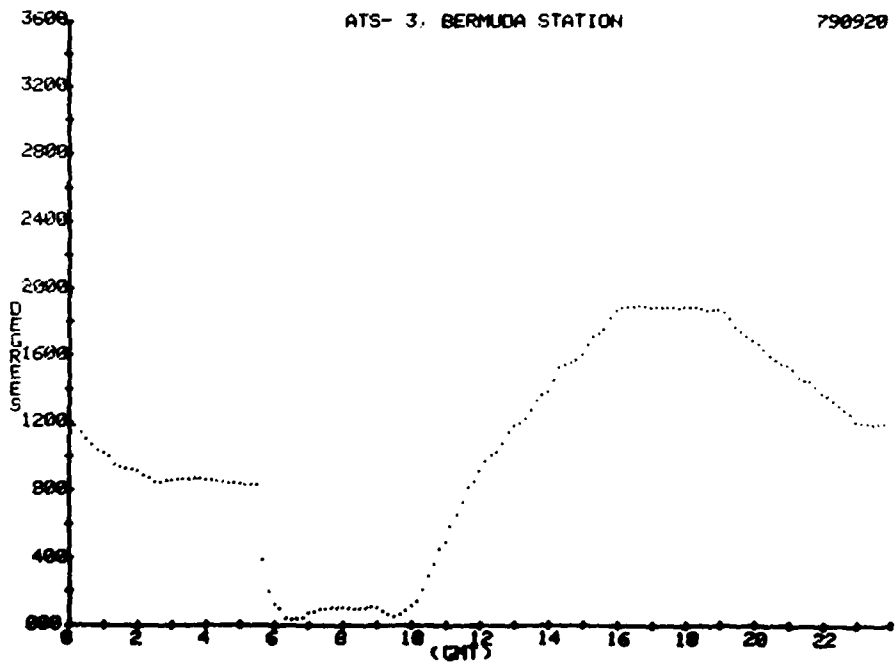
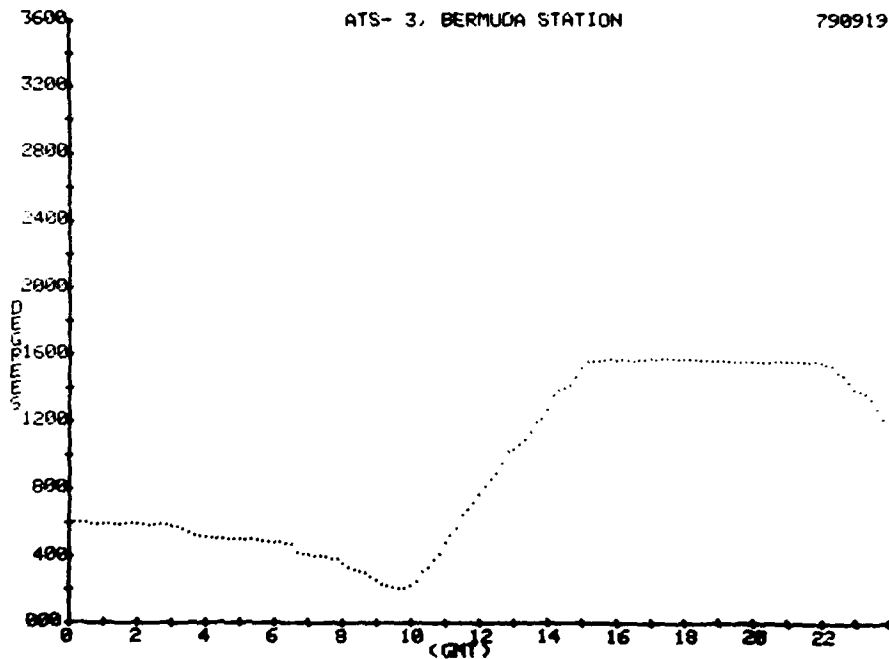
Appendix B

This appendix contains the Faraday rotation data for ATS-3 obtained between Sept. 17 and Sept. 23, 1979. The description of the Appendix A data applies to this data set also.

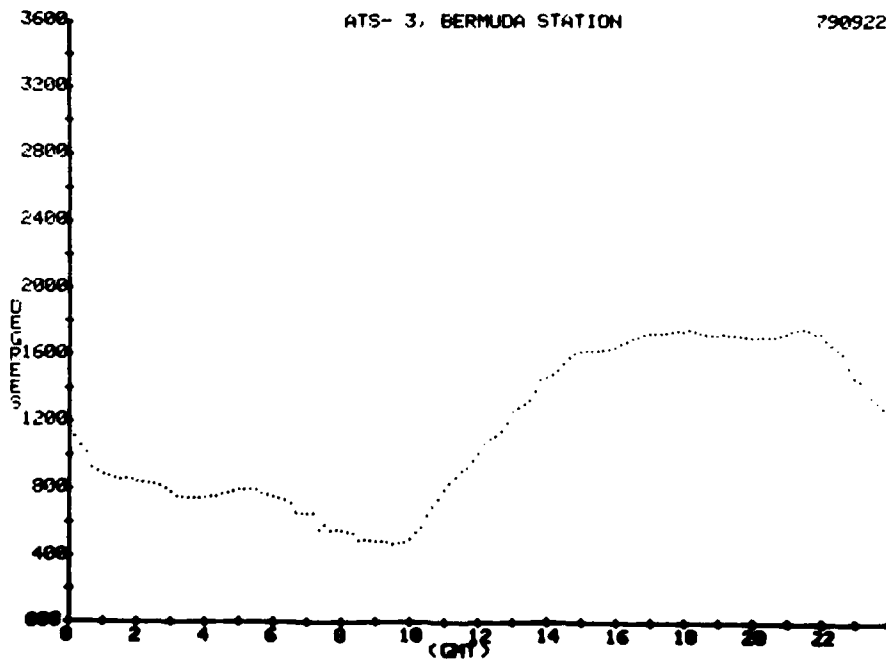
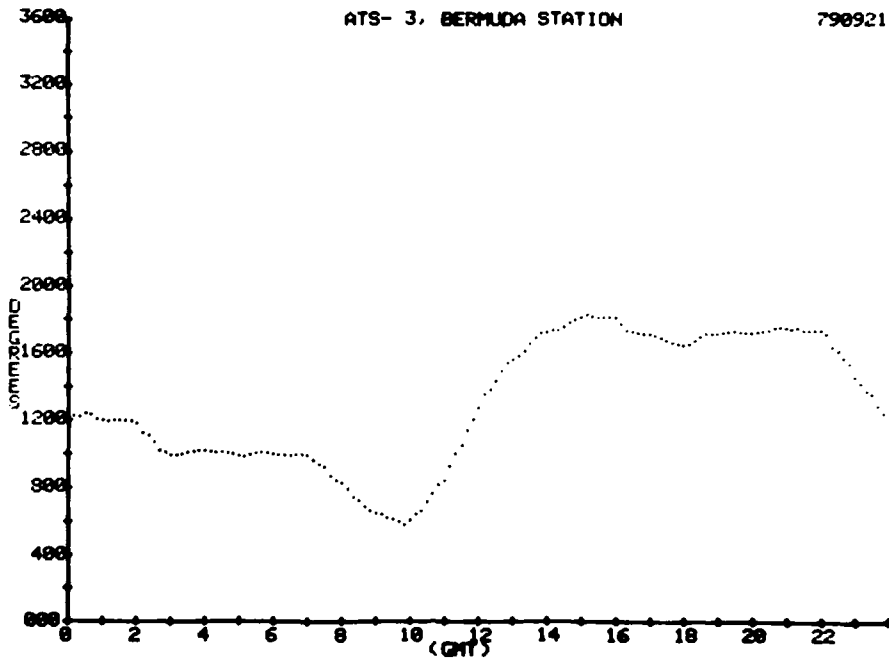
REILLY, HARNISH, AND GOODMAN



NRL MEMORANDUM REPORT 4517



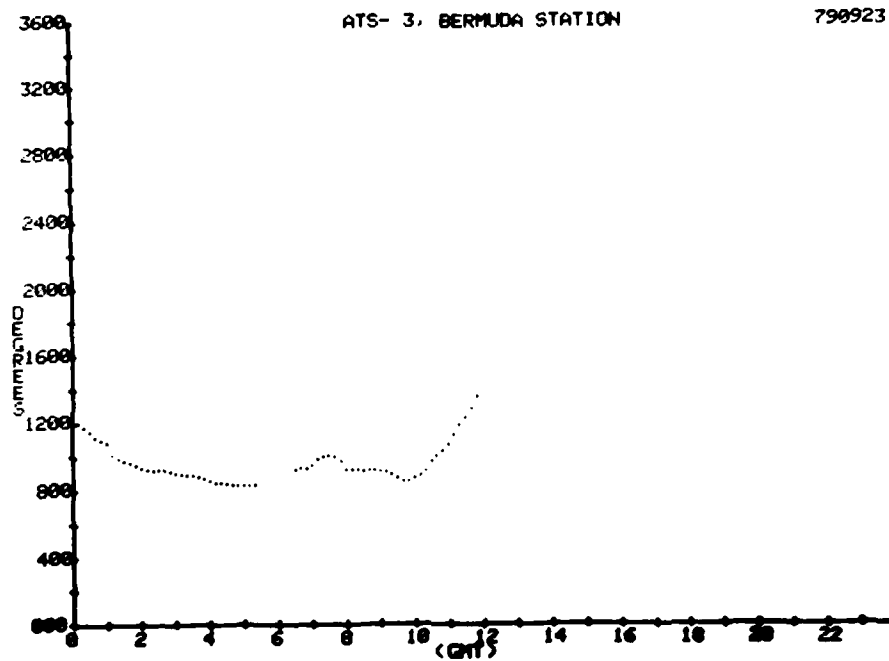
REILLY, HARNISH, AND GOODMAN



NRL MEMORANDUM REPORT 4517

ATS- 3, BERMUDA STATION

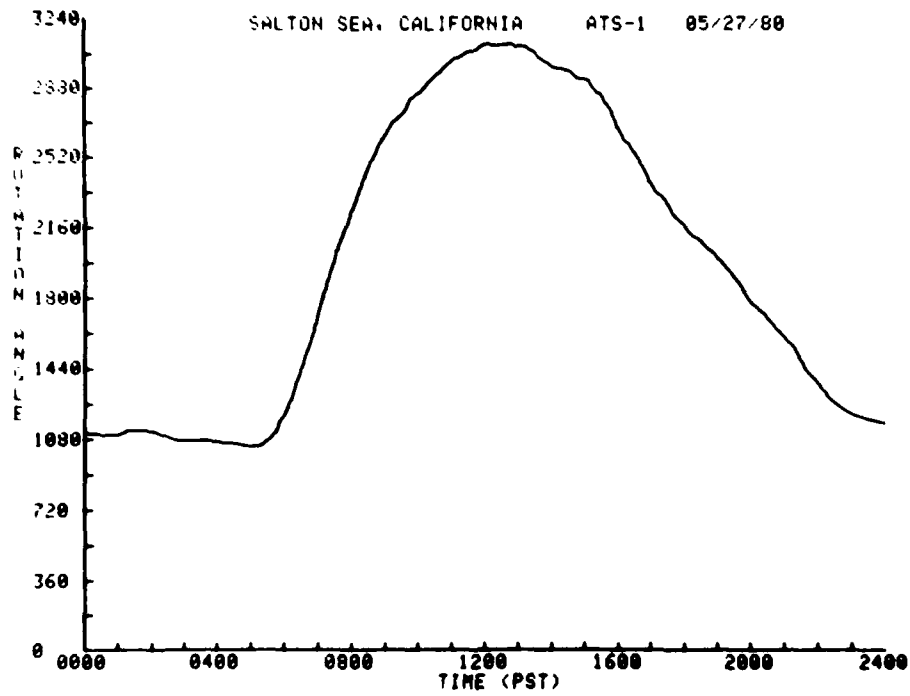
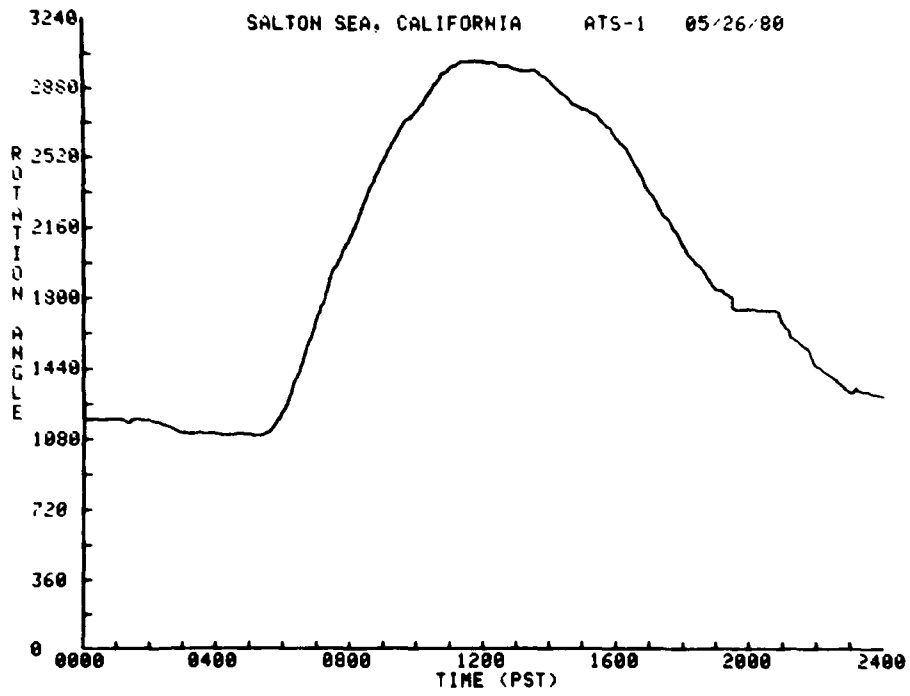
790923



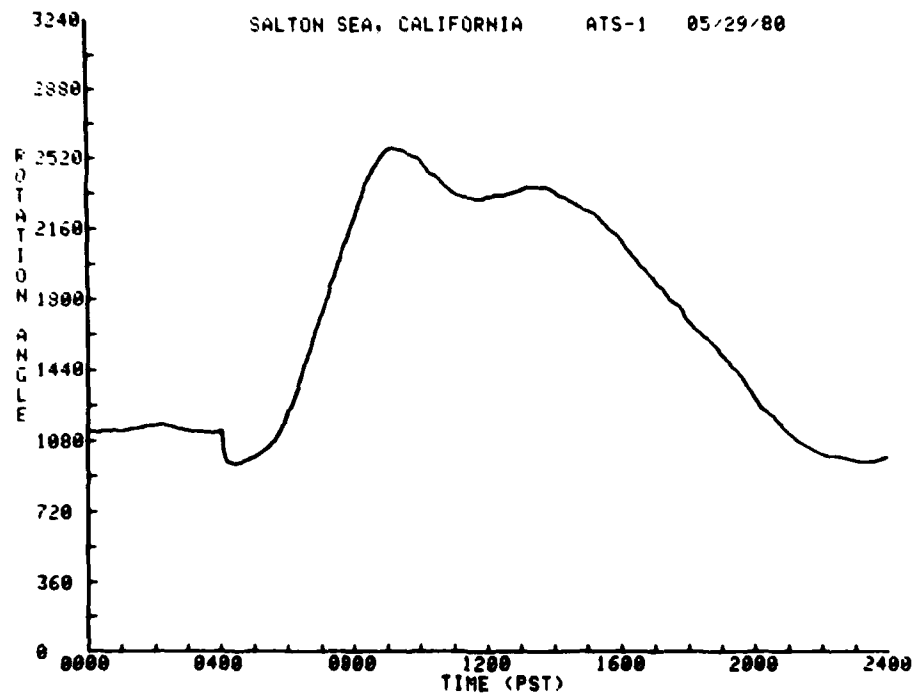
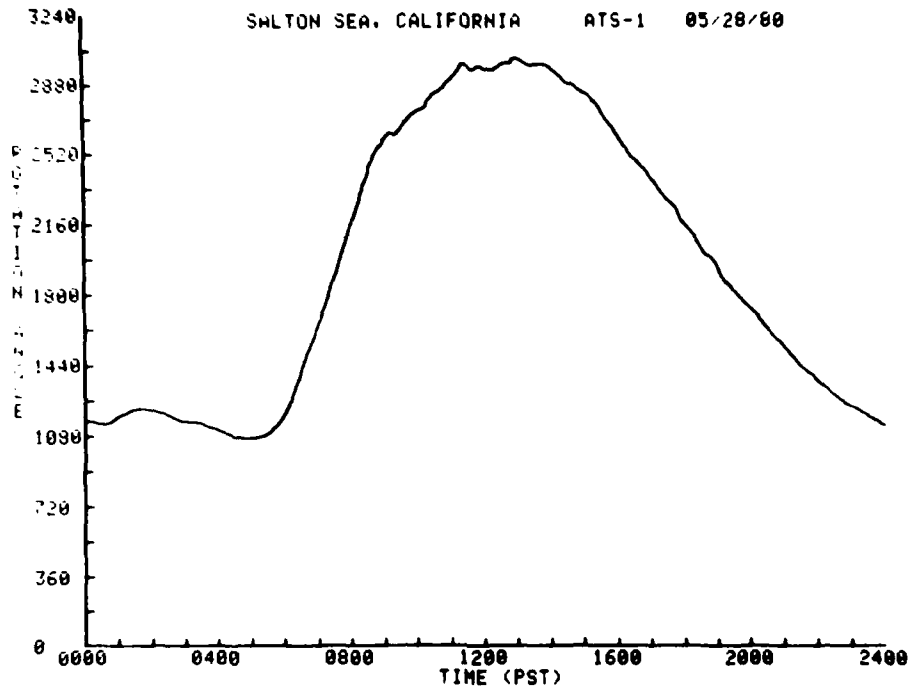
Appendix C

This appendix contains the Faraday rotation data for ATS-1 obtained at the Salton Sea site between May 26 and May 29, 1980. No attempt is made to remove the baseline ambiguity in this data. The time axis is local time (PST), 7 hours earlier than GMT or UT.

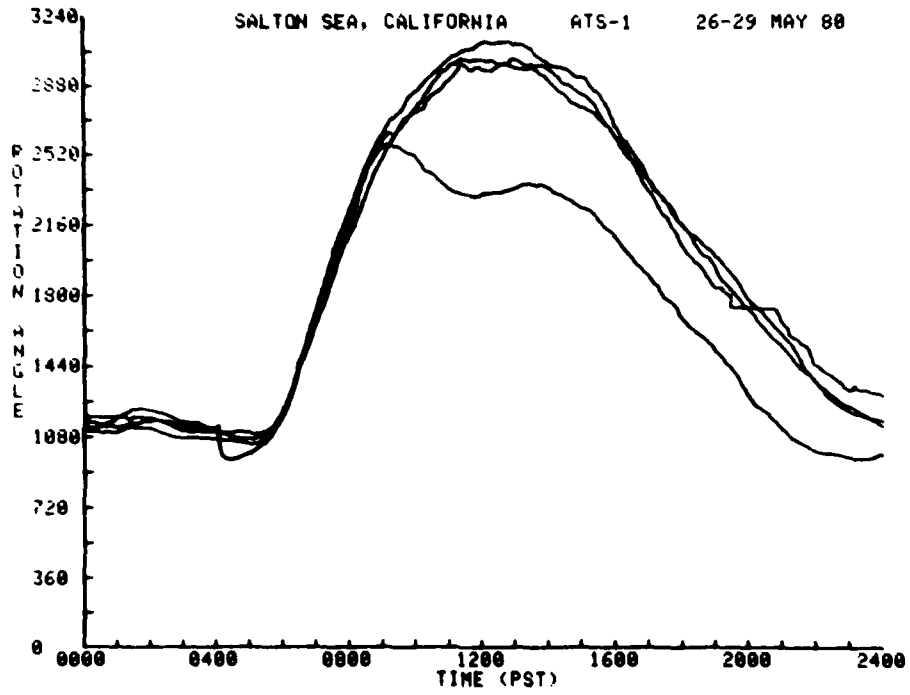
NRL MEMORANDUM REPORT 4517



REILLY, HARNISH, AND GOODMAN



NRL MEMORANDUM REPORT 4517



REPORT DISTRIBUTION LIST

Department of Defense

Assistant Secretary of Defense
Comm. Cmd. Cont & Intell
Washington, D.C. 20301

O1CY ATTN: J. Babcock
O1CY ATTN: M. Epstein
O1CY ATTN: Dr. T. P. Quinn
O1CY ATTN: Dr. H. Van Trees
O1CY ATTN: Dr. R. M. Davis
O1CY ATTN: COL E. W. Friday
O1CY ATTN: S. L. Zeiberg
O1CY ATTN: R. A. Moore

Defense Science Board
Washington, D.C. 20301
O1CY ATTN: Chairman Dr. E. G. Fubini

Assistant to the Secretary of Defense
Atomic Energy
Washington, D.C. 20301
O1CY ATTN: Executive Assistant

Director
Command Control Technical Center
Pentagon Rm BE 685
Washington, D.C. 20301
O1CY ATTN: C-650
O1CY ATTN: C-312 R. Mason

Joint Chiefs of Staff
Pentagon
Washington, D.C. 20301
O1CY ATTN: COL L.M. Hand
O1CY ATTN: COL C.H. Moss
O1CY ATTN: COL R.W. Seh
O1CY ATTN: Director C3 Systems
O1CY ATTN: COL W.H. Doyle
O1CY ATTN: Dep Director Tactical/
Theater C3 Systems
RADM M.J. Schultz Jr.
O1CY ATTN: CAPT B.L. Cloud
O1CY ATTN: COL G.A. Pons

Director
Defense Advanced Resch Proj Agency
Architect Building
1400 Wilson Blvd.
Arlington, VA. 22209
O1CY ATTN: Nuclear Monitoring Research
O1CY ATTN: Strategic Tech Office
O1CY ATTN: Tactical Technology Office

Advanced Research Projects Agency (ARPA)
Strategic Technology Office
Arlington, Virginia
O1CY ATTN: CAPT Donald M. Levine

Defense Communications Agency
8th and Courthouse Road
Arlington, VA. 22204
O1CY ATTN: Paul Rosen
O1CY ATTN: Dr. I. L. Lebow

Defense Communications Engineering Center
Derey Engineering Building
1860 Wiehle Avenue
Reston VA. 22090
O1CY ATTN: W. Heidig
O1CY ATTN: D. T. Worthington
O1CY ATTN: M. J. Raffensperger

Command and Control Technical Center
Plans, Prog. and Management Directorate
Pentagon
Washington, D.C. 20301
O1CY ATTN: COL J. L. Manbeck - 5200

Defense Intelligence Agency
1735 N. Lynn Street
Arlington, VA. 22209
O1CY ATTN: DT
O1CY ATTN: DT-1A
O1CY ATTN: DT-2C

Defense Mapping Agency
Red 56 NOBS
Washington, D.C. 20305
O1CY ATTN: R. D. Cook
O1CY ATTN: A. Mancini

Defense Mapping Agency
Hydrographic/Topographic Center
6500 Brookes Lane
Washington, D.C. 20305
O1CY ATTN: P. ...
O1CY ATTN: COL R. Kazanjian
O1CY ATTN: F. Kuwamura Jr.

Defense Nuclear Agency
Hybla Valley Federal Building
6801 Telegraph Road
Alexandria, VA. 20305
O1CY ATTN: DDST
O1CY ATTN: RAAE

Commander
Field Command
Defense Nuclear Agency
Kirtland AFB, NM 87115
OICY ATTN: FCPR

Chief
Livermore Division Fld Command Dna
Department of Defense
Lawrence Livermore Laboratory
P. O. Box 808
Livermore, CA 94550
OICY ATTN: FCPRL

Director
National Security Agency
Department of Defense
Ft. George G. Meade, MD 20755
OICY ATTN: R52
OICY ATTN: W14
OICY ATTN: W32
OICY ATTN: R5
OICY ATTN: Science Advisor

Institute for Defense Analysis
400 Army/Navy Drive
Arlington, VA 22202
OICY ATTN: Dr. W. Wasylkowskyj
OICY ATTN: J. M. Aein
OICY ATTN: Ernest Bauer
OICY ATTN: Hans Wolfhard
OICY ATTN: Joel Bengston

Defense Documentation Center
Cameron Station
Alexandria, Va 22314
OICY ATTN: TC
(12 copies if open publication,
other wise 2 copies)

Commander
U.S. Army Comm-Elec Engrg Instal Agy
Ft. Huachuca, AZ. 85613
OICY ATTN: CCC-EMEO George Lane

Commander
U.S. Army Foreign Science & Tech Ctr.
220 7th Street, NE.
Charlottesville, VA. 22901
OICY ATTN: DRXST-SD
OICY ATTN: R. Jones

Commander/Director
Atmospheric Sciences Laboratory
U.S. Army Electronics Command
White Sands Missile Range, NM 88002
OICY ATTN: Delas-Eo F. Niles

Director
BMD Advanced Tech Ctr.
5001 Eisenhower Avenue
Alexandria, VA. 22333
OICY ATTN: Dacs-3Mt J. Shea

Chief C-E Services Division
U. S. Army Communications CMD
Pentagon Rm 18269
Washington, D.C. 20310
OICY ATTN: C-E-Services Division

Commander
U.S. Army Material Dev & Readiness CMD
5001 Eisenhower Avenue
Alexandria, VA. 22333
OICY ATTN: DRCLDC J.A. Bender

Commander
U.S. Army Nuclear and Chemical Agency
7500 Backlick Road
Bldg. 2073
Springfield, VA. 22150
OICY ATTN: Library

Director
U.S. Army Ballistic Research Labs.
Aberdeen Proving Ground, MD. 21005
OICY ATTN: Tech Lib Edward Baicy

Commander
U.S. Army Satcom Agency
Ft. Monmouth, NJ 07703
OICY ATTN: Document Control

Commander
U.S. Army Missile Intelligence Agency
Redstone Arsenal, AL 35809
OICY ATTN: Jim Gamble

Director
U.S. Army Tradoc Systems Analysis Activity
White Sands Missile Range, NM 88002
OICY ATTN: ATAA-SA
OICY ATTN: TCC/F. Pavan Jr.
OICY ATTN: ATAA-TAC LTC J. Hesse

U. S. Army Aberdeen Research and Development Center
Ballistic Research Laboratory
Aberdeen, Maryland
01CY ATTN: Dr. J. Heimerl

Commander
FRADCOM Technical Support Activity
Department of the Army
Fort Monmouth, N.J. 07703
01CY ATTN: DRSEL-NL-RD H. Bennet
01CY ATTN: DRSEL-PL-ENV H. Bomke
01CY ATTN: J. E. Quigley

Commander
Harry Diamond Laboratories
Department of the Army
2800 Powder Mill Road
Adelphi, MD. 20783
(CNWDI-Inner Envelope: ATTN: DELMD-RBH)
01CY ATTN: DELHD-TI M. Weiner
01CY ATTN: DELHD-RB R. Williams
01CY ATTN: DELHD-NP F. Wizenitz
01CY ATTN: DELHD-NP C. Moazed

Headquarters CORADCOM
Department of Army
Ft. Monmouth, N.J. 07703
01CY ATTN: DRDCCO-COM-RF-5

Asst Secretary of Navy RE&S
Pentagon, Washington D.C. 20350
01CY ATTN: G. Cann
01CY ATTN: Dr. H. Rabin
01CY ATTN: J. Hull
01CY ATTN: T. Jacobs
01CY ATTN: W. Guinard

Office of Naval Research
BCT-1 800 N. Quincy Street
Arlington, VA. 22217
01CY ATTN: ONR-100-C
01CY ATTN: ONR-200
01CY ATTN: ONR-102-B
01CY ATTN: ONR-220
01CY ATTN: ONR-221
01CY ATTN: ONR-400
01CY ATTN: ONR-420
01CY ATTN: ONR-421
01CY ATTN: ONR-427 Dr. J. Dimmock
01CY ATTN: ONR Dr. H. Mullaney
01CY ATTN: ONR G. Joiner

Center for Naval Analysis (Contract Group)
2000 N. Beauregard Street
Alexandria, VA. 22311
01CY ATTN: J. K. Tyson
01CY ATTN: W. J. Hurley

Department of the Navy
Pentagon, Washington, D.C. 20350
01CY ATTN: NOP-094H Dr. R. Conlev
01CY ATTN: NOP-940B Dr. N. McAllister
01CY ATTN: NOP-940D
01CY ATTN: NOP-941
01CY ATTN: NOP-941C
01CY ATTN: NOP-941E
01CY ATTN: NOP-941F W. A. Fiegleson
01CY ATTN: NOP-941H
01CY ATTN: NOP-941J
01CY ATTN: NOP-942
01CY ATTN: NOP-944
01CY ATTN: NOP-951A
01CY ATTN: NOP-952C
01CY ATTN: NOP-952C4
01CY ATTN: NOP-952D
01CY ATTN: NOP-980
01CY ATTN: NOP-986
01CY ATTN: NOP-986C
01CY ATTN: NOP-986D
01CY ATTN: NOP-986E
01CY ATTN: NOP-986F
01CY ATTN: NOP-986J
01CY ATTN: NOP-009
01CY ATTN: NOP-06
01CY ATTN: NOP-60
01CY ATTN: NOP-64

U.S. Marine Corps
01CY ATTN: MC-LMC
01CY ATTN: MC-CC

Headquarters Naval Material Command
Crystal Plaza 5
2211 Jefferson Davis Highway
Arlington, VA. 20360
01CY ATTN: O8L J. W. Probus
01CY ATTN: O8TB
01CY ATTN: O8TC
01CY ATTN: O8T2
01CY ATTN: O8T21
01CY ATTN: O8T22
01CY ATTN: O8T23

Trident System Project Office (PM-2)
National Center 3
2531 Jefferson Davis Highway
Arlington, VA. 20362

01CY ATTN: PM2-00
01CY ATTN: PM2-001
01CY ATTN: PM2-10

Naval Air Systems Command
Jefferson Plaza 1
1411 Jefferson Davis Highway
Arlington, VA. 20360

01CY ATTN: NAIR-03
01CY ATTN: NAIR-03C
01CY ATTN: NAIR-302
01CY ATTN: NAIR-310
01CY ATTN: NAIR-360
01CY ATTN: NAIR-370
01CY ATTN: NAIR-370C
01CY ATTN: NAIR-370P
01CY ATTN: NAIR-370G
01CY ATTN: NAIR-370R
01CY ATTN: NAIR-05
01CY ATTN: NAIR-06

Naval Electronics Systems Command
National Center 1
2511 Jefferson Davis Highway
Arlington, VA. 20360

01CY ATTN: NELEX-00B D. J. Lawson
01CY ATTN: NELEX-091
01CY ATTN: PME-108
01CY ATTN: PME-108-14
01CY ATTN: PME-108T
01CY ATTN: PME-117-201A
01CY ATTN: PME-119
01CY ATTN: PME-121
01CY ATTN: NELEX-095
01CY ATTN: NELEX-953
01CY ATTN: PME-106.T
01CY ATTN: PME-106-1
01CY ATTN: PME-106-2
01CY ATTN: PME-106-3
01CY ATTN: PME-106-4
01CY ATTN: PME-106-5
01CY ATTN: PME-106-6
01CY ATTN: ELEX-02
01CY ATTN: ELEX-03
01CY ATTN: ELEX-03A
01CY ATTN: ELEX-310
01CY ATTN: ELEX-310A
01CY ATTN: ELEX-330
01CY ATTN: ELEX-350

01CY ATTN: ELEX-04
01CY ATTN: ELEX-05

Naval Electronics Systems Command
REWSON PME 107
Jefferson Plaza 1
1411 Jefferson Davis Highway
Arlington, VA. 20360

01CY ATTN: PME 107-5
01CY ATTN: PME 107-6 CAPT W. Flowers
01CY ATTN: PME 107-6 CDR H. Orejuella
01CY ATTN: PME 107-55

Naval Sea Systems Command
National Center 3
2531 Jefferson Davis Highway
Arlington, VA. 20362
01CY ATTN: NAVSEA-00
01CY ATTN: NAVSEA-003

Naval Telecommunications Command
4401 Mass. Ave.
Washington, D. C. 20390
01CY ATTN: CNTC
01CY ATTN: 01
01CY ATTN: 03
01CY ATTN: 05
01CY ATTN: 06
01CY ATTN: 08

Naval Security Group
3801 Nebraska Avenue, N.W.
Washington, D. C. 20390
01CY ATTN: Tech. Dir. Dr. G. S. Blevins
01CY ATTN: R. R. Rozanski
01CY ATTN: CAPT G. L. Jackson

Navy Tactical Support Activity
Naval Ordnance Laboratory
White Oak, MD. 20910
01CY ATTN: A. M. Letow

Fleet Weather Facility
FB #4

01CY ATTN: Operations Officer

Naval Communications Unit
Cheltenham, MD. 20390
01CY ATTN:

U. S. Naval Research Laboratory
4555 Overlook Avenue
Washington, D. C. 20375

01CY ATTN: 4100
02CY ATTN: 4101
01CY ATTN: 4120
01CY ATTN: 4130
01CY ATTN: 4140
01CY ATTN: 4150
01CY ATTN: 4160
01CY ATTN: 4170
30CY ATTN: 4180
01CY ATTN: 4190
01CY ATTN: 4700
01CY ATTN: 4701
01CY ATTN: 4780
01CY ATTN: 4320
01CY ATTN: 5000
01CY ATTN: 5300
01CY ATTN: 5306
01CY ATTN: 5320
01CY ATTN: 5700
01CY ATTN: 5700.1
01CY ATTN: 7000
01CY ATTN: 7500
01CY ATTN: 7506
01CY ATTN: 7570
01CY ATTN: 7580
01CY ATTN: 7900
01CY ATTN: 7903
01CY ATTN: 7960

Commander
Naval Space Surveillance System
Dahlgren, Va. 22448
01CY ATTN Capt J. H. Burton

Officer-in-Charge
Naval Surface Weapons Center
White Oak, Silver Spring, Md. 20910
01CY ATTN: Code F31

Director
Strategic Systems Project Office
Department of the Navy
Washington, D. C. 20376
01CY ATTN: NSP-2141
01CY ATTN: NSSP-2722 Fred Wimberly

Naval Space System Activity
P. O. Box 92960
Worldway Postal Center
Los Angeles, Ca 90009
01CY ATTN: Code 52

Commanding Officer
Naval Intelligence Support Center
4301 Suitland Road, Bldg. 5
Washington, D. C. 20390
01CY ATTN: Mr. Dubbin, STIC 12
01CY ATTN: NISC-50
01CY ATTN: Code 5404, J. Galet

Commander
San Diego, Ca. 92152
01CY ATTN: Code 532, W. Moler
01CY ATTN: Code 0230, C. Baggett
01CY ATTN: Code 81, R. Eastman
01CY ATTN: R. Rose
01CY ATTN: J. Richter
01CY ATTN: R.U.F. Hopkins
01CY ATTN: R. Lebahn
01CY ATTN: J. Caldwell

Director
Joint STRAT TGT Planning Staff
Offutt, AFB
Omaha, NB 68113
01CY ATTN: JLTW-2
01CY ATTN: JPST, G. Goetz

Commander
Aerospace Defense Command/DC
Dept of the Air Force
ENT AFB, CO 80912
01CY ATTN: DC, Mr. Long

Commander
Aerospace Defense Command/XPD
Department of the Air Force
ENT AFB, Co 80912
01CY ATTN: XPDQQ
01CY ATTN: XP

Air Force Geophysics Laboratory
Hancom AFB, Ma 01731
01CY ATTN: OPR, Harold Gardner
01CY ATTN: OPR-2, James C. Ulwick
01CY ATTN: LKB, Kenneth S.W. Champion
01CY ATTN: OPR Alva T. Stair

O1CY ATTN: Jules Aarons
O1CY ATTN: Jurgen Buchau
O1CY ATTN: John P. Mullen
O1CY ATTN: J. A. Klobuchar
O1CY ATTN: H. Whitney
O1CY ATTN: E. Huppi
Air Force Weapons Laboratory
Kirtland AFB, NM 87117
O1CY ATTN SUL
O1CY ATTN: CA Authur ,/ Guenther
O1CY ATTN: DYC, Capt. J. Barry
O1CY ATTN: DYC John M. Kamm
O1CY ATTN: DYT Capt. Mark A. Fry
O1CY ATTN: DES Maj. Gary Ganong
O1CY ATTN: DYC J. Janni

AFTAC
Patrick AFB, FL 32925
O1CY ATTN: TF/Maj. Wiley
O1CY ATTN: TN

Air Force Avionics Laboratory
Wright-Patterson AFB, Oh 45433
O1CY ATTN: AAD Wade Hunt
O1CY ATTN: AAD Allen Johnson

Deputy Chief of Staff
Research, Development, & Acq
Department of the Air Force
Washington, D. C. 20330
O1CY ATTN: AFRDQ

SAMSO/SZ
Post Office Box 92960
Worldway Postal Center
Los Angeles, Ca 90009
(Space Defense Systems)
O1CY ATTN: SZJ

Strategic Air Command/XPFS
Offutt AFB, NE 68113
O1CY ATTN: SPS Maj. B. Stephan
O1CY ATTN: WATE Maj. Bruce Bauer
O1CY ATTN: NRT
O1CY ATTN: DOK Chief Scientist

SAMSO/YA
P. O. Box 92960
Worldway Postal Center
Los Angeles, Ca 90009
O1CY ATTN: YAT Capt. L. Blackwelder

SAMSO/SK
P. O. Box 92960
Worldway Postal Center
Los Angeles, Ca 90009
O1CY ATTN: SKA (Space COMM Systems)
M. Clavin

SAMSOMN
Norton AFB, Ca 92409
(Minuteman)
O1CY ATTN: MNN LTC Kennedy

Commander
Rome Air Development Center, AFSC
Hanscom AFB, Ma 01731
O1CY ATTN: EEP A. Lorentzen

Headquarters
Electronic Systems Division/DC
Department of the Air Force
Hanscom AFB, Ma 01731
O1CY ATTN: DCKC Maj. J. C. Clark

Commander
Foreign Technology Division, AFSC
Wright-Patterson AFB, Oh 45433
O1CY ATTN: NICD Library
O1CY ATTN: ETOP B. Ballard

Commander
Rome Air Development Center, AFSC
Griffiss AFB, NY 13441
O1CY ATTN: Doc Library/TSLD
O1CY ATTN: OCSE V. Coyne

Headquarters
Electronic Systems Division/XR
Department of the Air Force
Hanscom AFB, MA 01731
O1CY ATTN: XR J. Deas

Headquarters
Electronic Systems Division/YSEA
Department of the Air Force
Hanscom AFB, Ma 01731
O1CY ATTN: YSEA

Air Force Global Weather Central
Air Weather Service
Offutt AFB, NE 68113
O1CY ATTN:

Director of Space Environmental Laboratory
NOAA
325 S. Broadway
Boulder, Co 80302

01CY ATTN: Dr. A. Glenn Jean
01CY ATTN: Dr. G. W. Adams
01CY ATTN: Dr. D. N. Anderson
01CY ATTN: Dr. K. Davies
01CY ATTN: Dr. R.F. Donnelly
01CY ATTN: Dr. David Evans
01CY ATTN: Dr. R. Grubb
01CY ATTN: Dr. G. Reid

National Center for Atmospheric Research
World Data Center A
325 Broadway
Boulder, Co 80303

01CY ATTN: R. Conkright
01CY ATTN: W. Paulishak

Harvard University
Harvard Square
Cambridge, Ma 02138

01CY ATTN: Dr. M. B. McElroy
01CY ATTN: Dr. R. Lindzen

Pennsylvania State University
University Park, Pa 16803

01CY ATTN: Dr. J. S. Nisbet
01CY ATTN: Dr. P. R. Rohrbaugh
01CY ATTN: Dr. D. E. Baran
01CY ATTN: L. A. Carpenter
01CY ATTN: Dr. M. Lee
01CY ATTN: Dr. R. Divant
01CY ATTN: Dr. P. Bennett
01CY ATTN: Dr. E. Klevans

University of California, Los Angeles
405 Hillgard Avenue
Los Angeles, Ca 90024

01CY ATTN: Dr. F. V. Coroniti
01CY ATTN: Dr. C. Kennel

University of California, Berkeley
Berkeley, Ca 94720

01CY ATTN: Dr. M. Hudson

Utah State University
4th N. and 8th Streets
Logan, Ut. 84322

01CY ATTN: Dr. P. M. Banks
01CY ATTN: Dr. R. Harris

01CY ATTN: Dr. V. Peterson
01CY ATTN: Dr. R. Megill
01CY ATTN: Dr. K. Baker

Cornell University
Ithaca, NY 14850

01CY ATTN: Dr. W. E. Swartz
01CY ATTN: Dr. R. Sudan
01CY ATTN: Dr. D. Farley
01CY ATTN: Dr. M. Kelley

NASA

Goddard Space Flight Center
Greenbelt, Md 20771

01CY ATTN: Dr. S. Chandra
01CY ATTN: Dr. K. Maedo

General Electric Company
Tempo-Center for Advanced Studies
816 State Street

P. O. Drawer QQ
Santa Barbara, Ca 93102

01CY ATTN: DASIAC
01CY ATTN: Don Chandler
01CY ATTN: Tom Barrett
01CY ATTN: Tim Stephas
01CY ATTN: Warren S. Knapp
01CY ATTN: William McNamara
01CY ATTN: B. Gambill
01CY ATTN: Mack Stanton

General Electric Tech. Services Co., Inc.
Court Street

Syracuse, NY 13201

01CY ATTN: G. Millman

General Research Corporation
Santa Barbara Division
P. O. Box 6770

Santa Barbara, Ca 93111
01CY ATTN: John Ise, Jr.
01CY ATTN: Joel Garbarino

Geophysical Institute

University of Alaska
Fairbanks, AK 99701

01CY ATTN: T. N. Davis
01CY ATTN: Neal Brown
01CY ATTN: Technical Library

GTE Sylvania, Inc.
Electronics Systems GRP-Eastern Div.
77 A Street
Needham, Ma 02194
01 CY ATTN: Marshal Cross

University of Illinois
Department of Electrical Engineering
Urbana, Il 61803
01CY ATTN: K. Yeh
01CY ATTN: S. Bowhill

HSS, Inc
2 Alfred Circle
Bedford, Ma 01730
01CY ATTN: Donald Hansen

International Telephone and
Telegraph Corporation
500 Washington Avenue
Nutley, NJ 07110
01CY ATTN: Technical library

Jaycor
1401 Camino Del Mar
Del Mar, Ca 92014
01CY ATTN: S. R. Goldman

Johns Hopkins University
Applied Physics Laboratory
Johns Hopkins Road
Laurel, MD 20810
01CY ATTN: Document Librarian
01CY ATTN: Thomas Potemra
01CY ATTN: John Dassoulas

Lockheed Missiles & Space Co. Inc.
P. O. Box 504
Sunnyvale, Ca 94088
01CY ATTN: Dept 60-12
01CY Attn: D. R. Churchill

Lockheed Missiles and Space Co., Inc.
3251 Hanover Street
Palo Alto, Ca. 94304
01CY ATTN: Martin Walt - Dept 52-10
01CY ATTN: W. L. Imof - Dept 52-12

Kaman Sciences Corp.
P. O. Box 7463
Colorado Springs, Co 80933
01CY ATTN: T. Meagher

Linkabit Corporation
10453 Roselle
San Diego, Ca 92121
01CY ATTN: Irwin Jacobs

University of Lowell
RSCH Foundation
450 Aiken Street
Lowell, Ma 01854
01CY ATTN: K. Bibl

M.I.T. Lincoln Laboratory
P. O. Box 73
Lexington, Ma 02173
01CY ATTN: D. M. Towle
01CY ATTN: Dr. J. V. Evans
01CY ATTN: P. Waldron
01CY ATTN: L. Loughlin
01Cy ATTN: D. Clark
01Cy ATTN: R. Wand

Martin Marietta Corporation
Orlando Division
P. O. Box 5837
Orlando, Fl 32805
01CY ATTN: R. Heffner

McDonnell Douglas Corporation
5301 Bolsa Avenue
Huntington Beach, Ca 92647
01CY ATTN: N. Harris
01CY ATTN: J. Moule
01CY ATTN: George Mroz
01CY ATTN: W. Olson
01CY ATTN: R. W. Halprin
01CY ATTN: Technical Library Services

Mission Research Corporation
735 State Street
Santa Barbara, Ca 93101
01CY ATTN: P. Fischer
01CY ATTN: W. F. Crevier
01CY ATTN: Steven L. Gutsche
01Cy ATTN: D. Sappenfield
01CY ATTN: R. Bogusch
01CY ATTN: R. Hendrick
01CY ATTN: Ralph Kilb
01CY ATTN: Dave Sowle
01CY ATTN: F. Fajen
01CY ATTN: M. Scheibe
01CY ATTN: Conrad L. Longmire
01CY ATTN: Warren A. Schlueter

Mitre Corporation
P. O. Box 208
Bedford, Ma 01730

01CY ATTN: John Morganstern
01CY ATTN: G. Harding
01CY ATTN: C. E. Callahan

Mitre Corporation
Westgate Research Park
1820 Dolly Madison Blvd.
McLean, Va 22101

01CY ATTN: W. Hall
01CY ATTN: W. Foster

Pacific-Sierra Research Corp
1456 Coverfield Blvd.
Santa Monica, Ca 90404

01CY ATTN: E. C. Field, Jr.

Pennsylvania State University
Ionosphere Research Lab
318 Electrical Engineering East
University Park, Pa. 16802

* (Do not send classified to this address)
01CY ATTN: Ionospheric Research Lab

Department of Energy
Albuquerque Operations Office
P. O. Box 5400
Albuquerque, NM 87115

01CY ATTN: Doc Control
D. Sherwood

Department of Energy
Library, Room G-042
Washington, D. C. 20545

01CY Attn: Document Control
A. Labowitz

EG&G, Inc.
Los Alamos Division
P. O. Box 809
Los Alamos, NM 85544

01 Cy Attn: Document Control
J. Breedlove

University of California
Lawrence Livermore Laboratory
P. O. Box 808
Livermore, Ca. 94550

01 Cy Attn: Doc Con for Tech. Info. Dept.
01 Cy Attn: Doc Con for L-389 R. Ott

01 Cy Attn: Doc con for L-31 R. Hager
01 Cy Attn: Doc con for L-46 F. Seward

Los Alamos Scientific Laboratory
P. O. Box 1663
Los Alamos, NM 87545

01Cy Attn: Doc con for R. F. Taschek
01Cy Attn: Doc con for E. Jones
01Cy Attn: Doc con for J. Malik
01Cy Attn: Doc con for R. Jeffries
01Cy Attn: Doc con for J. Zinn
01Cy Attn: Doc con for P. Keaton
01Cy Attn: Doc con for D. Westervelt
01Cy Attn: M. Pongratz
01Cy Attn: D. Simons
01Cy Attn: G. Barasch
01Cy Attn: L. Duncan

Sandia Laboratories
P. O. Box 5800
Albuquerque, NM 87115

01Cy Attn: Doc con for J. Martin
01Cy Attn: Doc con for W. Brown
01Cy Attn: Doc con for A. Thornbrough
01Cy Attn: Doc con for T. Wright
01Cy Attn: Doc con for D. Dahlgren
01Cy Attn: Doc con for 3141
01Cy Attn: Doc con for Space Project Division

Sandia Laboratories
Livermore Laboratory
P. O. Box 959
Livermore, Ca 94550

01Cy Attn: Doc con for B. Murphey
01Cy Attn: Doc con for T. Cook

Office of Military Application
Department of Energy
Washington, D. C. 20545

01Cy Attn: Doc Con for D. Gale

Central Intelligence Agency
Attn. RD/51, Rm 5G48, HQ Bldg.
Washington, D. C. 20505

Department of Commerce
National Bureau of Standards
Washington, D. C. 20234

(All Corres: Attn: Sec Officer for)
01Cy Attn: R. Moore

Department of Transportation
Office of the Secretary
TAO-44.1, Room 10402-B
400 7th Street, S. W.

Institute for Telecommunication Sciences
National Telecommunications & Info Admin
Boulder, Co 80303

01Cy Attn: A. Jean (Unclass only)
01Cy Attn: W. Utlaut
01Cy Attn: D. Crombie
01Cy Attn: L. Berry
01Cy Attn: Dr. C. Rush

Aerospace Corporation
P. O. Box 92957

Los Angeles, Ca. 90009
01Cy Attn: I. Garfunkel
01Cy Attn: T. Salmi
01Cy Attn: V. Josephson
01Cy Attn: S. Bower
01Cy Attn: N. Stockwell
01Cy Attn: D. Olsen
01Cy Attn: F. Morse
01Cy Attn: SMFA for PW

Analytical Systems Engineering Corp.
5 Old Concord Road
Burlington, Ma 01803
01Cy Attn: Radio Sciences

Berkeley Research Associates, Inc.
P. O. Box 983
Berkeley, Ca 94701
01Cy Attn: J. Workman

The Boeing Company
P. O. Box 3707
Seattle, Wa 98124
01Cy Attn: G. Keister
01Cy Attn: D. Murray
01Cy Attn: G. Hall
01Cy Attn: J. Kenney

California At San Diego
University of IPAPS, 8-019
LaJolla, Ca 92093
01Cy Attn: Henry G. Booker

Brown Engineering Company, Inc.
Cummings Research Park
Huntsville, Al 35807
01Cy Attn: Romeo A. Deliberis

Charles Stark Draper Laboratory, Inc.
555 Technology Square
Cambridge, Ma 02139

01Cy Attn: D. B. Cox
01Cy Attn: J. P. Gilmore

Computer Sciences Corporation
6565 Arlington Blvd.

Falls Church, Va. 22046
01Cy Attn: H. Blank
01Cy Attn: John Spoor
01Cy Attn: C. Nail

COMSAT Laboratories
Linthicum Road
Clarksburg, Md. 20734
01Cy Attn: G. Hyde

Cornell University
Department of Electrical Engineering
Ithaca, NY 14850
02Cy Attn: D. T. Farley, Jr.

Electrospace Systems, Inc
Box 1339
Richardson, Tx 75080
01Cy Attn: H. Logston
01Cy Attn: Security (P. Phillips)

ESL, Inc.
495 Java Drive
Sunnyvale, Ca. 94086
01Cy Attn: J. Roberts
01Cy Attn: James Marshall
01Cy Attn: C. W. Prettie

Ford Aerospace & Communications Corp
3939 Fabian Way
Palo Alto, Ca. 94303
01Cy Attn: J. T. Mattingley

University of Texas
Applied Research Laboratories
P.O. Box 8029
Austin, Tx 78717
01CY Attn: R. Altenburg
01CY Attn: J.R. Clynych

Emmanuel College
Physics Department
400 The Fenway

Boston, Ma. 02115
OICY Attn: Santimay Basu
OICY Attn: Sunada Basu

Syracuse, NY 13201
OICY Attn: F. Reibert

Boston University Department of Astronomy
725 Commonwealth Ave.
Boston, Ma 02215

United Technologies Research Center
Silver Lane: Mail Stop 85
East Hartford, Conn. 06108
OICY Attn: G. Meltz

OICY Attn: J. Baumgardner
OICY Attn: C. Chacko
OICY Attn: C. Crabb
OICY Attn: M. Mendillo
OICY Attn: G. LaQuadra
OICY Attn: B. Vance

Argonne National Laboratory
Energy and Environmental Systems Div.
9700 S. Cass Ave.
Argonne, Il 60439
OICY Attn: D. Rote

Arecibo Observatory
P.O. Box 995
Arecibo, Puerto Rico 00612
OICY Attn: R. Behnke

Photometrics, Inc.
442 Marrett Road
Lexington, Ma 02173
OICY Attn: I.L. Kofsky
OICY Attn: D. Villanucci

Stanford University
Radioscience Laboratory
Stanford, Ca. 94305
OICY Attn: P.A. Bernhardt

General Electric Company
Space Division
Valley Forge Space Center
Goddard Blvd King of Prussia
P. O. Box 8555
Philadelphia, Pa 19101
OICY Attn: M. H. Bortner
Space Science Lab.

SRI International
Radiophysics Laboratory
333 Ravenswood Laboratory
Menlo Park, Ca 94025
OICY Attn: M. Cousins

General Electric Company
P. O. Box 1122
Syracuse, NY 13201
OICY Attn: F. Reibert

US Army Electronics Command
AMSEL-NL-H-4
Fort Monmouth, N.J. 07703
OICY Attn: F. Gorman
OICY Attn: H. Solcher

Defense Advanced Research Project Agency
1400 Wilson Blvd.
Arlington, VA 22209

General Electric Company
Space Division
Valley Forge Space Center
Goddard Blvd King of Prussia
P. O. Box 8555
Philadelphia, Pa 19101
OICY Attn: M. H. Bortner
Space Science Lab.

ATTN: Lt. Col. G. Bulin (NMRO)
Mr. R. W. Alewine (SSTO)

General Electric Company
P. O. Box 1122

Lockheed Palto Alto Research Laboratory
Dept 52-12, Bldg. 205
3251 Hanover Street
Palto, Alto, CA 94304

ATTN: Dr. Joseph B. Reagan
Dr. Richard D. Sharp

The University of Chicago
The Enrico Fermi Institute
933 East 56th Street
Chicago, IL 60637

ATTN: Dr. John Simpson

University of Wyoming
Dept. of Physics
Laramie, WY 82070

ATTN: Dr. T. J. Pepin

ONR Pasadena
1030 E. Green Street
Pasadena, CA 91106
ATTN: Mr. Bob Lawson

Radio Science Lab
Department of Electrical Engineering
Stanford University
Stanford, CA 94305

ATTN: R. Helliwell

Office of Naval Research Q-043
Scripps Institute of Oceanography
La Jolla, CA 92093

ATTN: Dr. Bob Stevenson

Headquarters, U. S. Air Force (RDS)
Washington, D.C. 20330

ATTN: Maj. Robert R. Wilde

Air Force Space Division (YLT)
P.O. Box 92960
Worldway Postal Center
Los Angeles, CA 90009

ATTN: Col. R. B. Kehl
Lt. I. Falto

Analytic Services, Inc.
400 Army-Navy Drive
Arlington, VA 22202

ATTN: Dr. John Baker

Commanding Officer
Office of Naval Research
Eastern/Central Regional Office
Bldg. 114, Section D
6... Summer Street
Boston, MA 02210

ATTN: Dr. F. Quelle

END

DATE
FILMED

7-8-1

DTIC